AIRS V6 Test Report Supplement:

Performance of AIRS+AMSU vs. AIRS-only retrievals

Analysis of the impact of the loss of AMSU-A2

Edited by:

Qing Yue and Bjorn Lambrigtsen

Contributions by:

Ali Behrangi, Luke Chen, Van Dang, Eric J. Fetzer, Evan Fishbein, Fredrick W. Irion, Brian Kahn, Peter Kalmus, Evan Manning, Edward Olsen, Baijun Tian, R. Chris Wilson, and Sun Wong

Jet Propulsion Laboratory, California Institute of Technology

Pasadena, February 10, 2017

This research was carried out at the Jet Propulsion Laboratory, California Institute of Technology, under a contract with the National Aeronautics and Space Administration

Preface

This report presents the results of analysis to assess the impact of the loss of AMSU-A2 on the AIRS data products. The function of that microwave radiometer, with its two "window channels", has been to provide estimates of total column water content, both vapor and liquid, in the presence of clouds and thus plays a role in "cloud clearing", an important step in the AIRS retrieval process. It has also been used to provide information about the surface type. The AIRS Project and science team had already developed an alternative retrieval system that does not require microwave data, in anticipation of the eventual failure of the microwave sounders, and two parallel data product streams have been generated, both covering the entire mission. The "AIRS-only" products have been viewed as secondary, and in our report on the performance of the V6 retrieval system released in 2012 only rudimentary comparisons between the two were made (Dang et al. 2012). In the present report, we show the results of analysis in depth. This report is therefore a supplement to the main V6 report (Dang et al. 2012).

Executive Summary

The results of the analysis show that the quality of AIRS-only retrievals is nearly equal to that of the AIRS-AMSU retrievals, but with a few exceptions. At a global level the results are nearly indistinguishable, and AIRS therefore still meets Level 1 requirements, as illustrated in the example figure below for temperature profiles.

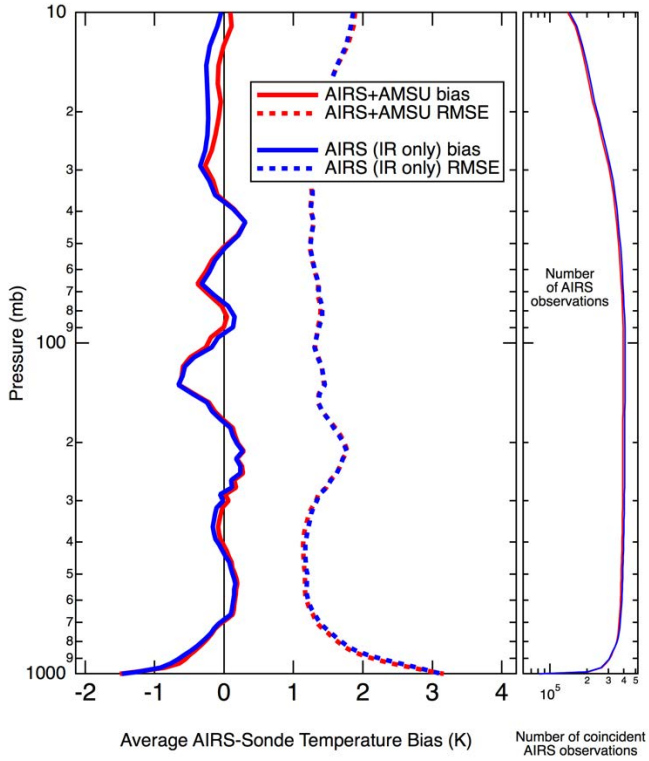

Figure 1. Vertical profiles of the global average temperature bias and RMSE for AIRS+AMSU and AIRS-only retrievals versus the National Center for Environmental Prediction (NCEP) quality-controlled radiosondes. Observations were made during June-July-August 2006, with the AIRS observations within 3 hours and 100 km of each sonde launch time and location AIRS retrievals with quality flag 2 (bad quality) were not included. The right panel shows the number of AIRS observations matched to sondes.

There are two main exceptions to this, both regional in nature: 1) cases with frozen land and 2) cases with low-lying clouds over tropical ocean. In both cases the effect of losing AMSU-A2 is a reduction in yield. In the case of frozen land, there is also some degradation in accuracy (precision). In the case of low clouds over ocean accuracy (precision) is almost unchanged. This is discussed in detail in subsequent sections.

The likely explanation for the frozen-land effect is that AMSU-A2 could detect snow on the ground, which AIRS by itself cannot do. There is therefore an error and uncertainty in the surface emissivity first guess, which leads to errors in the retrievals. The likely explanation for the cloud effect is that AIRS by itself often cannot detect low lying clouds, where the thermal contrast between the cloud tops and the surface may be very small. (In contrast, AMSU-A2 sees a very large thermal contrast over water.) This makes a difference in oceanic low-cloud cases where the cloud clearing process would normally succeed and retrievals be obtained with AMSU-A2.

An effort is under way to improve the retrieval results in the two cases noted above, using AMSU-A1 and possibly other sources that can provide information on frozen land and low clouds over ocean.

Table of Contents

Table of Tables

Table of Figures

1. Technical Summary

On September 24, 2016 power to the AMSU-A2 instrument on Aqua was lost. A series of attempts to restore it to normal operation have been unsuccessful. The presumed but unverified cause is that a current surge inside AMSU-A2 caused a fuse in a power supply unit on the spacecraft side to blow. If true, there is no possibility of recovery. AMSU-A includes two separate instrument modules, AMSU-A1 with 13 temperature-sounding channels between 50 and 90 GHz and AMSU-A2 with two transparent "surface" channels at 23.8 and 31.4 GHz. While AMSU-A1 is still operational (although 3 of its channels have degraded to the point where they are no longer used), this report addresses the consequences of losing both A1 and A2. This is because a retrieval system that does not use AMSU data is already in production, and we report here on the results of comparisons between it and the baseline retrieval system, which does use AMSU data. In the future, we will explore the possibility of using AIRS with AMSU-A1 only, but this report does not address that option.

This document characterizes the various AIRS core data product differences between the Version 6 (V6) AIRS/AMSU infrared and microwave combined (IR+MW) and AIRS infrared only (IR) retrieval algorithms. Comparisons with other well-validated data sources, such as radiosondes and other satellite and reanalysis datasets, are provided for a limited set of variables. This report does not provide detailed documentation on the differences in algorithms; instead, this document aims at estimating quantitatively the differences in the outputs of the two algorithms and identifying the potential regions and/or regimes where users should expect potential changes in the AIRS core product between AIRS IR+MW and IR retrievals.

AIRS is a suite of microwave and infrared instruments on the Aqua satellite launched on May, 2002 into a sun-synchronous orbit with an equatorial crossing time of 1:30 PM on the ascending (northward-moving) orbital node. The AIRS instrument, which is a hyper-spectral infrared grating spectrometer with 2378 channels between 3.7 and 15.4 μm, is the primary source of information for the retrieval algorithm, and the AMSU-A, with 15 microwave channels between 23 and 90 GHz (Aumann et al. 2003), is the secondary source. The nadir spatial resolution for the AIRS instrument is 13.5 km and clusters of 3×3 AIRS footprints are co-registered to a single AMSU footprint (Lambrigtsen and Lee 2003) with an FOV of 45 km. The AIRS system was designed to retrieve temperature with a 1K root-mean-square error (RMSE) in 1-km layers in the troposphere and water vapor with 15% RMSE per 2-km layer.

In addition to the standard AIRS/AMSU (IR+MW) products, the AIRS V6 data release includes an AIRS IR-only retrieval capability in the Level 2 (L2) software. The IR-only L2 and L3 products are both available for the full mission. The combination of infrared and microwave radiances facilitates the retrieval in cloudy conditions up to an infrared effective cloud fraction (ECF) of approximately 0.7 (Susskind et al. 2006) to 0.9 (Yue et al. 2013a; Yue et al. 2013b), depending on the cloud regime. Microwave channels provide additional information about surface classification, especially when differentiating frozen and non-frozen surfaces (both over land and ocean) during cold seasons. As a result, changes on the AIRS products from IR+MW to IR retrievals mainly

occur under cloudy conditions (ECF > 70%) and high latitude regions especially during cold seasons, causing a decrease of yield (i.e. the fraction of successful, high quality retrievals) by 10% to 30% in these conditions. The changes in the L3 products (Sec. 3.3) are mainly a result of this sampling difference.

Comparisons of the L2 products at the pixel scale (Sec. 3.2) indicate subtle changes in cloud-cleared radiances (CC-Rad), clouds and surface properties, and atmospheric states including temperature (T), water vapor (Q), carbon dioxide (CO_2), and Ozone (O_3). The AIRS L2 data products include a variable-by-variable, case-by-case, level-by-level quality control (QC) indicator. The name of each QC indicator is the same as the name of the corresponding parameter with "_QC" appended to the name. QC=0 indicates the highest quality retrieval, where the data products individually meet the AIRS accuracy requirements and may be used for data assimilation and statistical climate studies. QC=1 indicates good quality retrievals, where data may be used for studies with temporal and/or spatial averaging. QC=2 indicates the use of such data is not recommended. The V6 IR+MW and IR retrievals have different sets of QC indicators. Correct interpretation of the AIRS data requires the application of the appropriate QC flags to corresponding L2 products.

Table 1.1 provides a summary of test results for the L2 products and Table 1.2 for the L3 products. Table 1.3 shows a list of variables with no values (filler with -9999) in the IR retrievals due to the absence of microwave observations. By comparing with collocated MODIS clear-sky radiances (Sec.3.2.1), the AIRS CC-Rads show negligible differences between the two data products but a larger yield is found with QC=0&1 in the IR+MW than IR. This is due to the microwave's ability to sense the atmosphere through thick clouds. By comparing with collocated radiosonde data (Sec. 3.2.2), the AIRS team found very small differences in both the absolute biases (accuracy) and RMSEs (precision) on temperature and water vapor profiles, with IR retrievals having slightly larger RMSEs in the boundary layer (~5% for Q and 0.5K for T).

Table 1.1. Summary of L2 test results

Variable	"Truth" Data	Method	Findings
Cloud-cleared radiances: CC-Rads	N/A	Granule scale differences	• Max Bias is within +/- 0.8K • Max RMSE is within 1.0K • Yield for QC=1 for IR is higher than in IR+MW, but yield for QC=0 is lower for IR than IR+MW.
	MODIS clear radiances	Comparisons between AIRS convolved CC-Rad with MODIS radiances	• Differences between IR and IR+MW are smaller than the accuracy of the collocation scheme between AIRS and MODIS. • Both IR and IR+MW CC-Rad QC procedures are accurately categorizing the fidelity of CC-Rad from AIRS. • Higher (lower) yield for QC=1 (QC=0) in IR than in IR+MW, corresponding with reduced ability to sense atmosphere through thicker clouds without microwave.
Temperature and water vapor profiles: T(P) Q(P)	Dedicated Sonde and ECMWF	21 stations in three latitude bands	• Differences between IR and IR+MW are not significant. • Larger RMSE (<10%) in specific humidity in the tropical and polar lower troposphere. • Mean bias for T increases by 0.5 K in IR compared with IR+MW in the tropical upper troposphere. • Differences between the IR and IR+MW are smaller in physical retrieval than those in the Neural Network (NN) first guess.
	MAGIC Sonde and	Collocated; by longitude bins	• T bias increases by 0.2K for pressure (P) > 850 hPa and RMSE increase by 0.2K for P > 950hPa in IR compared to IR+MW.

	ECMWF		• Q bias is the same in IR and IR+MW with RMSE increased by 0.5g/kg for P > 800hPa in IR. • These changes are within the uncertainty range of MAGIC radiosonde measurements. • Sudden increases in IR retrieval yield at a particular longitude in the MAGIC region possibly associated with specific cloud regime.
	PREPQC radiosonde	Collocated; Trend of T bias profiles	• Difference in T profile between IR and IR+MW is very small, both products have less than 1K bias against sondes. • Differences in the T drift are small. Both products have less than 0.05K/yr drift which is within the uncertainty limit of sondes.
Total precipitable water: TPW	GPS Ground (US)	multi-year; conditioned on cloud, land-only	• Yield decreases for larger ECF: by 5-10% for 0.6-0.8 ECF, same yield for ECF>0.9. • Slightly larger biases and RMSE for IR-only at all ECFs.
Near surface air temperature and water vapor: NSAT and NSWV	Buoy over ocean and Mesonet over land (Western US)	Collocated	• Larger impact seen for NSWV than for NSAT with loss of MW. • The nighttime IR retrievals produce a comparable (for NSAT) or smaller (for NSWV) mean bias than IR+MW, while the RMS increases by 0.1~0.3K for NSAT and 2-5% for NSWV going from IR+MW to IR. The magnitude of bias increases as ECF increases. • Daytime NSAT from IR+MW and IR is similar in terms of both bias and RMS, while the NSWV IR-only retrievals produce a much larger dry bias than IR+MW and the RMS increases by more than 5% for ECF > 70%. • Very small differences between the two retrievals over CONUS.
Clouds	N/A	IR and IR+MW granule-scale comparisons on cloud and atmosphere	• Over 75% agreement on the nCld retrievals. The cloud property change is consistent with the cloud vertical structure changes between IR and IR+MW.
CO_2	HIPPO	Convolved HIPPO profile; 24hr collocation	• The loss of MW has no direct influence upon the AIRS CO_2 post-processing algorithm because the algorithm has used channels that have minimal radiance contribution from the surface and the very lowest atmospheric layers. Thus, the difference of retrieved CO_2 exhibits essentially no bias when AMSU/AIRS and AIRS (IR Only) are compared against one another or compared separately against airborne validation measurements.

Table 1.2. Summary of L3 test results

Variable	"Truth" Data	Method	Findings
TPW	AMSRE and TMI	Multi-sensor comparison, Monthly mean maps	• The AIRS IR-Only and IR+MW TPW have dry biases over the tropical deep convective or high cloud regions and wet biases over the subsiding or low cloud regions and mid-latitude snow-covered land regions. The IR only retrievals have biases with the same spatial pattern but larger magnitudes than the IR+MW combined retrievals. • Biases are larger in the ascending node but much smaller in the descending node. This indicates a spurious cycle in AIRS TPW.
SurfSkinTemp	N/A	Monthly mean maps, IR minus IR+MW	• Large difference (3K) over high latitude region but less than 1K elsewhere. • IR yield decreases by 10-30% in high latitude regions and the subtropics.
SurfAirTemp	N/A	Monthly mean maps, IR minus IR+MW	• Large differences (±3K) over high latitude regions (e.g., Canada, Siberia, and Alaska coast), generally small (< 1 K) over most other regions. • 15-30% yield reduction in IR over high latitude regions (e.g., Canada and Siberia), generally small (< 10%) over most other regions.
Tropopause height, pressure, and temperature	GPS RO	Multi-sensor comparison, Monthly mean maps	•Large differences between IR+MW and IR tropopause parameters (300m, 20hPa, and 2K for height, pressure, and temperature, respectively) in the extra-tropics. •These differences are much smaller than the differences between the AIRS and GPSRO tropopause quantities.
Temperature	N/A	Monthly mean	• The lower troposphere (850 hPa) temperature difference can reach 3K

profile		maps, IR minus IR+MW	over the mid- and high-latitude regions in the cold season, but is relatively small over other regions (magnitude less than ±0.6K). • The middle troposphere (500 hPa) temperature difference can reach ±1K over high-latitude and tropical deep convective regions, especially over land. • In the upper troposphere (250 hPa), the IR-Only temperature is about 1 K warmer than IR+MW over the tropical deep convective regions and about 1 K colder than IR+MW over high-latitude regions (e.g., the NH mid-latitudes). • In the lower stratosphere (70 hPa), the temperature difference between IR-Only and IR+MW is very small.
Water vapor mixing ratio: MMR	N/A	Monthly mean maps, IR minus IR+MW	• The IR MMR in the lower and middle troposphere (850, 500 hPa) is lower (by about 2g/kg at 850 hPa and 0.1 g/kg at 500 hPa) than IR+MW over tropical deep convective or high cloud regions, while it is higher than IR+MW by about 1 g/kg and 0.1g/kg than IR+MW over subsiding or low cloud regions. • At 250 hPa, IR MMR is higher than IR+MW by 0.008 g/kg over tropical deep convective or high cloud regions.
Relative Humidity: RelHum	N/A	Monthly mean maps, IR minus IR+MW	• The RelHum differences between the IR and IR+MW result from the combination of changes in both temperature and water vapor mixing ratio at each level. • Compared to IR+MW, IR-only RelHum at the lower and middle troposphere is lower over tropical deep convective region and higher over subtropical subsiding regions. • The difference between the IR-Only and IR+MW RelHum at the upper troposphere is generally small except in Polar Regions
CO_2	N/A	Time series, by latitude, map of monthly difference	• Changes on L3 CO2 are purely due to yield change. • Increased IR-only yield for low stratus cloud
Total Column Ozone	OMI	Multi-sensor comparison	• The differences in total column ozone between IR+MW and IR-only are much smaller than the differences between AIRS and OMI
Clouds: cloud top temperature (CTT) and effective cloud fraction (ECF)	N/A	Difference between IR and IR+MW, global, monthly data	• Upper layer CTT decreases/decreases in the tropics/mid and high latitudes. • Fewer lower layer cloud especially in the broken low cloud region with IR-only • Upper layer ECF is reduced in low lat and increased in high lat in the IR data. Lower layer ECF shows changes with opposite sign. • Significant increase in ice cloud optical depth in the high lat regions. Slightly reduced optical depth in thicker cloud region and slightly increased optical depth in the thin cirrus over the W. Pacific region. • Changes in ice particle effective size have similar spatial pattern but opposite sign.

Table 1.3. Variables with no values (filled with -9999) in the IR retrievals

Mnemonic Name	**ESDT Shortname**	**Variables**
L2_Standard_cloud-cleared_radiance_product	AIRS2CCF	None
L2_Standard_atmospheric&surface_product	AIRS2RET	TAirMWOnlyStd MWSurfClass sfcTbMWStd EmisMWStd EmisMWStdErr totH2OMWOnlyStd GP_Height_MWOnly totCldH2OStd totCldH2OStdErr
L2_Support_atmospheric&surface_product	AIRS2SUP	TAirMWOnlyErr MWSurfClass sfcTbMWStd EmisMWStd EmisMWStdErr totH2OMWOnlyStd totCldH2OStd totCldH2OStdErr satzen_amsu satazi_amsu lwCDSup lwCDSupErr clWSup Phys_resid_AMSUA MWCheck_Resid_Ratio MWsurf_T0 MWsurf_Tinf MWsecant_ratio MWseaice_conc MWresidual_temp MWresidual_mois MWresidual_AMSUA MWresidual_HSB MWiter_temp MWiter_mois cloud_ice final_AMSU_ret
L3_Standard_Daily L3_Standard_Multiday L3_Standard_Monthly	AIRS3STD AIRS3ST8 AIRS3STM	ascending_MW_only grid descending_MW_only grid
L3_Support_Daily L3_Support_Multiday L3_Support_Monthly	AIRS3SPD AIRS3SP8 AIRS3SPM	SurfCLass_Count for some frozen types MWSST MW_Emis_*
L3_Research_Daily L3_Research_Multiday L3_Research_Monthly	AIRS3RED AIRS3RE8 AIRS3REM	TAirMWOnly H2OCDMWOnly MW_SurfClass_Count totCldH2OStd Phys_resid_AMSUA Tdiff_IR_MW_ret AMSU_Chans_Resid MWCheck_Resid_Ratio

2. Approach

The tested version of the product is V6.06, which is the standard AIRS V6 data release. The test results are shown in Section 3 for a set of AIRS core products at both Level 2 and Level 3 (please see Tables 1.1 and 1.2). The purpose of this report is to document the differences between the V6 IR+MW and IR retrievals. The reader should not interpret the analyses as validation but rather as indicators of the characteristics of the products from the two retrieval algorithms and how they differ from each other.

The AIRS product files contain a large number of parameters, ranging from quality flags to retrieved data values. Complete lists of the parameters can be found in the AIRS V6 Released Processing File Description (http://disc.sci.gsfc.nasa.gov/AIRS/documentation/v6_docs/v6releasedocs-1/V6_Released_Processing_File_Description.pdf). Only a small subset of these parameters, representative of the core retrieved variables, have been assessed and included in this report. This subset includes the cloud cleared radiances, thermodynamic quantities (T, Q, cloud parameters), trace gases (CO_2, O_3), and surface parameters. The test results are organized first by the processing level, and then by the parameters. The reader is referred to the table of contents. Two examples are given in Sec. 3.4 to illustrate the differences for one research analysis (variance scaling analysis of T and Q profiles) and one application (AIRS drought study) using the AIRS IR+MW and IR data.

As discussed in the executive summary, the impacts upon the cloudy scenes and cold surfaces in the high latitude cold season are highlighted in Sec. 3.1, with detailed reports in the following sections.

3. Test Results

3.1 The major impacts of losing microwave observations

3.1.1 Surface classification in IR+MW and IR retrieval algorithm and its impact

Contributor: Evan Manning, Bjorn Lambrigtsen, Qing Yue, Baijun Tian

Table 3.1.1 shows how surface types are determined in the IR+MW and IR algorithms. Land/water/coast are all determined from geolocation and a digital elevation model in both retrievals. In the IR+MW retrieval, microwave radiances are used to distinguish snow and ice from bare land or liquid water surfaces. Since microwave emissivity information is not available for the IR-only retrieval, the surface temperature from forecast (tsurf_forecast) or climatology if forecast is not available is used to differentiate frozen and non-frozen surfaces (frozen land if tsurf_forecast < 273.15 K; frozen water if tsurf_forecast < the sea water freezing point temperature). As a result, IR-only retrievals have less accurate discrimination of the surface types and hence the surface emissivity in the high latitude regions, which affects both the retrieval yield, accuracy, and precision of various parameters in these regions. Figure 3.1.1 shows the differences (IR minus IR+MW) in the number of non-frozen pixels in January and July, 2015 over ocean and over land. These differences are much larger during the cold season than the warm season. The spatial patterns of differences in the frozen/non-frozen surface classifications are highly correlated with the changes in both the yield and values of L3 parameters in the high latitude regions. The surface skin temperature (SurfSkinTemp) is shown as an example in Figure 3.1.2 and the same effect is also seen in Figure 3.1.4 for total precipitable water vapor. For surface skin temperature, note that differences are less than ±0.5K within most of the tropics and ±1.0K within most of the midlatitude regions. Over the ocean, AIRS SST data have been validated against three data sets: the European Center (ECMWF) analyses, operational buoys, and a ship born radiometer (Fetzer et al. 2003). Differences against the three datasets are -0.8K±1.0K, -0.8K±1.1K, and -0.85K±1.2K, respectively, in addition to a sampling bias of 3K when comparing with the SST from National Centers for Environmental Prediction (NECP) forecast. Therefore, the IR and IR+MW differences on SST are well within the uncertainty limit of AIRS products.

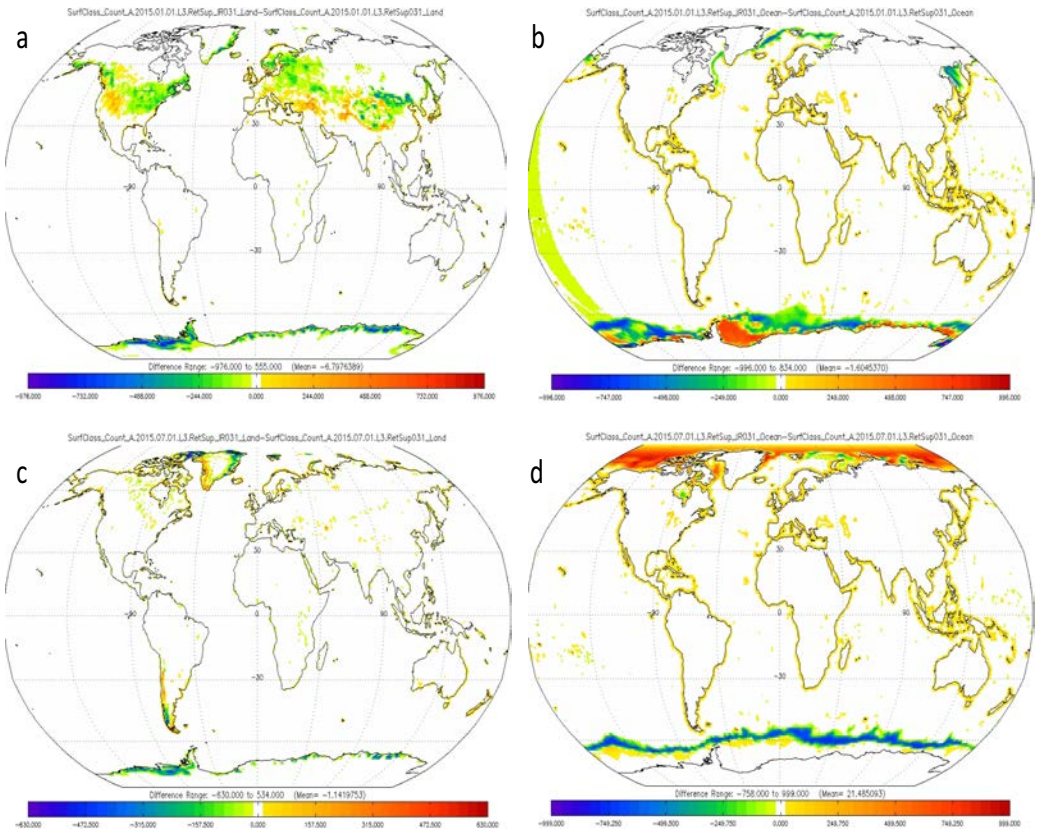

Figure 3.1.1. The differences (IR minus IR+MW) in the number of nonfrozen pixels on January (a and b) and July (c and d), 2015 over land (a and c) and over ocean (b and d).

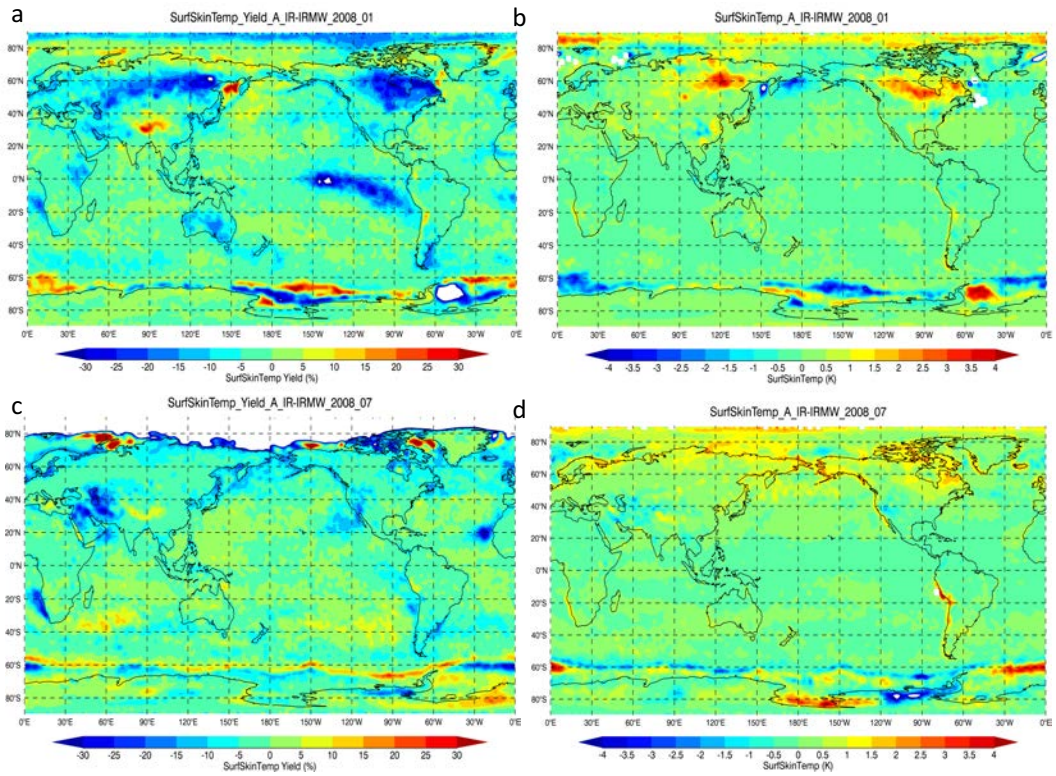

Figure 3.1.2. The V6 IR and IR+MW retrieval differences on L3 monthly surface skin temperature yield (left) and values (right). Data from January (top) and July (bottom) 2008 is used. The white region in the left panel represents values between -35 and -30%. Narrower color bars are used to show finer regional patterns.

Table 3.1.1. Surface classification in V6 IR+MW and IR retrievals

Surface Classification	IR+MW	IR
1	Coast	Coast
2	Land	Land
3	Ocean	Ocean
4	High microwave emissivity sea ice	Sea ice if tsurf_forecast < sea water freezing point
5	Low microwave emissivity sea ice	Not available, filled by -9999
6	Snow Covered Land (high microwave emissivity)	Frozen land if tsurf_forecast < 273.15 K
7	Glacier/Snow	Not available, filled by -9999
8	Snow Covered Land (Low microwave emissivity)	Not available, filled by -9999

3.1.2 Reduced retrieval yield within cloudy conditions (ECF>70%) in the IR retrieval

Contributor: Qing Yue, Baijun Tian

The yield of AIRS retrievals is highly dependent on the cloud state within the field of view (FOV) (Yue et al. 2011) and generally decreases as effective cloud fraction increases. Figure 3.1.3 shows the frequency of occurrence as a function of AIRS effective cloud fraction (ECF) for pixels with QC indicator values of 0 (top), 1 (middle), and 2 (bottom) for AIRS V6 L2 total precipitable water vapor. Nine years (2006-2014) of AIRS data over the United States SuomiNet GPS stations are used. V5 AMSU/AIRS results are also shown for comparison. Both V6 IR+MW and IR retrievals have much higher successful retrieval yield at all cloud fractions than V5. Although a sudden drop in the IR yield (increase in IR QC=2 frequency) is noticed when ECF is between 70% and 90%, the yields for IR+MW and IR are similar for ECF bins smaller or larger than this range, which is consistent with reduced QC=0&1 yields for CC-Rads (Sec. 3.2.1).

This reduced yield in very cloudy conditions is the main cause of the change in various parameters in the cloudy regions. As shown in Figure 3.1.4, the IR total precipitable water vapor shows a decreased yield in these regions and 5-10% less total water vapor values compared with IR+MW. A small increase (<15% relative to IR+MW climatology) in the total water vapor is found in IR compared to IR+MW over the subtropical oceans dominated by boundary layer clouds, which is consistent with a moister boundary layer retrieved in the IR-only algorithm in this region (see Sec. 3.2.2.2).

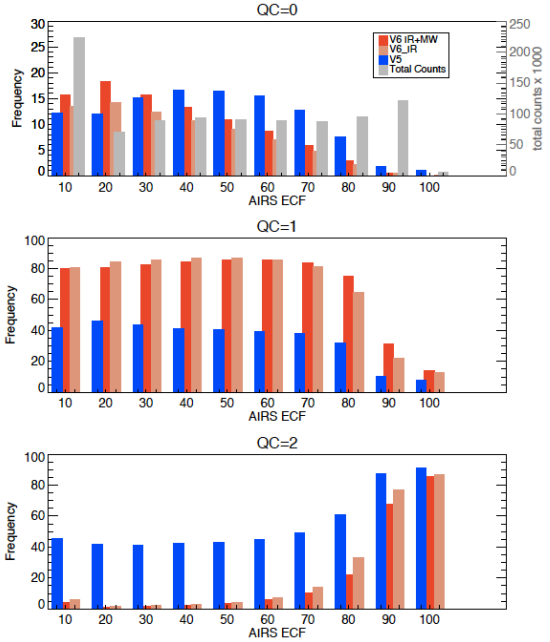

Figure 3.1.3. Frequency of occurrence as a function of AIRS effective cloud fraction (ECF) for pixels with QC indicator values of 0 (top), 1 (middle), and 2 (bottom) for AIRS V6 L2 total precipitable water vapor. Data from 2006 to 2014 that can be collocated with the SuomiNet GPS ground observations are used. The gray bars indicate the number of pixels. V6 IR+MW and IR results are shown with red and pink bars, separately. V5 AIRS/AMSU result is shown with blue bars for comparison.

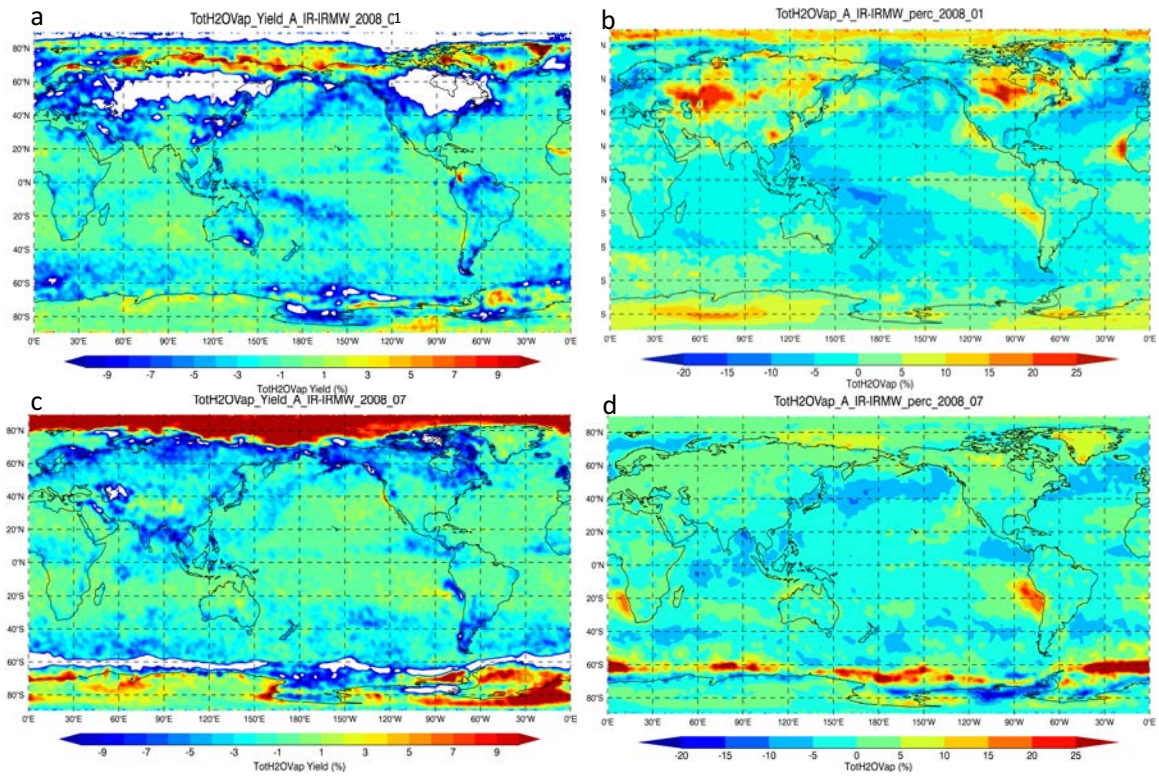

Figure 3.1.4. The V6 IR and IR+MW retrieval differences in L3 monthly total precipitable water vapor yield (left) and values (right). Data from January (top) and July (bottom) 2008 is used. The white region in the left panel represents values between -10 and -30% related to the surface classification issue discussed in Section 3.1.1. Narrower color bars are used to show finer regional patterns.

3.2 Test results for L2 products

This section presents the results for various L2 parameters. For a summary of these results, please refer to Table 1.1.

3.2.1 Cloud-cleared radiances (CC-Rad)

The CC-Rad product is an estimate of the upwelling, spectrally resolved radiances AIRS would observe if the scene were cloud-free. Nominally an independent estimate of clear sky radiances in some channels is used to estimate the entire clear-sky spectrum (Susskind et al. 2003; Susskind et al. 1997; Susskind et al. 1984). Both IR+MW and IR-only algorithms start with a neural-network (NN) trained against observed AIRS radiances and clear-sky radiances calculated using the ECMWF operational 3-hr forecasts (Blackwell and Chen 2005). The IR+MW NN uses the infrared and microwave radiances, while the IR-only NN uses the infrared radiances only. Then both algorithms proceed with sequential physical retrievals, where additional differences arise due to whether or not microwave information is included.

Two different tests are carried out for the CC-Rad product. The first one documents the changes in the entire AIRS spectrum from the IR+MW and IR data products (Sec. 3.2.1.1) The second one applies the collocated cloud observation from MODIS and makes comparisons of the AIRS CC-Rad convolved to the MODIS spectral response functions with the narrow band clear sky radiances observed by MODIS (Sec. 3.2.1.2).

3.2.1.1 Pixel scale assessment on the CC-Rad product

Contributor: Evan Fishbein, Luke Chen

The analyses presented here compare CC-Rad from the V6 IR-only and IR+MW products. The products are derived from the same software package, but follow slightly different logic paths. Specifically, the latter uses microwave brightness temperature (BT) to identify snow cover, while the former uses skin temperature to identify frozen conditions but cannot identify snow cover. Also, the topology of the two neural networks (NN) is different owing to the differences in inputs and training data. Two granules of data are used in this analysis, granules 32 and 71 from 2002-09-06.

Granule 32 is a descending (night) granule over the North Atlantic. Figure 3.2.1-1 summarizes the characteristics of the granules and the differences of cloud-cleared brightness temperatures between infrared (IR) and infrared combined with microwave (IR+MW) products. The lower left panel shows a map of the brightness temperature of the 1231 cm^{-1} channel, this is a cloud and surface-sensing channel with a modest radiometric contribution from the water continuum. The granule features a moderate mid-latitude cyclone and the radiances show the stratus clouds associated with the warm front in the left side of the image and the colder cumulus clouds associated with the cold front in the upper left. The lower-right panel shows a map of the differences in cloud-cleared brightness temperatures. Comparing the two maps, the largest differences in cloud-cleared radiances (after QC) do not occur in either the coldest clouds or clearest scenes, but along the edges of cloudy regions.

The upper-right panel examines the application of quality control and how yield depends on channel (frequency). Quality control is applied channel-by-channel comparing the cloud-cleared radiance noise against channel-dependent thresholds. Yield applied to comparisons of two products is strongly dependent on whether quality control is based on the intersection of quality-controlled sets, or the quality control of either product independently. The highest yield for good quality is achieved with the IR product, the lowest using the intersection. This is surprising in the sense that the IR+MW products contains the additional information from the MW observations and therefore should have higher quality. However, the best quality has the expected behavior. Water vapor sounding channels in the 6μm region have lower quality requirements and therefore higher yields; surface-sensing channels in the 8−12μm have higher requirements and therefore lower yields.

The upper left panel shows the spectrum of mean difference and root-mean square differences between the two products (IR − IR+MW); the intersections of good and best quality control are applied. The largest differences occur in channels sensing the surface and lower troposphere, and the changes in the best quality data are half that of the good quality. Mid-troposphere to stratosphere temperature-sounding and water-vapor-sounding channels show the smallest differences. Although this analysis documents differences between products, it does not represent comparisons against validation data sets and does not purport to suggest either product has better quality.

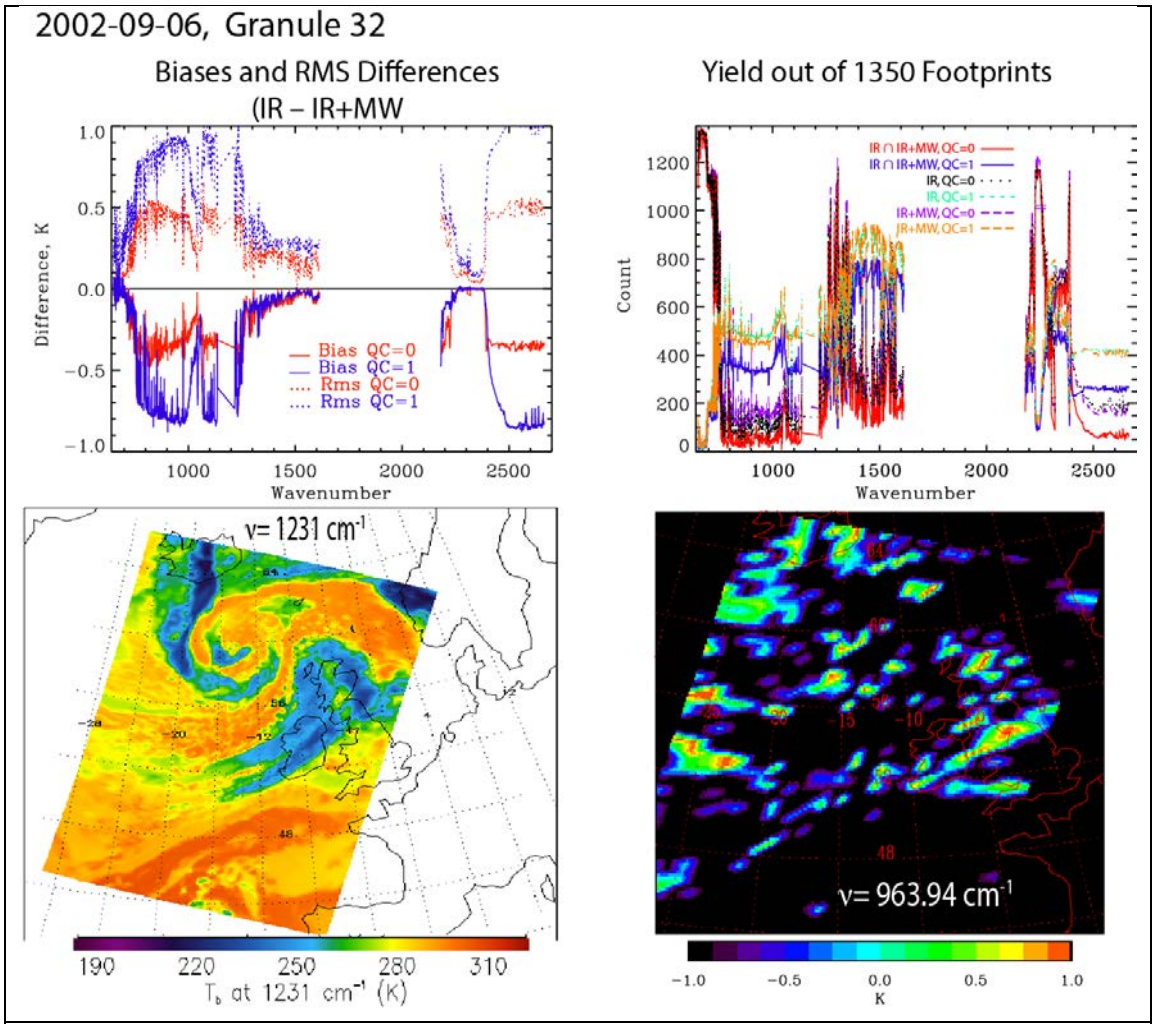

Figure 3.2.1-1. Granule 32, 6 Sep. 2002, Cloud-cleared radiance statistics. The lower left panel shows the raw 1231cm^{-1} brightness temperatures. The lower right panel shows differences between IR and IR+MW derived cloud-cleared brightness temperature; the data is filtered using the highest quality controlled (QC=0). The upper left panel shows mean and RMS differences between IR and IR+MW derived cloud-cleared brightness temperatures using both highest and medium quality control. The upper right panel shows the dependence of quality control (yield) on frequency using highest and medium quality control for the IR and IR+MW products; also shown is the yield when quality control is jointly (intersection) applied.

Figure 3.2.1-2 shows histograms of differences between cloud-cleared brightness temperatures for the 868.4, 963.84 and 2616.33 cm^{-1} channels, which are surface-sensing channels with decreasing contributions from water vapor continuum from long-wave to short-wave. Whereas Figure 3.2.1-1 showed that the mean differences vary slowly with frequency in the surface-sensing region, here we see that the probability density functions are complicated functions of channel and atmospheric conditions.

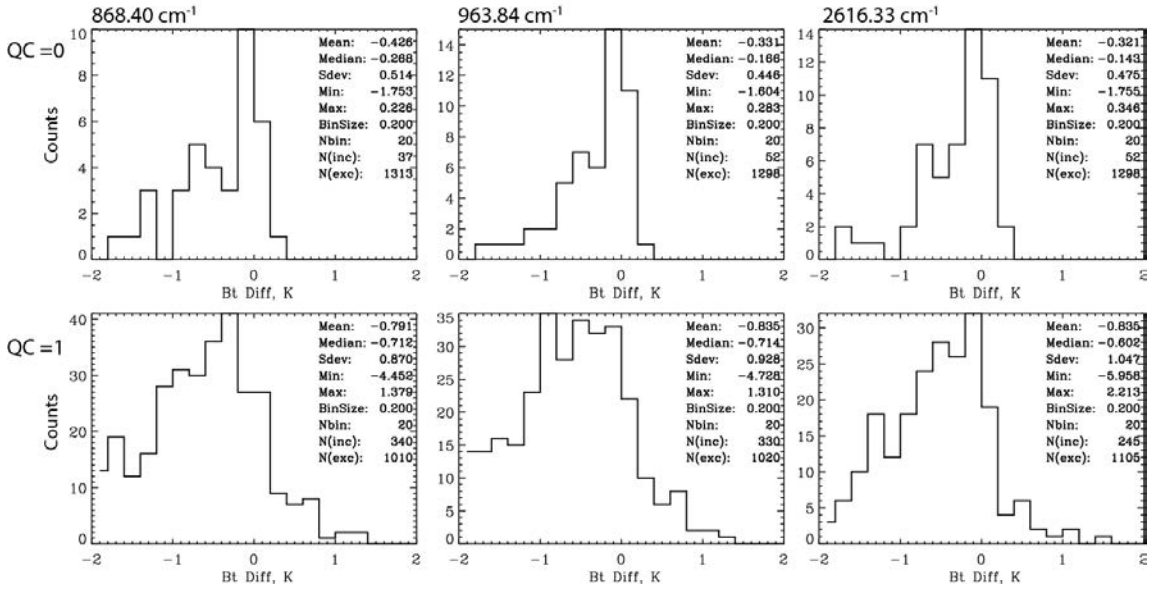

Figure 3.2.1-2. Granule 32, 6 Sep. 2002, Histograms of differences of cloud-cleared radiance IR minus IR+MW for channels: 868.40, 963.84 and 2616.33 cm^{-1}. Quality controls are "good" and "best", respectively, in the lower and upper panels using the intersection.

Figures 3.2.1-3 and 3.2.1-4 are the same as 3.2.1-1 and 3.2.1-2, but for Granule 71. This nighttime granule crosses the Antarctic coastline west of the Antarctic Peninsula and includes footprints containing sea ice and glacial ice. Although the yields for mid tropospheric to stratospheric temperature channels and water vapor channels are comparable to Granule 32, yields from surface sensing channels are 10x smaller. Good quality surface channel cloud-cleared radiances occur over sea and glacial ice are uncorrelated to cloudiness. However, the differences between the good quality brightness temperatures in the two data sets are smaller. Like the previous granule, the differences in the "best" data are 50% smaller than in the "good". Lastly, the probability density functions are more uniform across the surface-sensing channels and the differences are more closely distributed near the mean difference.

In summary:

1. The average and RMS BT difference increase from QC=0 to QC=1 in the long/short wave window channels for a mid-latitude ocean night granule. The slope of the difference spectrum also changes the sign between 800 and 1000 cm^{-1} from QC=0 to QC=1, corresponding to different type of clouds in the sample. This is expected, as the loss of MW channels would have a negative impact on cloud clearing. The differences for upper troposphere and stratosphere channels are relatively small as low clouds have small effects on these channels.
2. The range for the difference varies from granule to granule but is generally within +/-1K.
3. There are more QC=1 FOVs for IR-only than for IR+MW resulting in cloudier FOVs being misidentified as clear scenes. For the polar granule, the yields are extremely low for window channels even for AIRS/MW for both QC=0 and QC=1. This may result from the contamination of the frozen surface below.

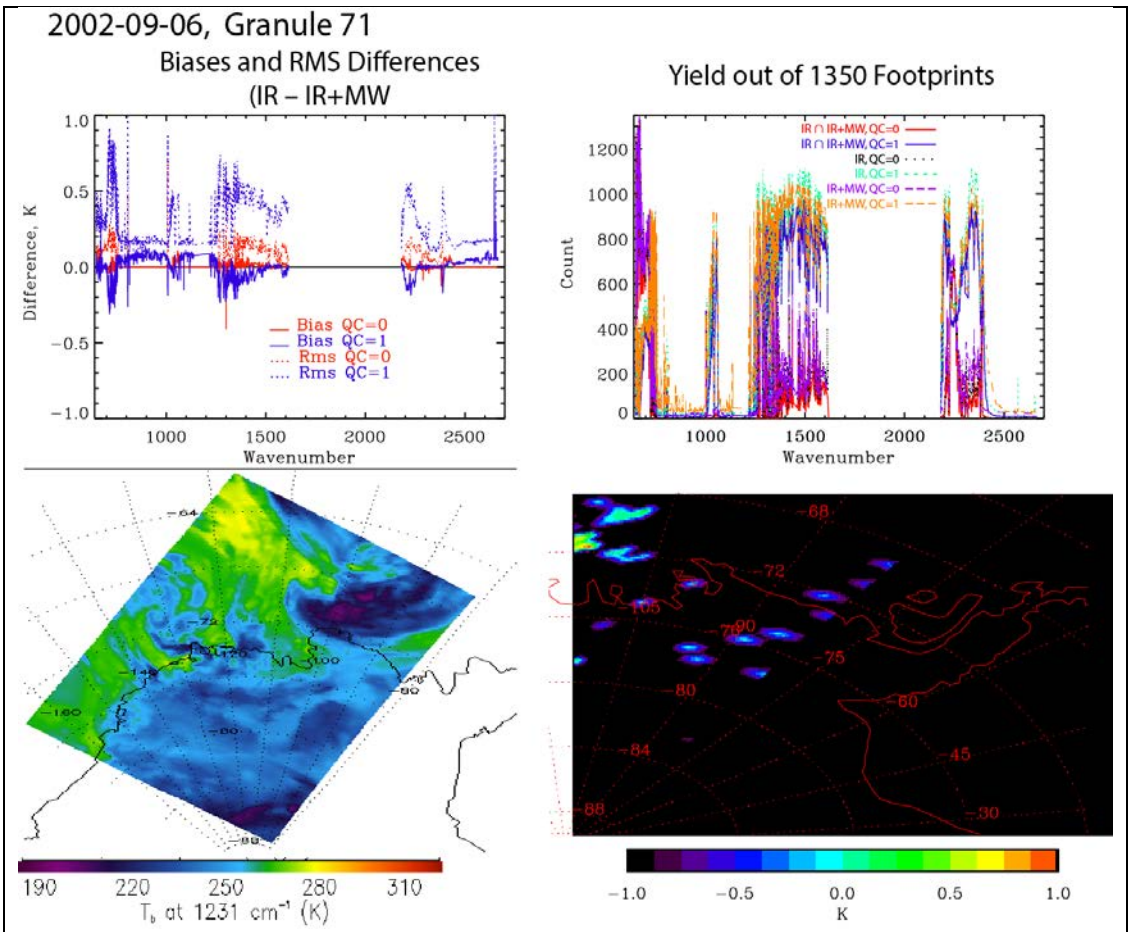

Figure 3.2.1-3. Granule 71, 6 Sep. 2002, Cloud-cleared radiance statistics. Equivalent to Figure 3.2.1-1, except for Granule 71. This is a night granule over the Antarctic coast, west of the Antarctic Peninsula.

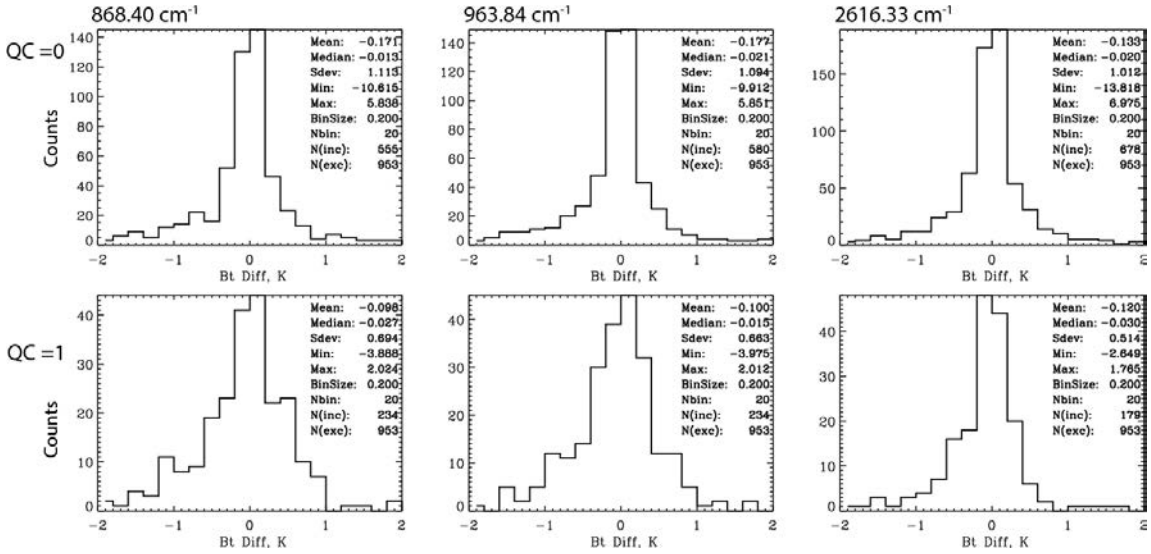

Figure 3.2.1-4. Equivalent to Figure 3.2.1-2, except for granule 71.

3.2.1.2 CC-Rad products from IR+MW and IR assessed using MODIS clear radiances

Contributor: R. Chris Wilson

Introduction

This analysis compares CC-Rads (CCRs) computed with AIRS/AMSU (IR+MW) to radiances computes with only AIRS (IR). The CCRs are spectrally convolved to MODIS channels 22, 24, 28, 32, 33, 34, and 35, while clear MODIS radiances are spatially convolved to the AIRS field of regard. All AIRS CCRs for February 3, 2013 are compared to clear MODIS. Figure 3.2.1-5 shows the spectral response functions that convolve AIRS CCRs to MODIS channels.

The method for convolving and comparing clear MODIS radiances with AIRS CCRs is validated by convolving all the MODIS pixels in the AIRS field of regard with spectrally convolved Level 1b AIRS radiances. Without spectral gaps in AIRS, and perfect knowledge of the field of regard and the AIRS spatial response function the matchups should have zero difference. Table 3.2.1-1 shows the bias, standard deviation, and percent of matchups between -0.5 and 0.5K. These MODIS channels were selected because there were not spectral gaps in AIRS and the collocation method generally had near zero bias and nearly 90 % of matchups with less than 0.5K differences.

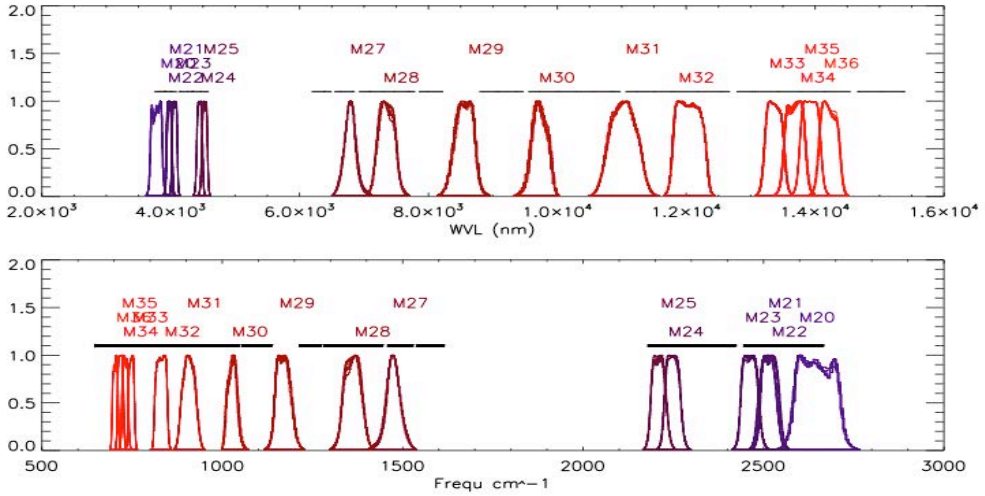

Figure 3.2.1-5. The spectral response function for MODIS channels.

Results

Only clear MODIS pixels as flagged by the MODIS clear 35 flag are used in the analysis. For an AIRS MODIS matchup to be included in the analysis at least 5 clear MODIS pixels must exist in the field of regard. Table 3.2.1-2 shows the results of AIRS CCRs-MODIS for IR+MW and IR products. In general, the IR+MW CCRs show a slightly smaller mean difference and standard deviation then the IR-only. This minor degradation (~.1K) of the IR only is smaller than the accuracy of the AIRS-MODIS convolution scheme as shown in Table 3.2.1-1.

Table 3.2.1-1. Comparison of AIRS L1B brightness temperature spectrally collocated with spatially collocated MODIS measurements.

MODIS Channel	Wavenumber (cm^{-1})	Main Influence	Bias (K)	SD (K)	% diff between -.5K to .5K
21	2525	Sfc/cld temp	-0.05	1.57	79
22	2465	Sfc/cld temp	-0.02	0.87	91
24	2236	CO_2/Atm temp	-0.43	0.79	99
28	1363	H_2O	-0.01	0.37	96
32	831	Sfc/cld temp	0.09	0.63	88
33	749	CO_2	-0.07	0.40	96
34	731	CO_2	-0.31	0.59	92
35	719	CO_2	-0.07	0.25	99

The AIRS CCR product contains QC flags for all channels. QC=0 means the expected error is less then 1K, QC=1means that the expected error is between 1 and 2.5K, and QC=2 means the expected error is greater than 2.5K. The expected error is based on a regression between the internal retrieval indicators, and agreement with ECMWF profiles. This study used a modified QC to assess the spectrally collocated AIRS CCRs. The expected error for the collocated AIRS is the average of the expected error for all AIRS channels located in the MODIS spectral response function. Each AIRS and MODIS channel matchup is then assigned a QC equal to 0, 1, or 2 based on the above QC description.

Table 3.2.1-2. Mean differences and standard deviations for AIRS CCRs-MODIS Clear radiances (Smaller in comparison with MODIS if highlighted in gray).

Channel	Mean diff IR+MW	Mean diff IR-only	SD diff IR+MW	SD IR-only
22	0.77	0.89	2.53	2.65
24	-0.09	-0.06	0.56	0.59
28	0.05	0.40	1.16	1.21
32	0.88	1.06	2.32	2.55
33	0.60	0.71	1.44	1.54
34	0.63	0.34	1.00	1.05
35	-0.43	0.30	0.76	0.75

Figure 3.2.1-6 shows the AIRS – MODIS bias and standard deviation for IR+MW and IR. There are slight differences between IR+MW and IR for QC=0 and QC=1. The bias of IR CCRs is lower compared to IR+MW for QC=2. The standard deviation of IR only is lower for QC=1 and QC=2. Both IR+MW and IR QC procedures for CCR products are accurately discriminating between the QC=0, 1, and 2 levels.

Figure 3.2.1-7 shows the percent of cases flagged as QC=0, 1, and 2 for IR+MW and IR CCR products. There are approximately 10 to 30 percent more QC=0 cases for the IR+MW compared to the IR-only. The reduction of the high quality CCRs in the IR-only seem to be evenly distributed in the IR+MW QC=1 and QC=2 cases.

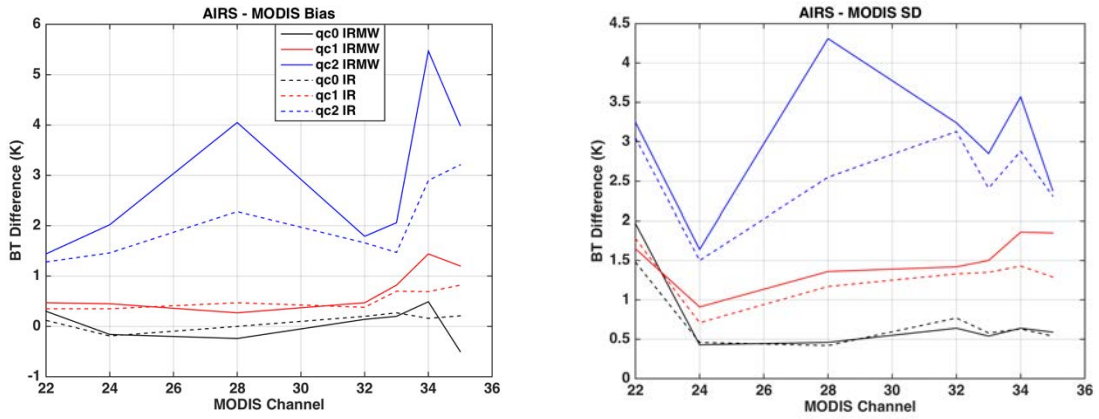

Figure 3.2.1-6. The AIRS CCRs – Clear MODIS bias (left) and standard deviation (right) for IR+MW and IR only.

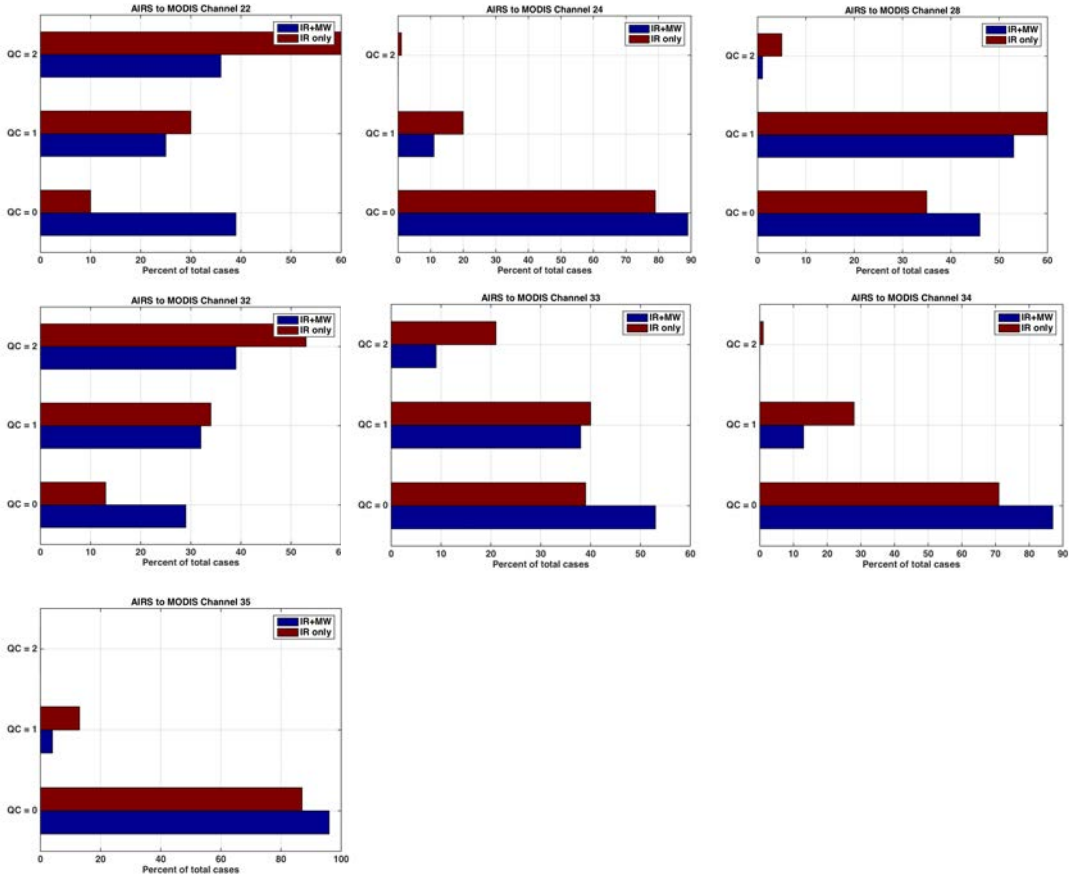

Figure 3.2.1-7. The percentage of cases with different AIRS convolved QC for IR+MW and IR only at various MODIS channels. QC=0 is expected error less then 1K, QC=1 is between 1 and 2.5K, and QC=2 is greater than 2.5K.

Conclusion

The differences in the CCRs from IR+MW and IR are less than the accuracy of the collocation scheme between AIRS and MODIS for QC=0 and 1, thus not significant. The IR-only CCRs show a smaller bias and standard deviation against collocated MODIS radiances for QC=2 cases. Both the IR+MW and IR-only QC procedures are accurately categorizing the fidelity of the CCRs. There are many more QC=0 cases for the IR+MW compared to the IR-only. This is likely because the microwave better characterizes the atmosphere in cloudier conditions.

3.2.2 Temperature (T) and water vapor (Q) vertical profiles

The IR+MW and IR differences in the L2 T and Q profiles are assessed against three different sets of *in situ* observations: dedicated sondes, radiosondes during the Marine ARM GPCI Investigation of Clouds (MAGIC) campaign, and PREPQC radiosondes. ECMWF model analysis data are also collocated to both AIRS and radiosondes measurements and included in the comparisons when available. The vertical profiles of mean biases, and root mean square (rms) errors of T and Q are calculated for IR+MW and IR-only L2 retrievals against these independent ground-based observations. The trend (drift) of temperature biases at each level is assessed against the PREPQC measurements and presented in Sec. 3.2.2.3.

3.2.2.1 Comparisons with dedicated sonde measurements

Contributor: Sun Wong

Data

V6 IR+MW and IR-only retrievals of temperature and specific humidity vertical profiles are validated against radiosonde measurements. Validation of co-located ECMWF forecast (EC) temperature and specific humidity profiles as well as the neural network (NN) profiles, which are used as the initial guess of the AIRS retrievals, are also included. Observations from dedicated radiosondes are used as the validation dataset, which were launched at certain sites in certain months 2002-2008. The radiosonde types being used are mainly RS92 so that specific humidity data are reasonably good in the upper troposphere (above 400 hPa). Moreover, dedicated radiosondes are not assimilated in EC so that they provide independent validation for EC data.

Methodology

Since measurements from dedicated radiosondes are sporadic in space and time, all samples within certain latitude bands are used for validation. The quality control is performed using the quality flag from the IR+MW products. It has been verified that the results do not change either using the flags for AIRS/AMSU retrieval or the flags for AIRS IR-only retrieval. Dedicated radiosondes were launched when Aqua overpassed the sites, ensuring close matchup between the measurements and remote sensing. The temporal tolerance of our data matching is within 2 hours, and the spatial tolerance is 1 degree in longitude and latitude differences. Biases and root-mean-squared errors (RMSEs) are computed for the V6 AIRS/AMSU, IR-only, EC, and NN temperature and specific humidity profiles against measurements of dedicated radiosondes.

The biases and RMSEs are calculated, respectively, as in Wong et al. 2015:

$$bias \equiv mean(x_{data} - x_{truth} - \varepsilon_m)$$

and

$$RMSE \equiv \sqrt{mean[(x_{data} - x_{truth} - \varepsilon_m)^2]}$$

where x_{truth} represents radiosonde measurements, x_{data} represents the data being validated (e.g., AIRS/AMSU, IR-only, or NN), and ε_m is the difference between the ECs collocated at the AIRS footprints and the radiosonde sites as the estimates of the biases caused by geographical differences. The means are taken over samples in three latitude bands, the tropics (30°S-30°N), Northern Hemispheric middle latitudes (30°-60°N) and polar region (60°-90°N). For specific humidity, the biases and RMSEs are divided by the means of the radiosonde measurements and reported as relative quantities in percentage.

Conclusions

Differences in specific humidity biases between AIRS/AMSU and IR-only retrievals are not evident (Fig. 3.2.2-1). The evident differences are the RMSEs for which IR-only retrievals have slightly larger values (< 10%) in particular in the tropical and polar lower troposphere.

Obvious differences in temperature biases between AIRS/AMSU and IR-only over polar region and tropical upper troposphere in NN are partially removed in the physical retrieval step (Fig. 3.2.2-2). In polar region, the consistently colder IR-only NN by ~0.5 K above 700 hPa is much reduced in the corresponding physical retrievals. The warmer IR-only NN by 1 K in the tropical upper troposphere is reduced to ~0.5 K in the corresponding physical retrievals. While the differences in RMSEs between the AIRS/AMSU and IR-only are small, IR-only generally has larger values particularly in the mid-latitude lower troposphere.

For specific humidity, the accuracies of AIRS/AMSU and IR-only retrievals are close to each other, with the IR-only having slightly less precision (i.e., larger RMSEs). For temperature, the accuracies between the two retrievals are close except in the tropical upper troposphere, where the IR-only is warmer by 0.5 K. The precisions of the two retrievals are also close, with IR-only having slightly larger RMSEs.

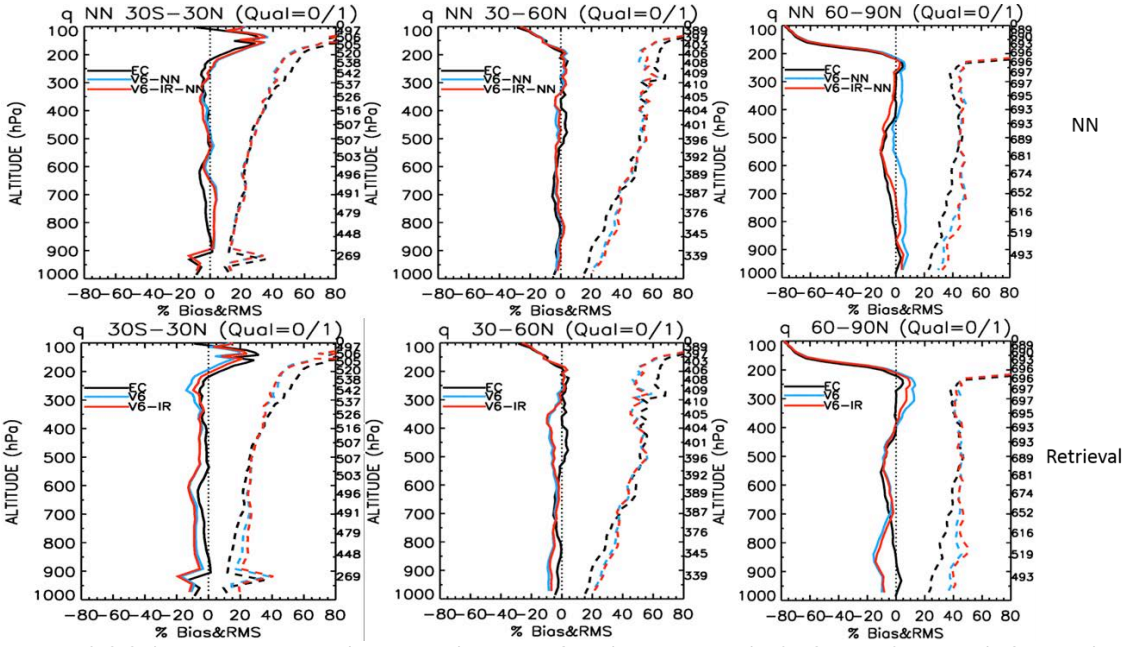

Figure 3.2.2-1. Relative biases (solid lines) and RMSEs (dashed lines) of ECMWF forecast (EC, black), V6 AIRS/AMSU (blue), and V6 IR-only (red) specific humidity retrievals. The upper panel is for neural network (NN), and the lower panel is for the physical retrievals. The numbers on the right axes are the sample sizes. The left column shows the results in the tropics (30°S-30°N), the middle column show the results in Northern middle latitudes (30°-60°N), and the right column shows the results in the Northern polar region (30°-60°N).

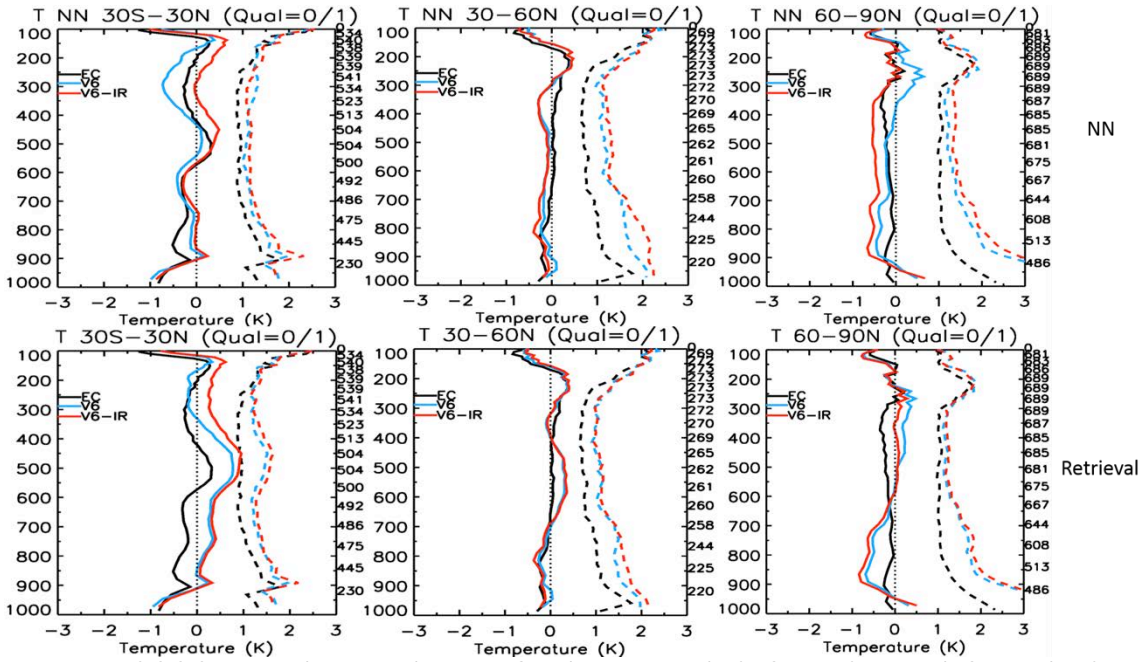

Figure 3.2.2-2. Biases (solid lines) and RMSEs (dashed lines) of ECMWF forecast (EC, black), V6 AIRS/AMSU (blue), and V6 IR-only (red) temperature retrievals. The upper panel is for neural network (NN), and the lower panel is for the physical retrievals. The numbers on the right axes are the sample sizes. The left column shows the results in the tropics (30°S-30°N), the middle column show the results in Northern middle latitudes (30°-60°N), and the right column shows the results in the Northern polar region (30°-60°N).

3.2.2.2 Comparisons with radiosonde measurements taken during the MAGIC field campaign

Contributor: Peter Kalmus

Data

L2 TAirSup (henceforth **T**) and L2 H2OCDSup (which is converted to specific humidity in units of g/kg, henceforth **q**) from AIRS/AMSU (IR+MW) and AIRS (IR) are examined by comparing with the collocated ECMWF reanalysis and the radiosonde measurements from the Marine ARM GPCI Investigation of Clouds (MAGIC) campaign.

We analyze approximately 550 vertical profiles for each variable (T and q) and each AIRS data type (airx2sup and airs2sup). Radiosondes from the ship-borne MAGIC campaign provide "truth" profiles for temperature and relative humidity (we convert the latter to specific humidity). The radiosonde manufacturer (Vaisala, model RS92-SGP) quotes two-sigma uncertainties of ±0.5 K and 5% for T and RH, respectively. The radiosondes provide T and RH to typical pressures of 15–30 hPa, at typical resolutions of 0.3–0.4 hPa.

The MAGIC campaign (9/2012–10/2013) included 19 round trips between Los Angeles and Honolulu. There is a data hiatus between January 2013 and May 2013 due to a ship refit, so most MAGIC data were taken in the months between June and December with some data in January and May. Radiosonde launches were attempted four times per day, near 5:30, 11:30, 17:30, and 23:30 UTC, except for Legs 14a and 14b which featured eight launch attempts per day. ECMWF data is also used, and is included in figures.

Methodology

The AIRS L2 retrievals are collocated with the MAGIC data with following criteria: temporally not more than 6 h before or after each MAGIC radiosonde launch time and spatially centered not more than 200 km from the radiosonde launch location. If more than one retrieval satisfies these constraints, the spatially nearest one is chosen. We find an AIRS L2 retrieval corresponding to the MAGIC radiosonde under these constraints for all but about 80 of the radiosonde launches.

We discard any matchups in which the L2 data quality is marked 2 for *either* data set (i.e. we exclude the matchup if the airs2sup QC equals 2 *or* if the airx2sup QC equals 2: dual QC). Results QCed by the corresponding QC flags in each product are also shown for comparison purpose. Comparison is carried out by:

a. Calculating profiles of mean bias and RMSE of all truth-AIRS pairs;
b. Calculating longitudinally-binned profiles of bias and RMSE, along the transect, of truth-AIRS pairs. In each bin, a mean bias and RMSE is calculated. This creates 2-dimensional longitude-pressure slices of bias and RMSE along the transect.

Conclusions

As shown in Fig. 3.2.2-3, in the MAGIC regime (marine northeast Pacific between California and Hawaii), comparing to the IR+MW, IR retrievals show a larger boundary-layer bias of T by 0.2K (in the warm direction) below 850 hPa and a larger RMSE of T by 0.2K near the surface (below 950 hPa). The Q biases in IR+MW and IR are very similar in the boundary layer, while the IR retrieved Q has an increased RMSE in the boundary layer, by 0.5 g/kg. As shown in the longitudinally-binned comparisons, the changes in T seem concentrated in the stratocumulus (Sc) regime, whereas changes in Q are seen throughout the MAGIC region (Sc and cumulus regimes).

IR seems to have a higher retrieval yield near the sc-cu transition region (Fig. 3.2.2-6) below 700 hPa by 10-20%. We examined the individual profiles in this region (about 228 longitude), and found that it corresponds with strong inversion cases with poor temperature retrievals not filtered out with the QC flags in the IR-only retrievals. These cases generally have a cold bias against the MAGIC observation, which decreases the mean temperature bias but increases the RMSE.

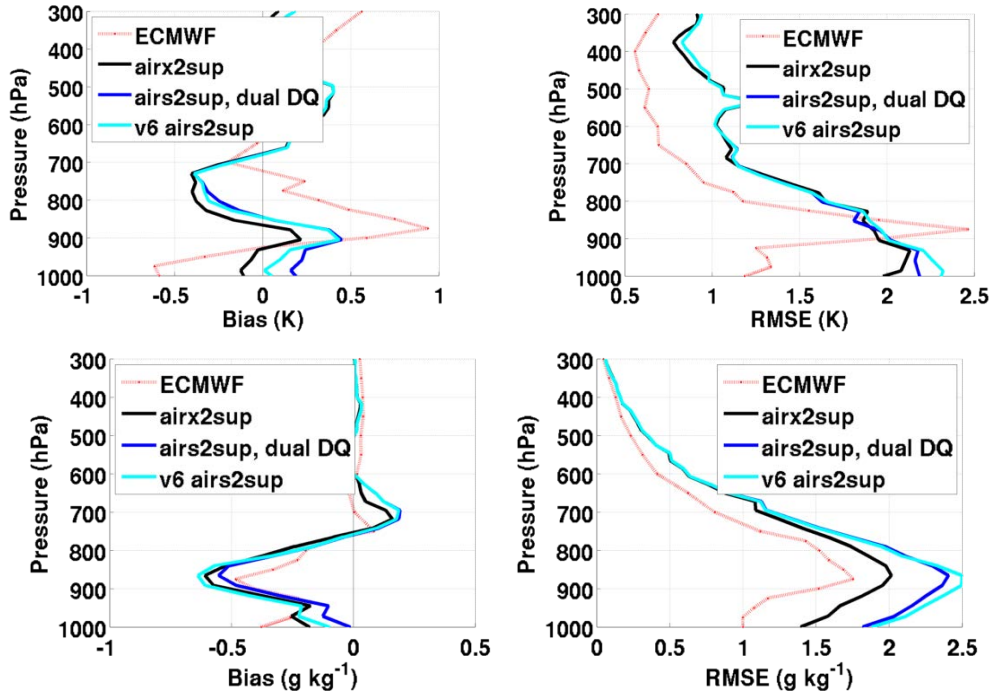

Figure 3.2.2-3. The bias (left) and RMSE (right) of temperature (T: upper) and water vapor (Q: lower) profiles against collocated MAGIC data. ECMWF (pink), AIRS/AMSU (airx2sup: black) and AIRS (airs2sup: navy) QCed by their corresponding QC flags, and AIRS-only retrievals QCed by dual QC flags (airs2up, dual DQ: light blue) are shown.

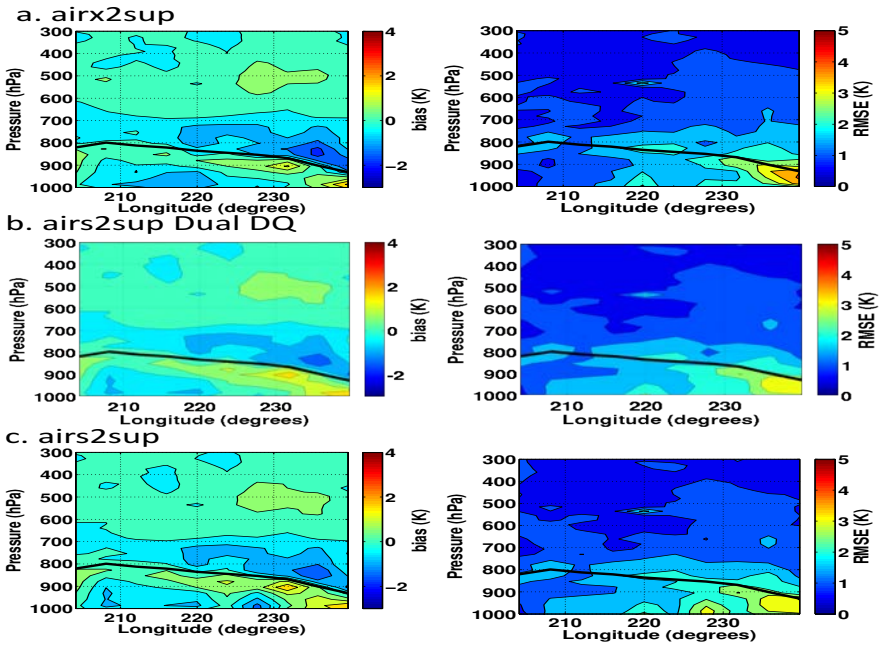

Figure 3.2.2-4. The longitudinally-binned bias (left) and RMSE (right) vertical profiles for temperature.

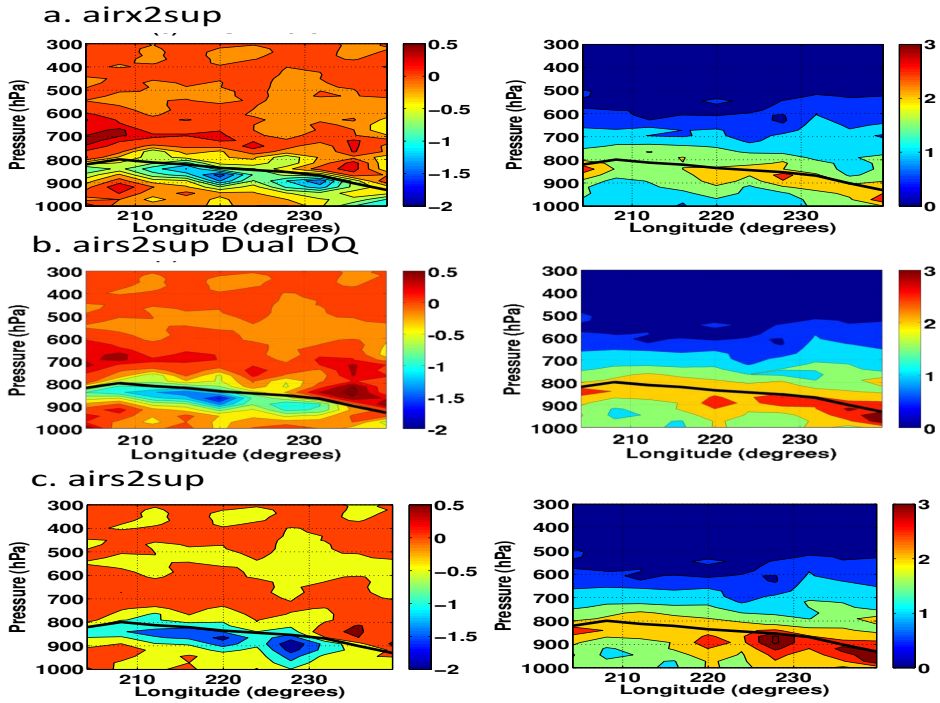

Figure 3.2.2-5. The longitudinally-binned bias (left) and RMSE (right) vertical profiles for temperature.

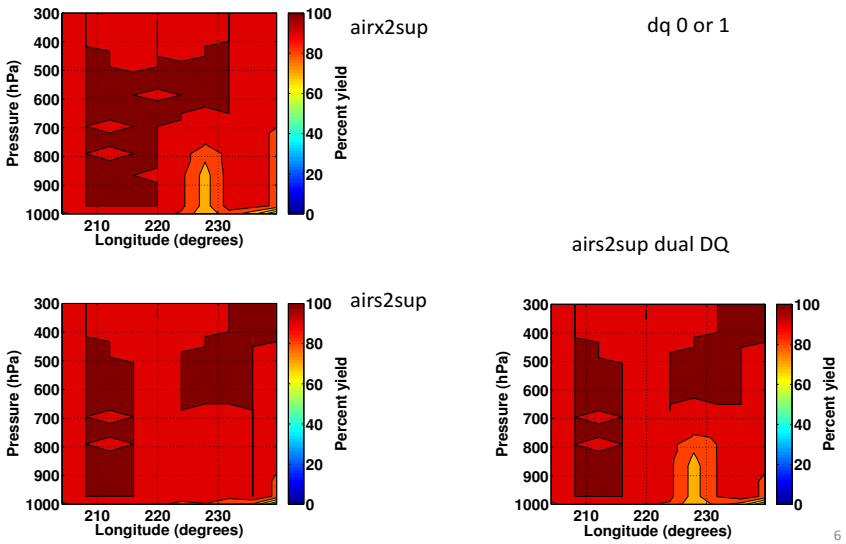

Figure 3.2.2-6. Frequency of occurrence with QC=0 or 1 for samples in the comparison.

3.2.2.3 Temperature bias and bias trends compared with PREPQC radiosondes

Contributor: Fredrick Irion

Data and Methodology

Versions 6 AIRS/AMSU (IR+MW) and AIRS (IR-only) retrieved temperatures (on the 100-level support grid) were compared against radiosonde observations in the National Centers for Environmental Prediction (NCEP) quality-controlled final observation (PREPQC) data files. The latter are from operational radiosondes mostly launched near 00 and 12 hrs GMT, with some launched near 6 and 18 hrs GMT. In addition to temperature, pressure and (often) specific humidity observations, the data records contain codes relating to quality control, correction methodology, radiosonde type etc., which were used in filtering the data before comparison to AIRS retrieval. To test and compare IR+MW and IR-only temperature retrievals, we matched radiosonde data to AIRS observations and calculated zonally-averaged differences as a function of pressure. This work has been previously described in the previous V6 test report (Dang et al. 2012). It is reproduced here specifically for V6 IR+MW and V6 IR-only comparison and testing for any major pathologies introduced by removing AMSU from processing AIRS data.

Radiosonde data were filtered by the following criteria:

1. For each pressure/temperature observation within a sonde profile:
   (a) If the "Temperature Program Code" (TPC) was 8, indicating that virtual temperature was given (T_V), the sensible temperature (T_s) was calculated from the formula:
   $$T_s = \frac{T_V}{1 + 0.608Q}$$
   where T_V, T_S are in Kelvin, and Q is the specific humidity using the same mass units (e.g., kg H_2O/kg dry air, not mg H_2O/kg dry air).
   (b) A single-level observation (but not necessarily the whole profile) would be rejected if either the "Temperature Quality Marker" (TQM), or the "Pressure Quality Marker" (PQM) was greater than 2.
   (c) An observation would be kept if the "Temperature Program Code" (TPC) and "Temperature Reason Code" (TRC) were matched as follows:
      (TPC = 8 and TRC = 1) (Virtual temperature reported calculated from sensible temperature and specific humidity), or
      (TPC = 1 and TRC = 100) (Temperature and quality marker unchanged from original values read into program "prepdata."), or
      (TPC = 6 and TRC = 1) (Rawinsonde has had a radiation bias correction with temperature and/or height recalculated), otherwise the observation would be rejected.
2. An entire sonde profile would be rejected if
   (a) The instrument type (ITP) was
      2 through 6, 8, or 9 (not radiosondes), or
      90 (radiosonde type unknown), or

100 through 109, or 112 through 225 (vacant, "not vacant", or reserved fields), or

(b) Accepted sonde temperature levels did not reach altitudes above the 90 mb level or altitudes below the 700 mb level, or

(c) A height gap in the accepted temperature observations was greater than 5 km (calculated from pressures assuming a 7km scale height).

For these comparisons, AIRS observations were land-only, and had to be made within 1 hour and 100 km of a sonde launch. (Note that this can lead to multiple AIRS observations matched to the same sonde profile.) Both daytime and nighttime observations are included, however comparisons are mostly at 0° in longitude and points eastward over Europe due to launch of sondes near noon GMT and the (ascending) 1:30PM equator crossing time of AQUA satellite. Figure 3.2.2-7 illustrates the locations of coincident observations used for bias calculations during JJA 2006. We selected a simple approach to maximize the number of coincidences while still avoiding poor retrievals: The only filters for AIRS data was that the surface temperature quality flag ("TSurfStd_QC" for V6) had to be 0 or 1 ("best" or "good"), and the V6 retrievals for a matched sonde had to be successful. We did not use AIRS quality flags for temperature profiles in filtering AIRS observations.

Radiosonde data were interpolated (by log pressure) to the AIRS 100-level vertical pressure grid prior to comparison. For direct measurements between AIRS and radiosonde temperatures, we did not extrapolate radiosonde data beyond their original range. In addition to direct comparisons between AIRS and radiosonde temperature profiles, we have also applied AIRS temperature averaging kernels to the radiosonde data ("kerned sondes").

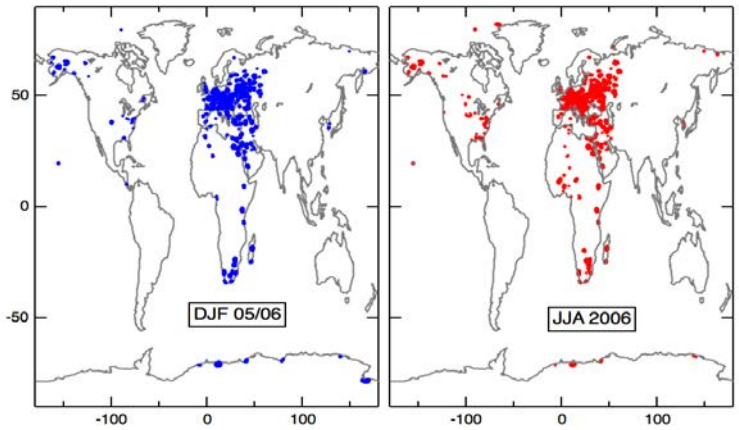

Figure 3.2.2-7. Locations of AIRS – radiosonde matchups for December 2005-January-February 2006 (left panel), and June, July, August 2006 (right panel).

The averaging kernel, **A** (a matrix), contains information on the vertical smoothing and sensitivity of a retrieval, and is calculated for each retrieved AIRS profile. Put simply, it relates the change of a retrieved state vector, $\hat{\mathbf{x}}$, to a change in the "true" state vector, $\mathbf{x}$:

$$\mathbf{A} = \frac{\partial \hat{\mathbf{x}}}{\partial \mathbf{x}} \qquad (1)$$

We apply the AIRS averaging kernel to the sonde data on the 100-level AIRS support grid as follows:

$$\mathbf{x}_{est} = \mathbf{x}_0 + \mathcal{T}\mathbf{A}\mathcal{T}'(\mathbf{x}_T - \mathbf{x}_0) \quad (2)$$

where: $\mathbf{x}_{est}$ is the temperature profile as AIRS "should have" seen it given its sensitivity to the *a priori* and limited vertical resolution,
$\mathbf{x}_0$ is the *a priori* temperature profile,
$\mathbf{x}_T$ is the radiosonde profile,
A is the averaging kernel,
T is a matrix describing the retrieval trapezoids (see *Susskind et al.* (2003)), and
$\mathcal{T}' = \left[\mathcal{T}^T\mathcal{T}\right]^{-1}\mathcal{T}^T$ is the least-squares inverse of T.

Details on the calculation of **A** for AIRS retrievals can be found in *Maddy et al.* (2008).

Note that as sondes do not extend to the lower pressures of the AIRS gridding, retrieved AIRS temperatures are used to fill in missing elements of $\mathbf{x}_T$ (e.g., pressures below the sonde burst); comparisons of temperatures between AIRS and kerned sondes may not be reliable in the mid-to-upper stratosphere since we are combining in-situ and AIRS remote measurements as 'truth' for this region. We also note that the AIRS averaging kernel is only calculated for the last step of the 'physical retrieval,' and does not account for information contained in the neural-network derivation of the *a priori* temperature profiles for the V6 or V6 AIRS-only retrievals.

AIRS minus Radiosonde Bias Calculation

To test changes in AIRS temperature retrievals between IR+MW and IR-only, we selected two three-month intervals, and binned comparisons on polar, mid-latitude and tropical regions. Figure 3.2.2-8 compares results for DJF 05/06. The left panels are the averages and root-mean-squares differences of profile temperatures between AIRS (IR+MW in blue, IR-only in red) and sonde observations. The middle panels show the number of observations in each bin. The right panels show differences of AIRS to 'kerned sonde temperatures,' that is, sonde temperatures that have been modified by the AIRS averaging kernel as in Eq. 2. Rows are by latitude bins. The average bias of both versions tend to be within 1K except at ground level and the southern mid-latitude stratosphere. Any differences in the biases to the PREPQC sonde data is quite small between the two versions.

Figure 3.2.2-9 compares biases for JJA 2006. Excluding the 90°S-60°S bin, biases tend to be within 1K except in the boundary layer from 60°N-90°N, and 60°S-30°S where cold biases greater than -1K can be seen. For the 90°S-60°S bin, zig-zag biases can be seen that are significantly larger during the austral winter months than what could seen during the austral summer in Figure 3.2.2-9. In the 90°S-60°S bin, a significantly different bias pattern can be seen in comparing AIRS to sondes on the left panel, and AIRS to kerned sondes on the right, indicating that shortcomings in both the *a priori* and the AIRS physical retrieval contribute to large biases. Again, however, differences in biases between IR+MW and IR-only are comparatively small.

AIRS Bias Drift Calculation

To calculate and compare any temperature bias drifts in IR+MW and IR-only retrievals, sonde profiles were filtered and matched to AIRS in the same manner described above, but this time for all available matchups from the beginning of 2004 through the end of 2011. (Dates after 2003 were used to avoid any 'jumps' resulting from calibration changes after the AIRS on-orbit shutdown of October 29 to November 14, 2003.) To avoid seasonal effects skewing the result, data were binned by calendar month, with the date of each matched observation set to the year+fraction-of-year. (For example, Feb 1, 2009 at 00:00GMT would have the date 2009.084931.) Data were then binned by pressure level, and a linear least-squares fit of the bias vs. the fractional date was calculated. The slopes from each calendar month were then averaged, and this average is presented in Figure 3.2.2-10 for each latitude bin and pressure. AIRS comparisons against sondes are on the left panels, and AIRS against kerned sondes are on the right. The thin lines show the standard deviation of the monthly averaged slope on each pressure level.

Drifts tend to be less than 0.05K/yr, except in the southern mid-latitude region (which, we caution, is the least well area observed by sondes), and in the southern polar upper troposphere and stratosphere. Differences in the drifts between IR+MW and IR-only are minor.

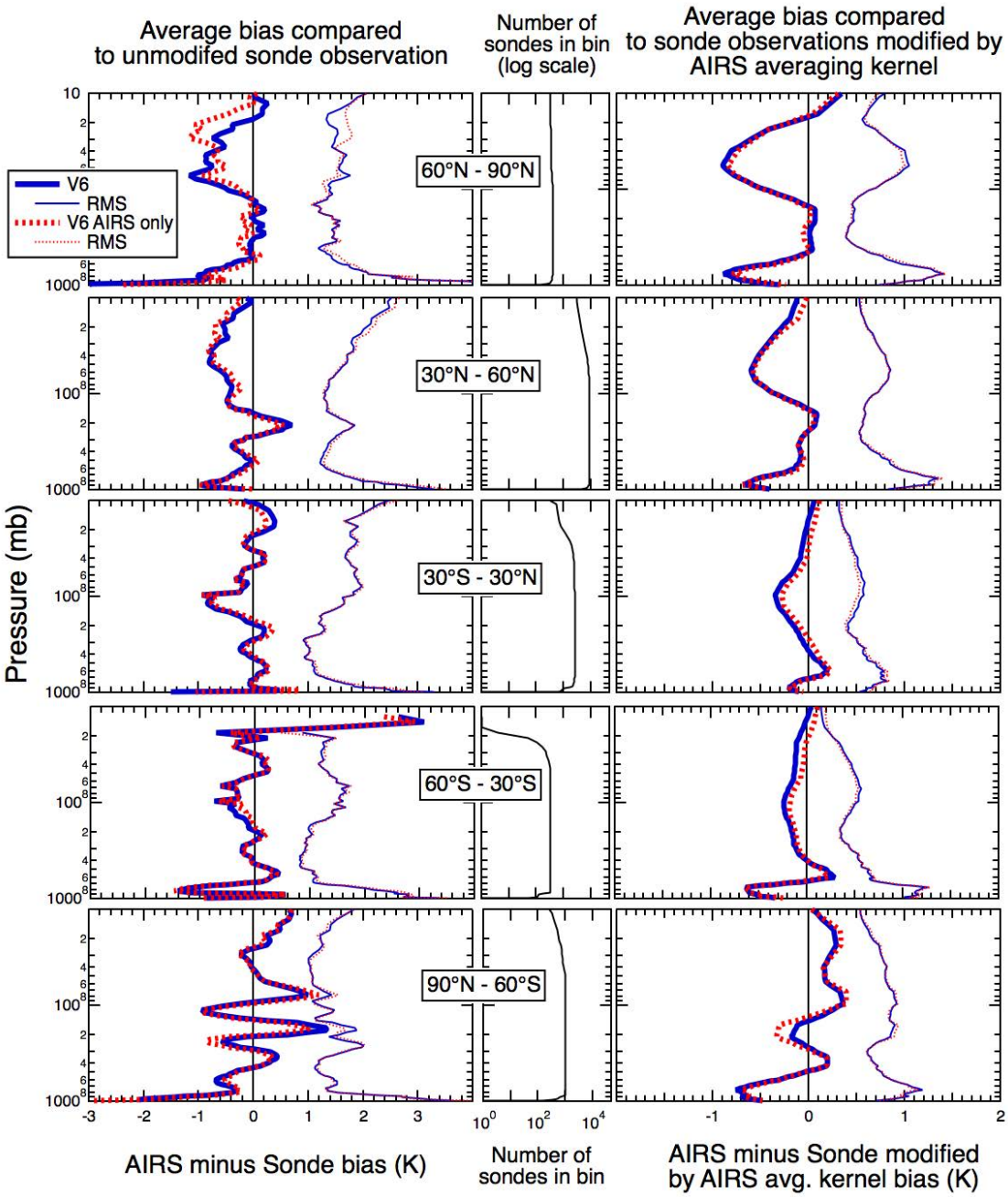

Figure 3.2.2-8. Zonally-averaged comparisons of AIRS V6 IR+MW and V6 IR-only minus radiosonde temperatures (left panels). The right panels show AIRS minus radiosonde temperatures modified by the AIRS averaging kernel as in Equation 2. Data are from December 2005 through February 2006. Note that the right panels have a shorter temperature scale than the left panels.

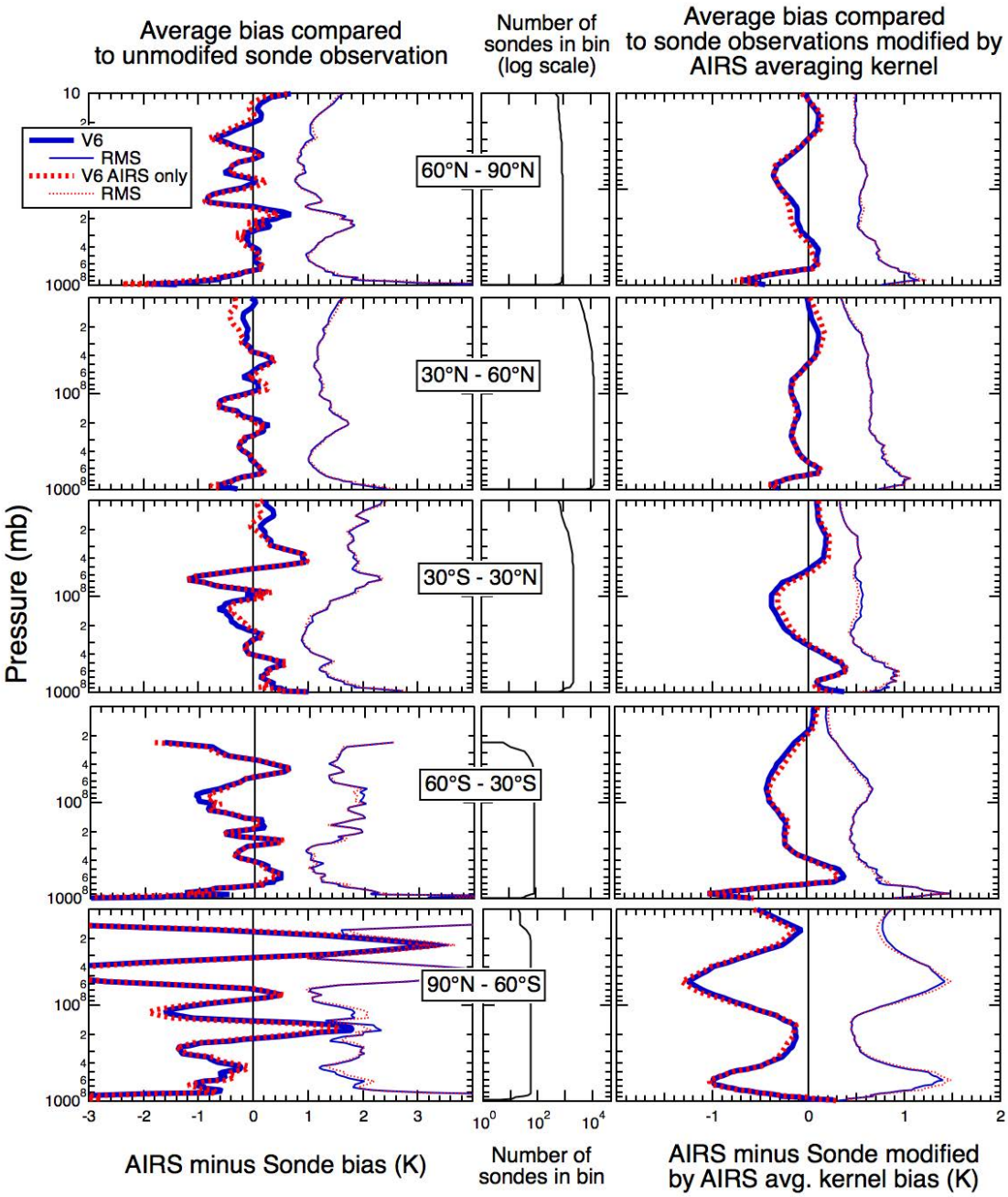

Figure 3.2.2-9. Zonally-averaged comparisons of AIRS V6 IR+MW and V6 IR-only minus radiosonde temperatures (left panels). The right panels show AIRS minus radiosonde temperatures modified by the AIRS averaging kernel as in Equation 2. Data are from June through August, 2006. Note that the right panels have a shorter temperature scale than the left panels.

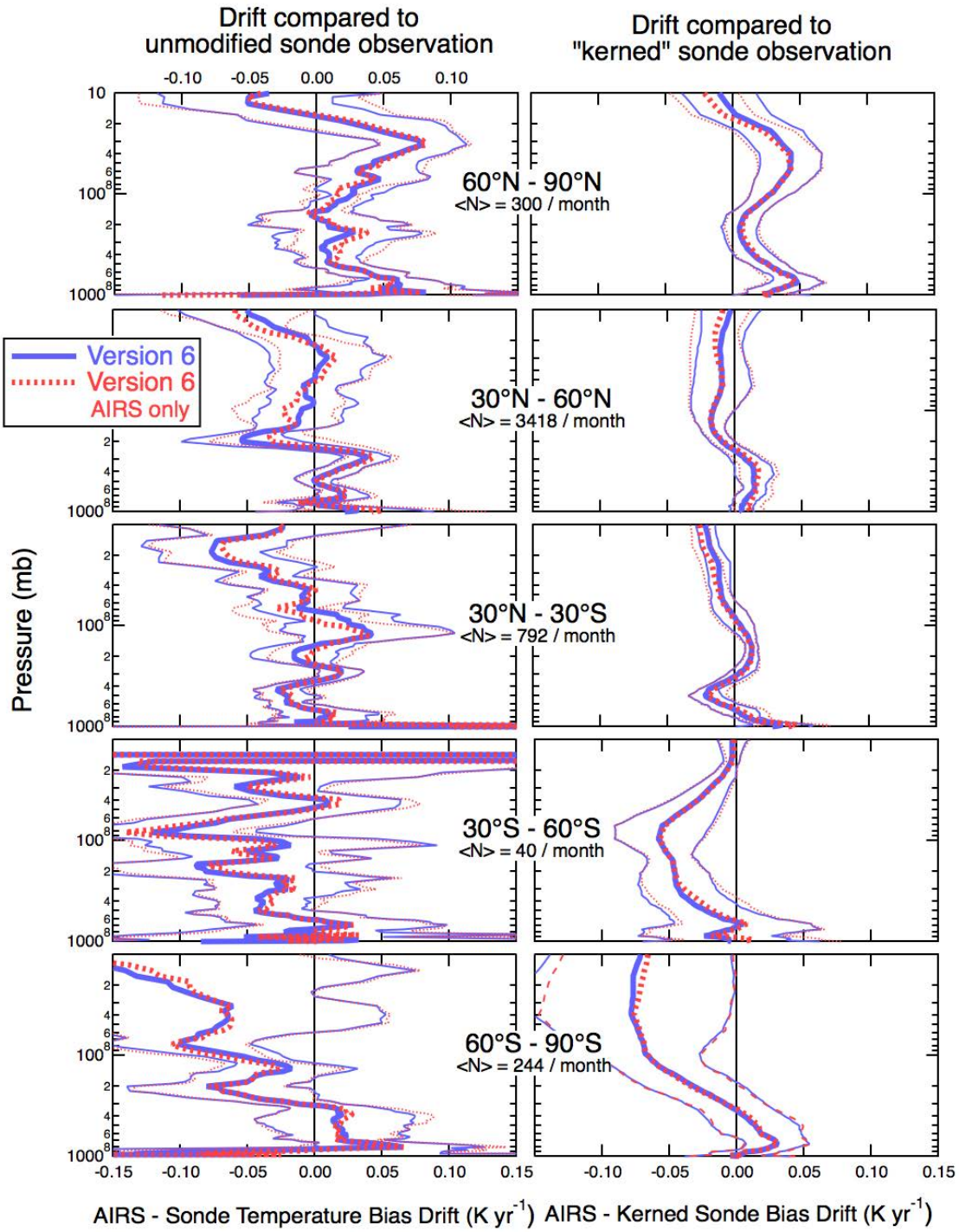

Figure 3.2.2-10. Zonally averaged temperature bias trends of AIRS V6 IR+MW and V6 IR-only minus operational radiosondes (left panels), and AIRS minus the radiosondes modified by the AIRS averaging kernels, as in Equation 2 (right panels). Trends were calculated by linear, least squares fitting though calendar month data from 2004 through 2011, with the average slope over all months shown above. The thinner lines are the standard deviation of the average slope at each pressure level.

3.2.3 Total precipitable water vapor (TPW) assessment using collocated GPS ground measurements over land.

Contributor: Qing Yue

Data and Methodology

The SuomiNet network is used in this study that provides a dense distribution of receivers/sites over the continental US (COUS) region. The SuomiNet network (Ware et al. 2000) is a university-based GPS network providing real-time TPW data for research and education since 1999, and maintained by the University Corporation for Atmospheric Research (UCAR). In this study, we use the SuimiNet data from 2006 to 2014 at 432 stations over CONUS region as shown in Figure 3.2.3-1. The retrieval of TPW from the GPS ground-based receivers has been well established and discussed in many previous studies. Using the empirical equations in Löfgren et al. (2010), a 1hPa error in surface pressure will induce an error of 0.36mm in TPW, and a 5K surface temperature error will cause a 0.13 mm TPW error (Dr. Angelyn Moore, personal communication). The error estimate reported in the SuomiNet dataset is less than 0.2 mm.

The criteria that are used to match AIRS TPW obtained at given FOV and the GPS-TPW are as follows:

1) AIRS observations within 30 min of the GPS observation time;
2) The center of AIRS FOVs within 100 km distance to the GPS station and;
3) The nearest neighbor method used, i.e. only the AIRS FOV nearest to a given GPS receiver is selected.
4) GPS reporting realistic TPW values (GPS-TPW less than 80 mm).

As a result, there are 968,000 pairs of matching observations obtained. Daytime and nighttime observations are separated by using the AIRS solar zenith angles (SZA): SZA $< 85°$ for daytime, and SZA $> 90°$ for nighttime points. The separation of day- and nighttime retrievals are necessary since AIRS L2 water vapor retrieval algorithm uses a combination of shortwave and longwave channels during daytime and longwave channels only during nighttime.

Five different AIRS TPW retrievals are included: Version 6 standard retrieval (IR+MW: V6), Version 6 AIRS only (V6_AO), Version 6 microwave only (V6_MW), Version 6 neural net (V6_NN), and Version 5 standard retrieval (V5). We investigate the measurement biases and sampling biases in the five AIRS TPW data products and their characteristics for different cloud condition, the seasonal variation, and the regional dependence.

Results and Conclusions

Figure 3.1.3 shows the retrieval yield of different AIRS TPW products and number of data points sorted by AIRS effective cloud fraction (ECF) bins and will not be repeated here. It is noteworthy that both V6 IR+MW and IR have much higher retrieval yields than V5, indicating improvement comparing with the previous version. Also shown are the sampling biases of different AIRS TPW data products. The sampling biases are calculated as the differences between the collocated GPS measurements

subsampled by AIRS QC flags and the collocated GPS data without the subsampling. Largest sampling biases are seen in the V6+MW data caused by very low (10%) yield over the land surface in the microwave retrieval. The V6 IR+MW and IR retrievals have the same magnitude of sampling bias (less than 0.5mm) except at ECF > 70% with IR values slightly larger than IR+MW. This is consistent with the reduced yield in IR at large ECF conditions.

Figure 3.2.3-2 shows the mean biases, the root-mean-square differences (RMS), and the correlation coefficients between the AIRS retrieved TPWs and collocated GPS measurements as a function of AIRS ECF values. The mean biases and rms are shown as the percentage of the GPS values. Although the yield is low, microwave retrieved TPW presents the smallest biases and highest correlation with collocated GPS data. The NN TPW shows slight dependence on cloud. The difference between IR+MW and IR in the V6 data is very small for all ECF values, and both V6 data products show significant improvement compared with V5. The bias and RMSE during daytime are larger than nighttime for both V6 IR+MW and IR AIRS retrievals, which is due to larger uncertainties in the radiative transfer with shortwave channels included in the daytime.

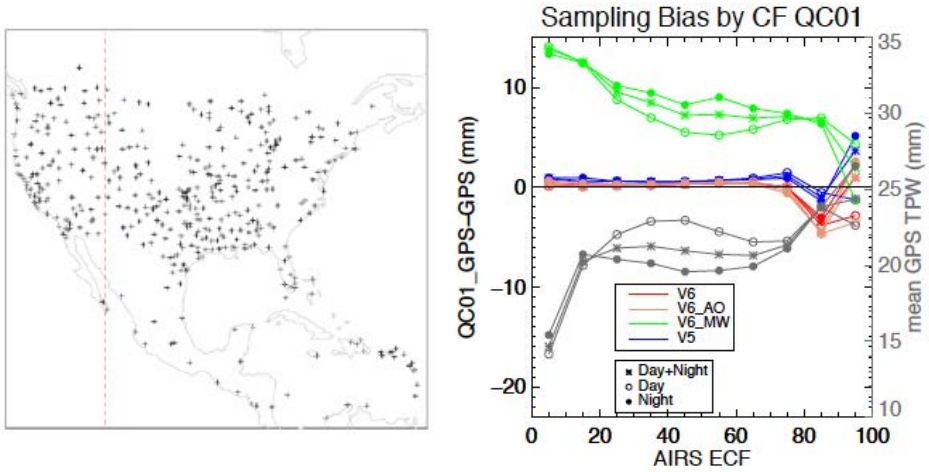

Figure 3.2.3-1. Left panel shows the location of 432 SuomiNet GPS stations located in the COUS used in the calculation. Right panel shows the sampling bias of AIRS retrieved TPW as a function of AIRS ECF overlayed with the mean TPW calculated from GPS measurements. Day, night, and combined day/night results are shown with different symbols. Different colors indicate different AIRS retrievals: blue for V5, red for V6 IR+MW, pink for V6 AIRS IR only, black for V6 IR+MW neural network used as initial guess in the IR+MW retrieval, and green for V6 MW-only retrieval.

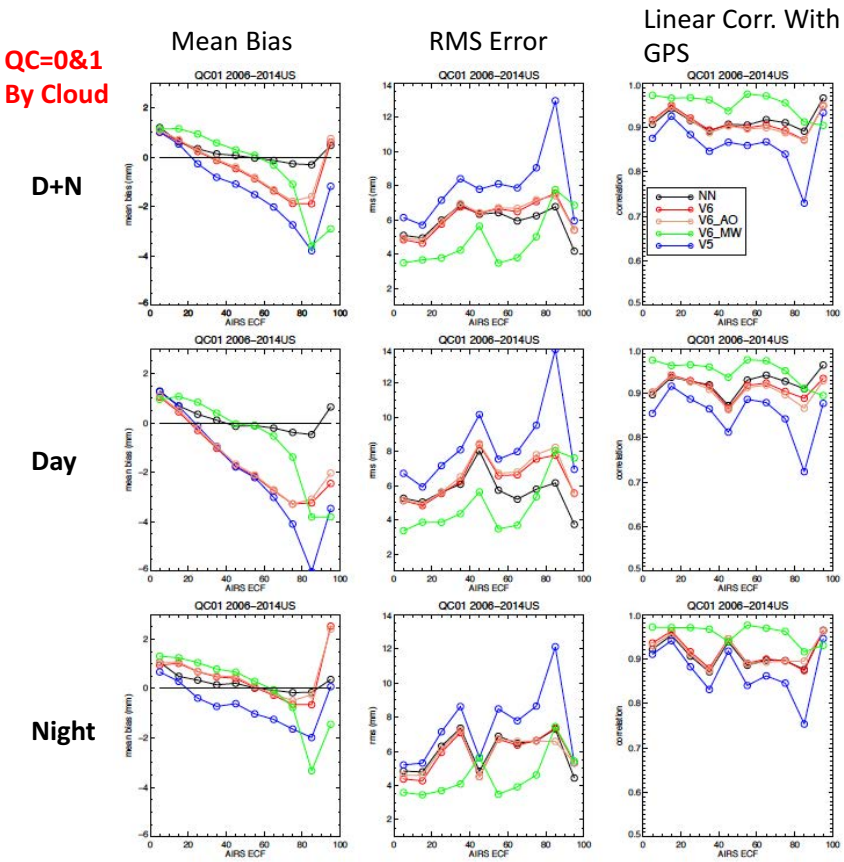

Figure 3.2.3-2. The mean bias, RMSE, and linear correlation with the collocated GPS measurements by effective cloud fraction (ECF) from AIRS. Different colors indicate different AIRS retrievals: blue for V5, red for V6 IR+MW, pink for V6 AIRS IR only, black for V6 IR+MW neural network used as initial guess in the IR+MW retrieval, and green for V6 MW-only retrieval.

3.2.4 The changes in the cloud properties and associated temperature and water vapor.

Contributor: Brian Kahn and Qing Yue

Data

The AIRS Standard Level 2 two-layer effective cloud fraction (ECF) and cloud top temperature (Tcld) and the Support Level 2 single layer ice cloud top temperature (Tcld,ice), optical thickness (tau) and effective diameter (De) is shown for granule #044 on September 6th, 2002. Temperature and water vapor retrievals at different levels for this granule are also shown. An entire day of granule maps was investigated (09-06-2002) with a wide variety of variations between AIRS/AMSU (IR+MW) and AIRS (IR) depending on the region, cloud regimes observed, land versus ocean, the presence of land or ocean ice, etc. We selected granule #044 for the test report as it shows a wide variety of the retrieval variations but it is located in the northern hemisphere subtropics, thus it does not contain some of the ice surface issues at the heart of the IR+MW and IR differences.

Methodology

All of the Tcld,ice, tau, and De parameters that meet the QC defined in Kahn et al. (2014) are kept in the analysis. In the case of ECF and Tcld, there is no QC applied so that we can understand some of the biggest changes in retrieval failures as well as outside of these areas. QC is applied when granule maps of T, q, and RH are shown. The same exact granule is shown and described in Kahn et al. (2014) for reference.

Discussion, Results, and Conclusions

Figure 3.2.4-1 shows results for the upper and lower layers of TCld and ECF (upper row), and the differences between IR+MW and IR (lower row). The bottom line is that there are very large changes in the TCld and ECF at the AIRS footprint and AMSU field of regard (~45km) that are consistent with the changes in cloud vertical structure determined by IR+MW and IR (see Figure 3.2.4-2), but less obvious are larger-scale systematic variations. The upper layer ECF in the northwest portion of the granule (low clouds behind a weak cold front) show some of the largest variations between the two retrievals. The way that the two retrievals obtain low clouds appears to be quite a bit different. The monthly map differences (Sec. 3.3.6) suggest that the IR retrieval shows some significant degradation in TCld and ECF for low clouds.

Figure 3.2.4-2 shows results for the ice cloud top temperature, optical thickness, and effective diameter, and also the differences between clear sky, single-layer, and two-layer cloud changes between IR+MW and IR. About 75% of AIRS FOVs remain the same between AIRS-MW and AIRS-IR; in other words, clear sky remains clear, single layer clouds remains single layer, and two-layer remain two layer. About 25% of AIRS FOVs show some changes from clear sky to cloudy (or vice versa), or flip between one or two layers. A slightly larger number of clouds appear to gain a second layer than those that

lose their second layer. The ice cloud optical thickness shows some significant pixel-scale variations that can either increase or decrease the value of optical thickness. This is especially true within deep convective clouds (see the tropical cyclone in the western part of the granule) compared to frontal regions (the upper portion of the granule). The ice cloud top temperature shows smaller differences compared to the standard Level 2 upper TCld field. In the case of ice cloud effective diameter, there are some spotty changes that increase or decrease the magnitude, but overall the changes are not large. This is not the case in some high latitude regions that are tied to surface skin temperature and emissivity changes.

Figure 3.2.4-3 shows the map of PGood for this granule. Given the various changes of cloud properties, the PGood values show very small change going from IR+MW to IR except some very localized variations. Figs 3.2.4-4, -5, -6 show the map of differences between IR+MW and IR at different levels for temperature, water vapor mixing ratio, and relative humidity from L2 support products. The AIRS team is still investigating the relationships of these changes to the changes on CC-Rad, cloud, and retrieval priori from neural network from IR+MW to IR. However, the changes from large differences without QC and much smaller differences with the correct QC are evident, indicating that although averaging over large number of cases shows very small differences between the IR+MW and IR retrievals of temperature and water vapor (Sec. 3.2.2), users should apply the correct QC to different products to ensure the quality of the data. Above 700 hPa, it seems the IR+MW shows generally colder T for this granule. For water vapor, drier 250 hPa is obtained in IR+MW than IR, however, at other levels, IR+MW retrievals seem to produce localized higher water vapor values than IR.

Further research is warranted to determine the cause of these differences, which could be some combination of yield, sampling in different cloud states, or changes in retrieval noise/RMSE. We have also quantified differences in the cloud thermodynamic phase algorithm in addition to these cloud properties. We decided not to show these results as they tend to be much smaller since the only way that they can change is through changes in ECF.

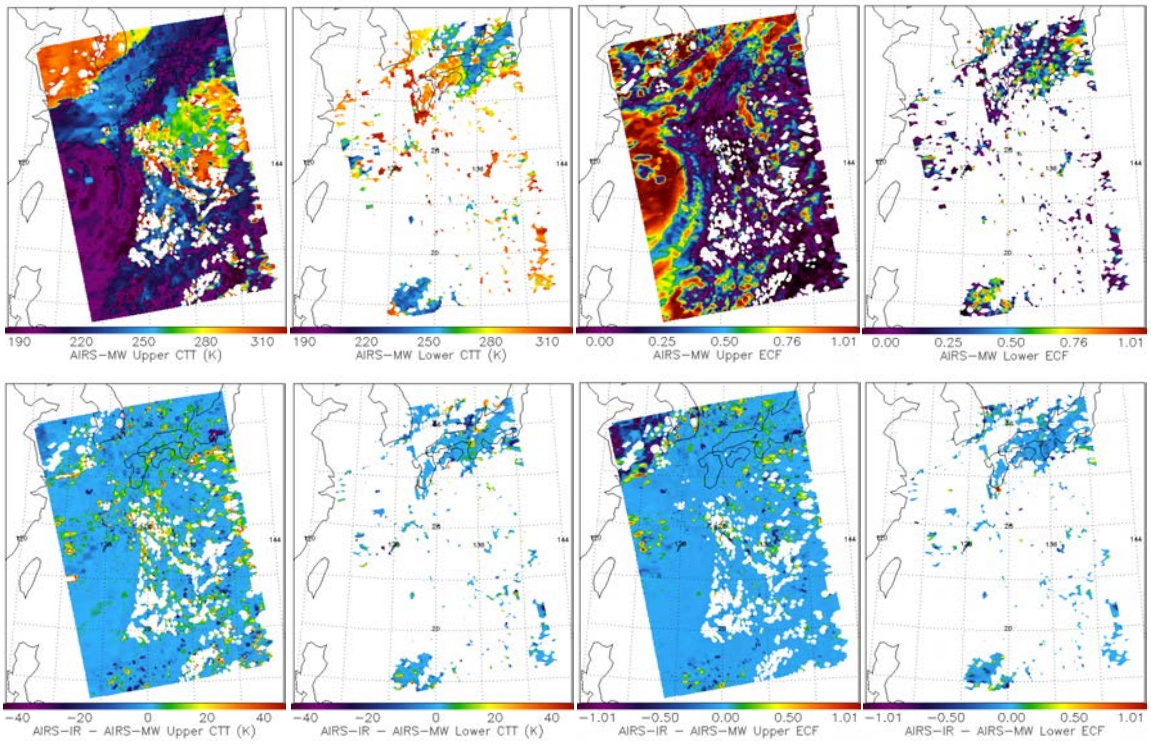

Figure 3.2.4-1. Left: AIRS-MW upper layer TCld for January 2009. Right: AIRS-IR minus AIRS-MW upper layer TCld for same time period.

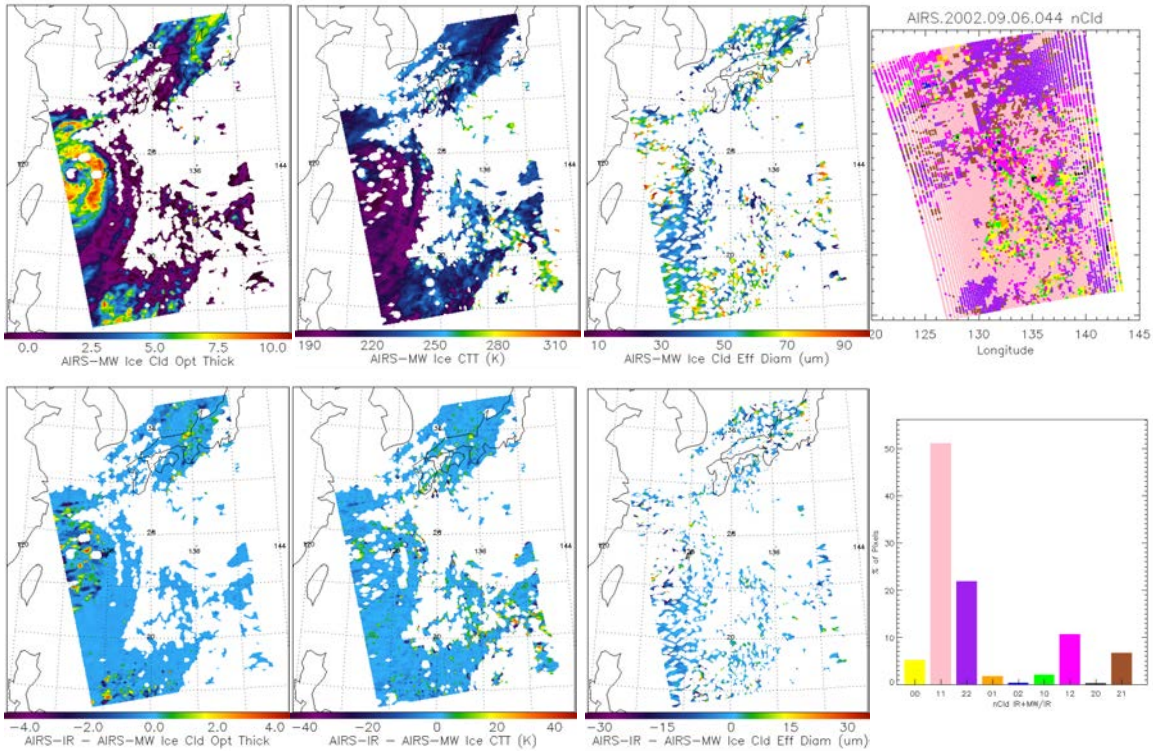

Figure 3.2.4-2. Top panels from left to right: IR+MW ice cloud optical thickness, IR+MW ice cloud top temperature, IR+MW ice cloud particle effective diameter, the spatial distribution of nCld (number of cloud layers) in the L2 product, for which the colors correspond with those used in the bar plot below. The labels of the bars are a series of two-digit numbers: the first digit is the nCld from IR+MW product, and the second digit is the nCld from IR product. The three bottom panels on the left show the differences between IR and IR+MW for ice cloud optical depth, cloud top temperature, and particle effective diameter for Granule 044 on Sep. 06, 2002.

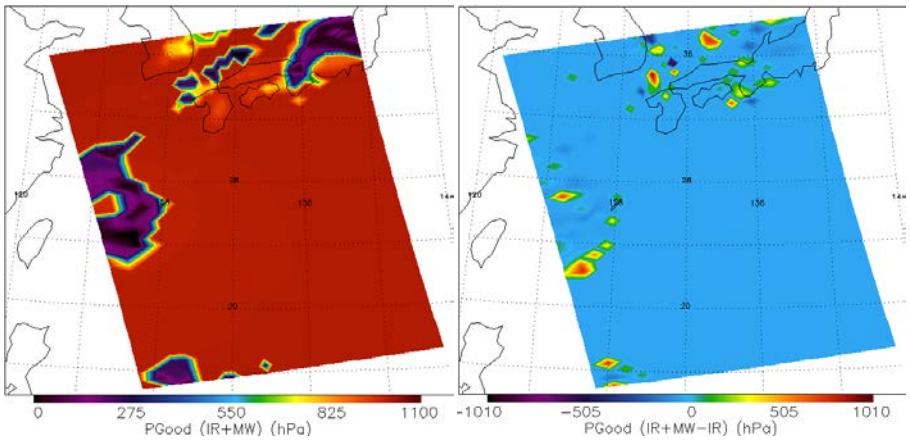

Figure 3.2.4-3. The value of PGood for Granule. 2002.09.06.044 from IR+MW (left) and its difference with the value from the IR retrieval (right).

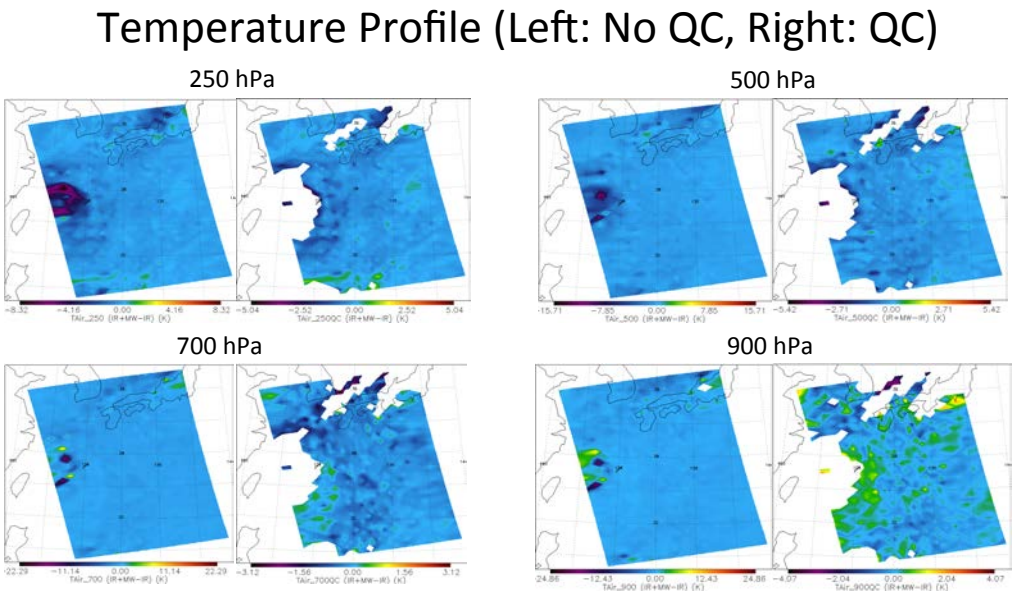

Figure 3.2.4-4. The differences in temperature between IR+MW and IR for granule 044 on 2002.09.06. Four different levels are shown: 250, 500, 700, and 900 hPa. At each level, the map on the left shows the difference without any QC, and the map on the right shows difference after applying individual QCs in IR+MW and IR retrievals to different data products respectively.

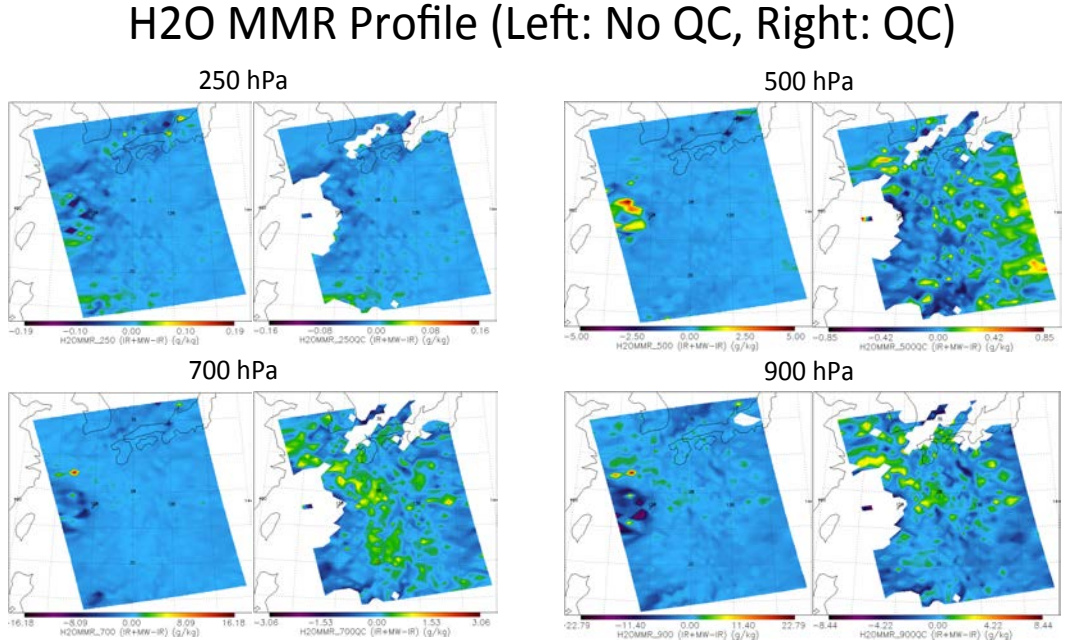

Figure 3.2.4-5. Same as Figure 3.2.4-4 but for water vapor mixing ratio.

RH (Left: No QC, Right: QC)

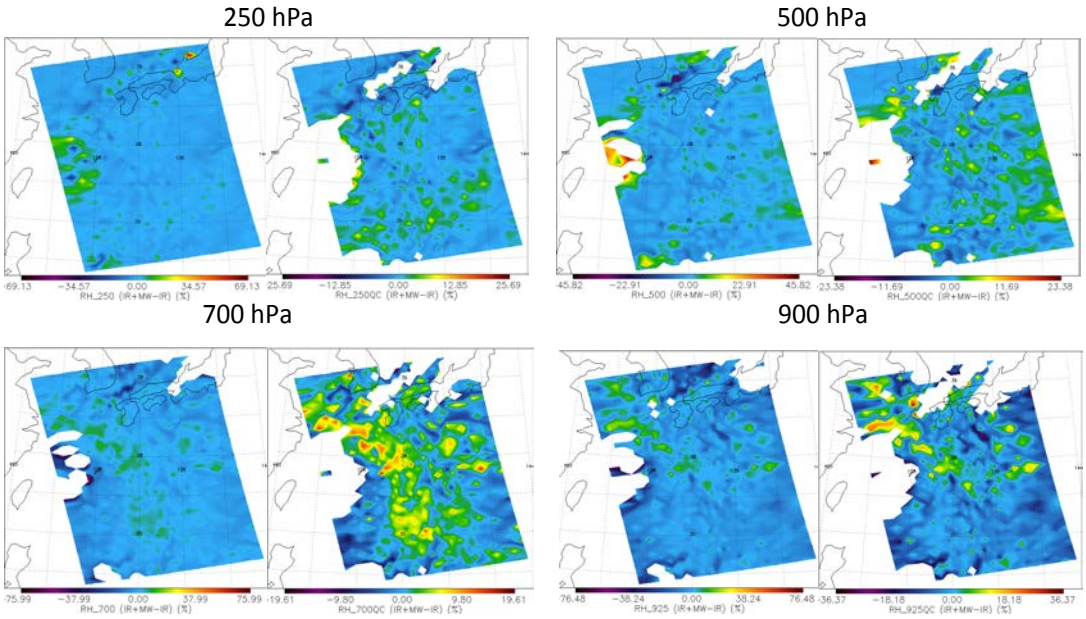

Figure 3.2.4-6. Same as Figure 3.2.4-4 but for relative humidity.

3.2.5 The near surface temperature and water vapor as compared with buoy and Mesonet observations

Contributor: Luke Chen and Van Dang

Data

AIRS/AMSU (IR+MW) and AIRS (IR) L2 near surface air temperature (TSurfAir) and water vapor data (H2OMMRSurf) are compared with collocated buoy observations for the ocean for Feb 2004, Feb 2010, Aug 2010, Feb 2011, and Mesonet observations for land surfaces for Feb 2004, Feb 2010, Aug 2010, and Aug 2013. We will refer to these comparisons as NSAT and NSWV in this report. Figure 3.2.5-1 and Figure 3.2.5-2 show the location of the buoys and Mesonet sites, respectively.

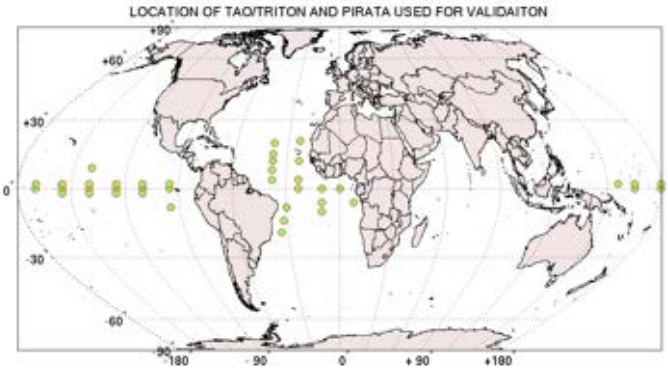

Figure 3.2.5-1. Location of the buoys used in this calculation, most of which are over the tropical ocean.

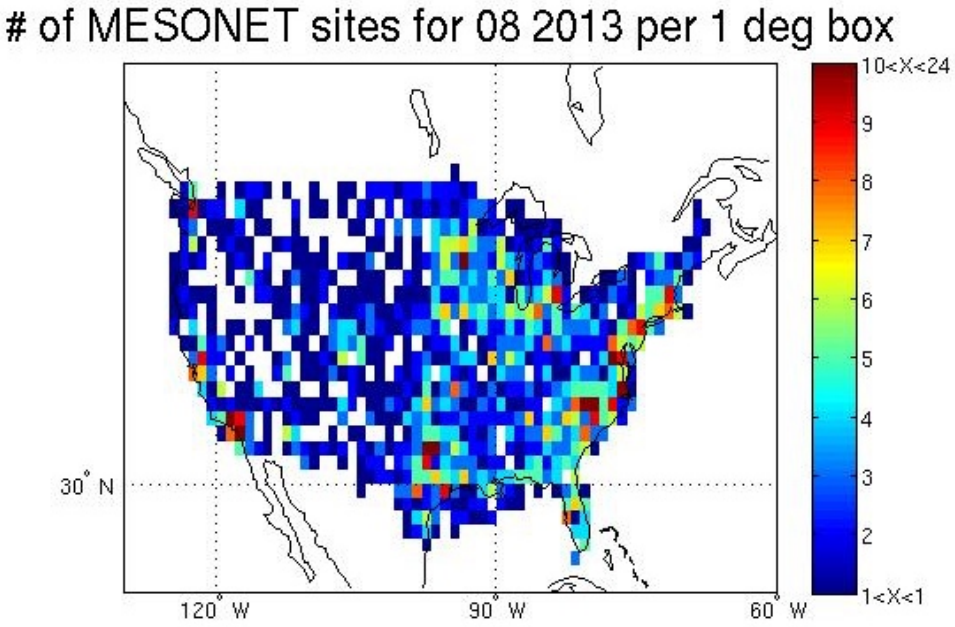

Figure 3.2.5-2. Distribution of the Mesonet sites used for land comparison over the ConUS

Methodology

TSurfAir_QC=(0,1), H2OMMRSurf_QC =(0,1), PSURF_CLR = PGOOD are used for quality checks. The buoy and Mesonet data are matched with AIRS retrievals to within 50 km. Correlation, averaged and rms difference between "truth" and AIRS data are calculated as a function of Effective Cloud Fractions(ECF).

Conclusions

1. *Buoy and AIRS Comparison*

Since AMSU channels 1 and 2 are sensitive to the total precipitable water in the atmosphere, the effect of losing AMSU channels can be readily seen in the plots in the right column of Fig. 3.2.5-3. which compares near surface water vapor between V6 data and collocated buoy measurements. The drop in correlation, increasing in the mean bias and the RMS difference between AIRS and Buoy data indicates lower information content in the boundary layer water vapor without the MW channels. In addition, MW channels are known for its ability to penetrate clouds and therefore contributing to the cloud clearing process. The graphs in the left column of Fig.3.2.5-3, which compare the near surface temperature, do not show significant differences between with and without AMSU channels.

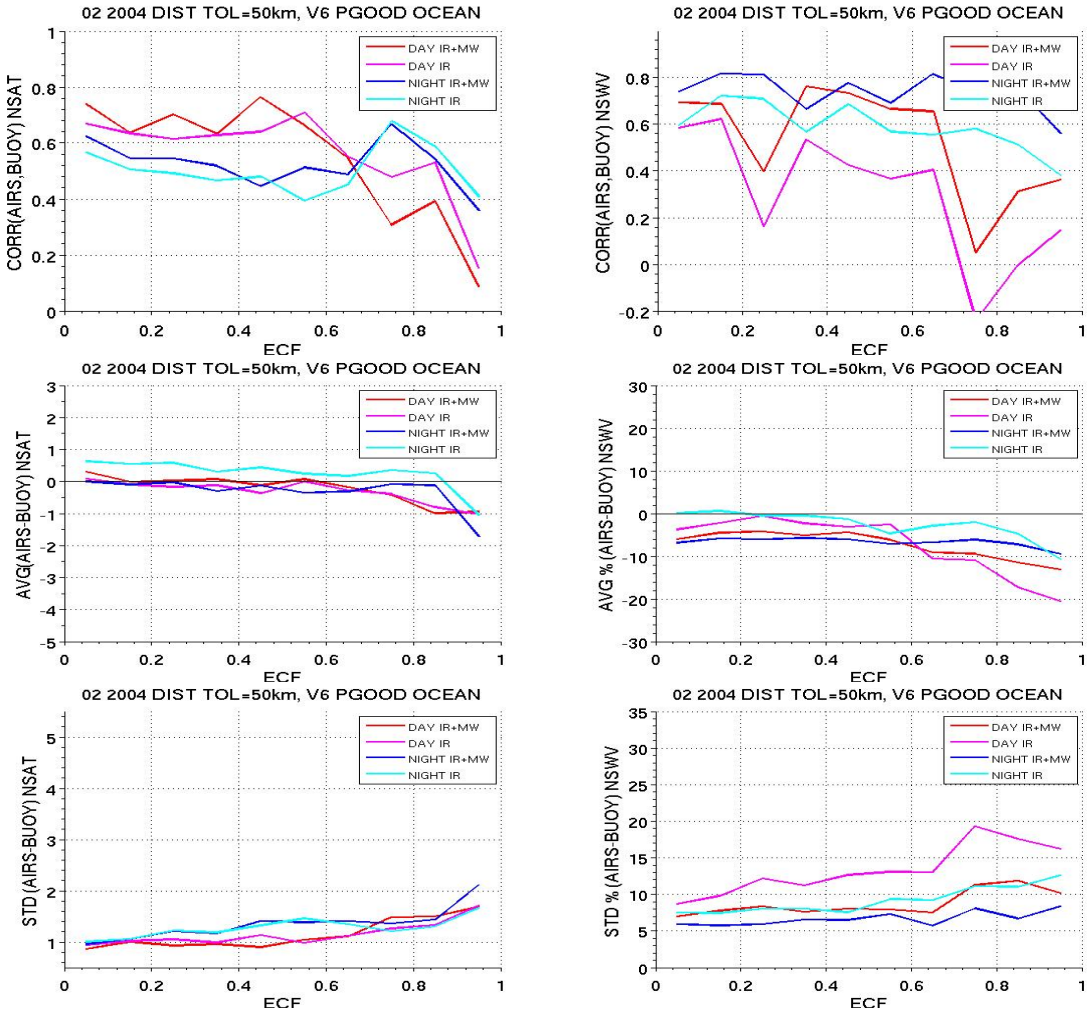

Figure 3.2.5-3. The correlation (top), mean bias (middle), and RMS (bottom) of the NSAT (left) and NSWV (right) of the comparison between V6 AIRS data products and collocated buoy observations. Both IR+MW and IR data are shown and results are separated by day and night for Feb 2004.

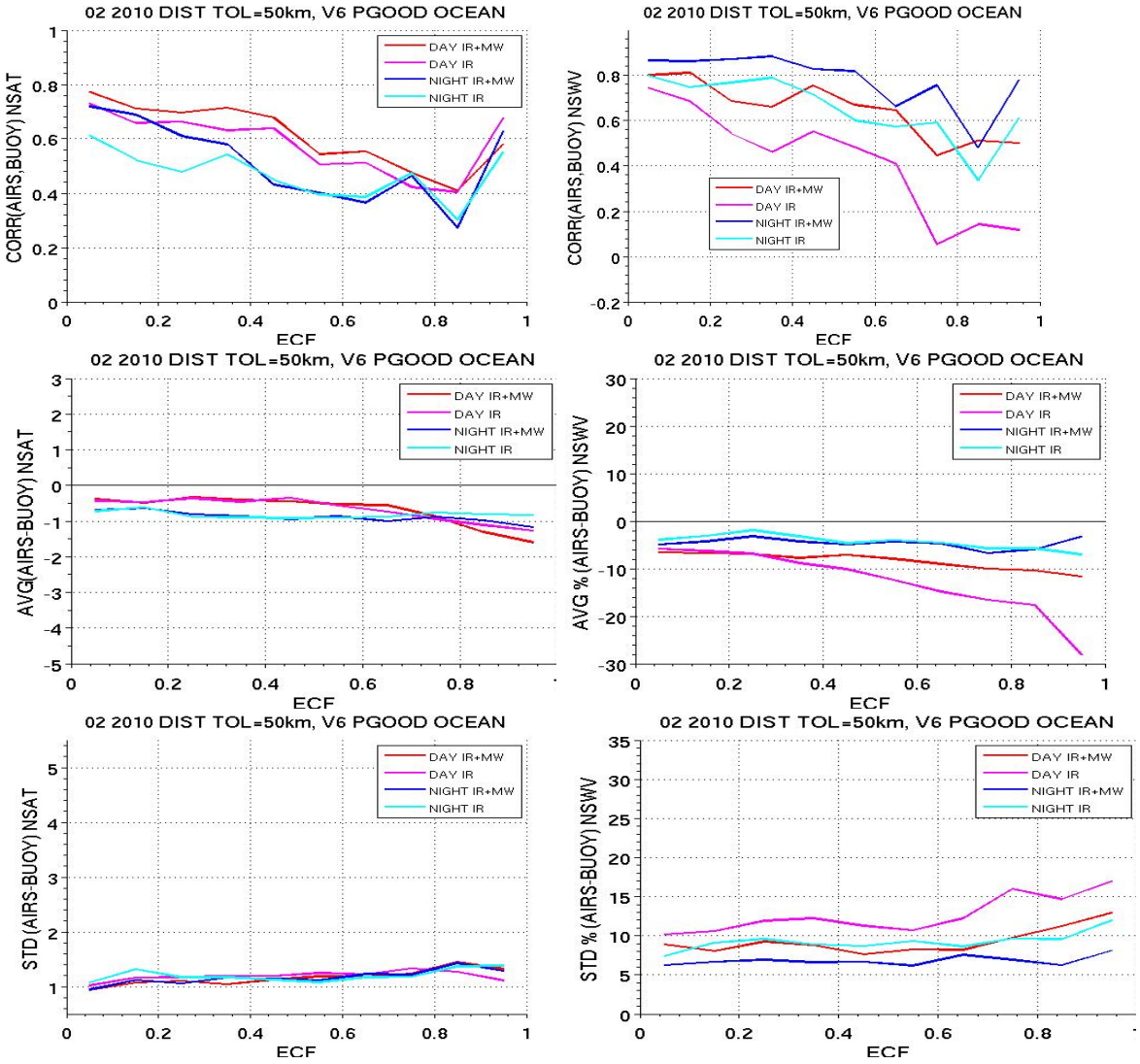

Figure 3.2.5-4. Similar to Figure 3.2.5-3, but for Feb 2010.

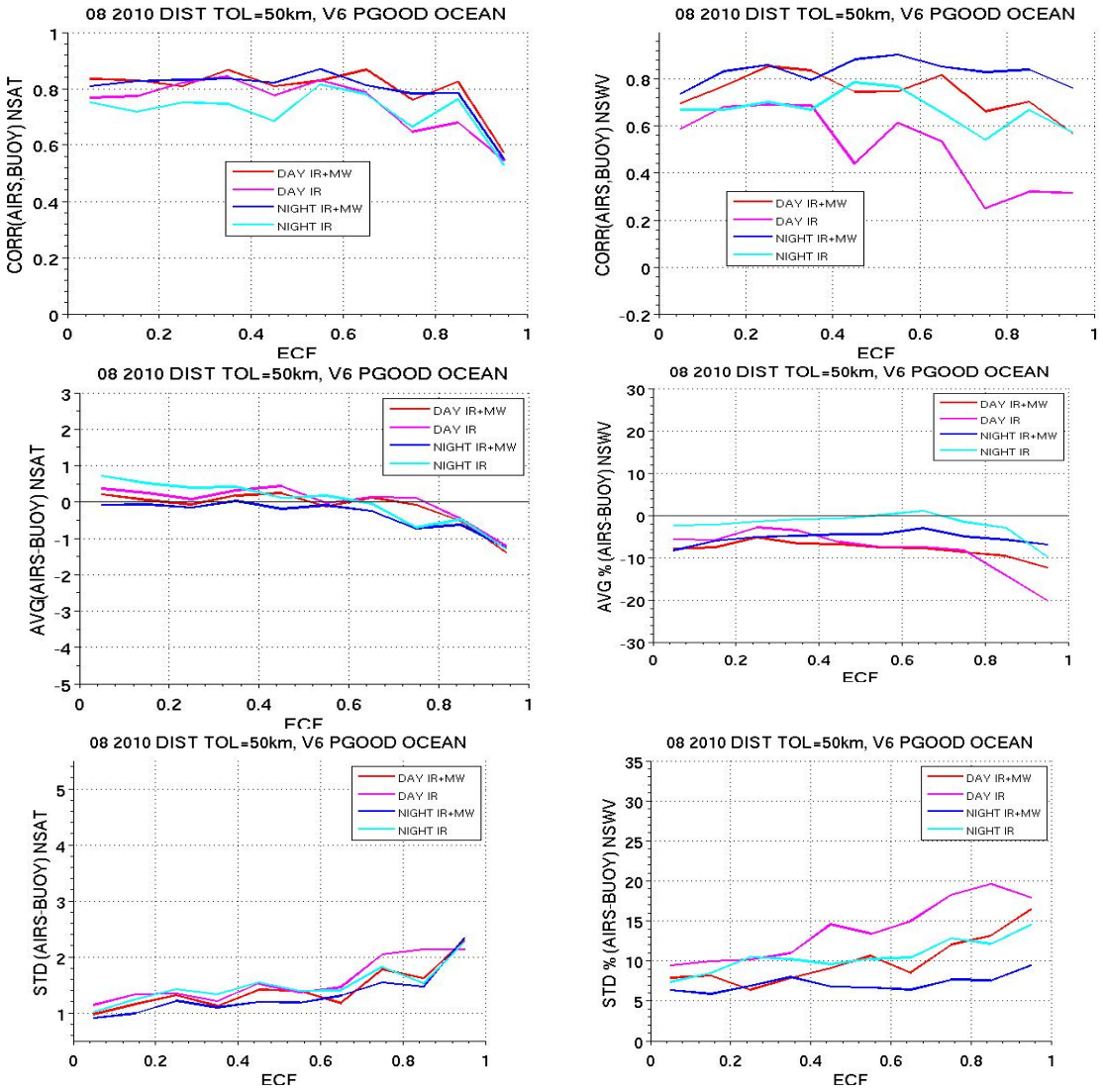

Figure 3.2.5-5. Similar to Figure 3.2.5-3, but for Aug 2010.

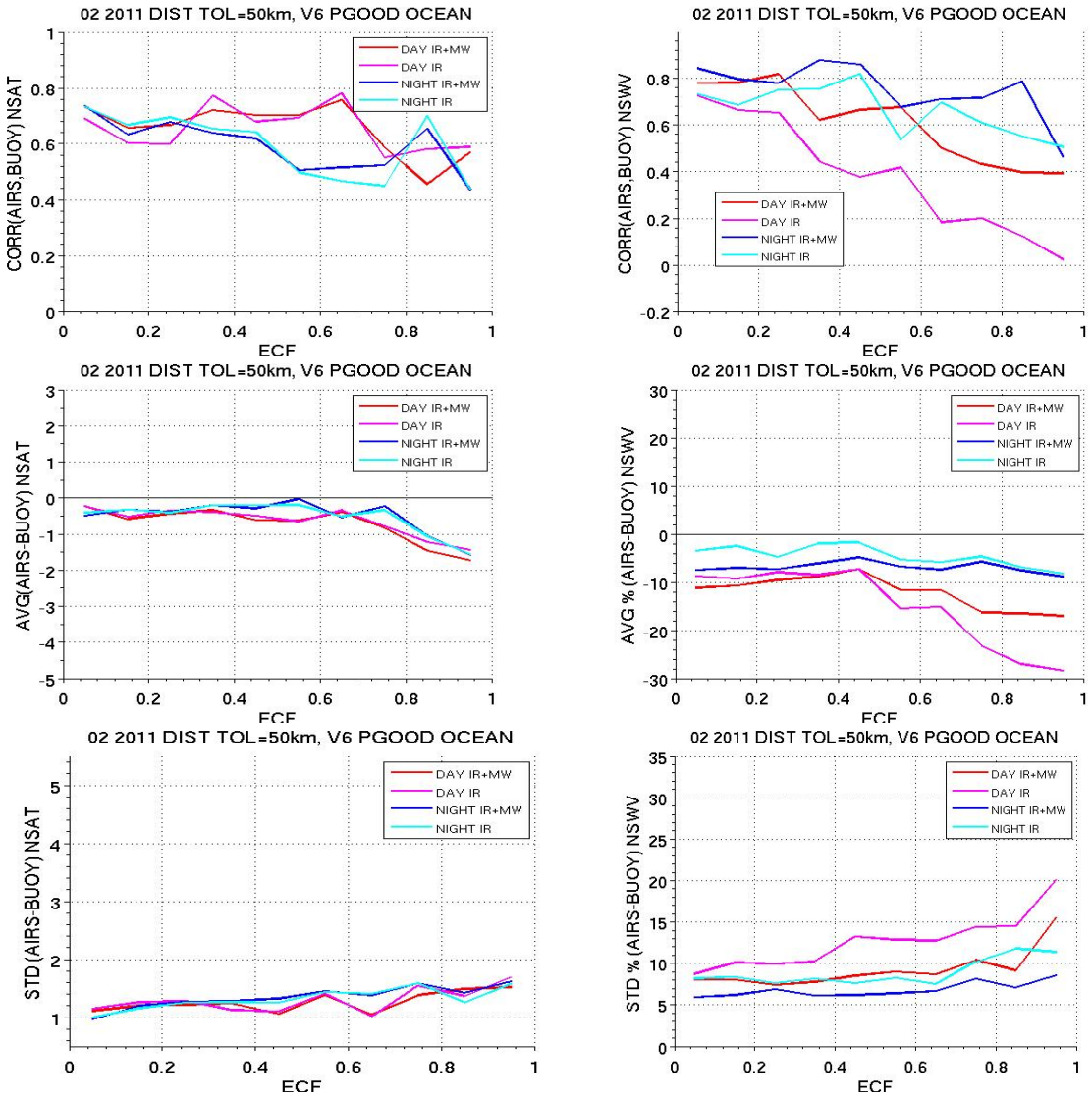

Figure 3.2.5-6. Similar to Figure 3.2.5-3, but for Feb 2011

2. Mesonet and AIRS Comparison

The differences in the near surface parameters retrieved by IR+MW and IR are much smaller over land than over ocean presumably due to the fact that there are much less near surface water vapor over land (see Figure 3.2.5-7 and Figure 3.2.5-8). Without MW channels, the correlation between Mesonet and AIRS decreases slightly for both NSAT and NSWV, the magnitude of RMS and mean bias decreases slightly in IR

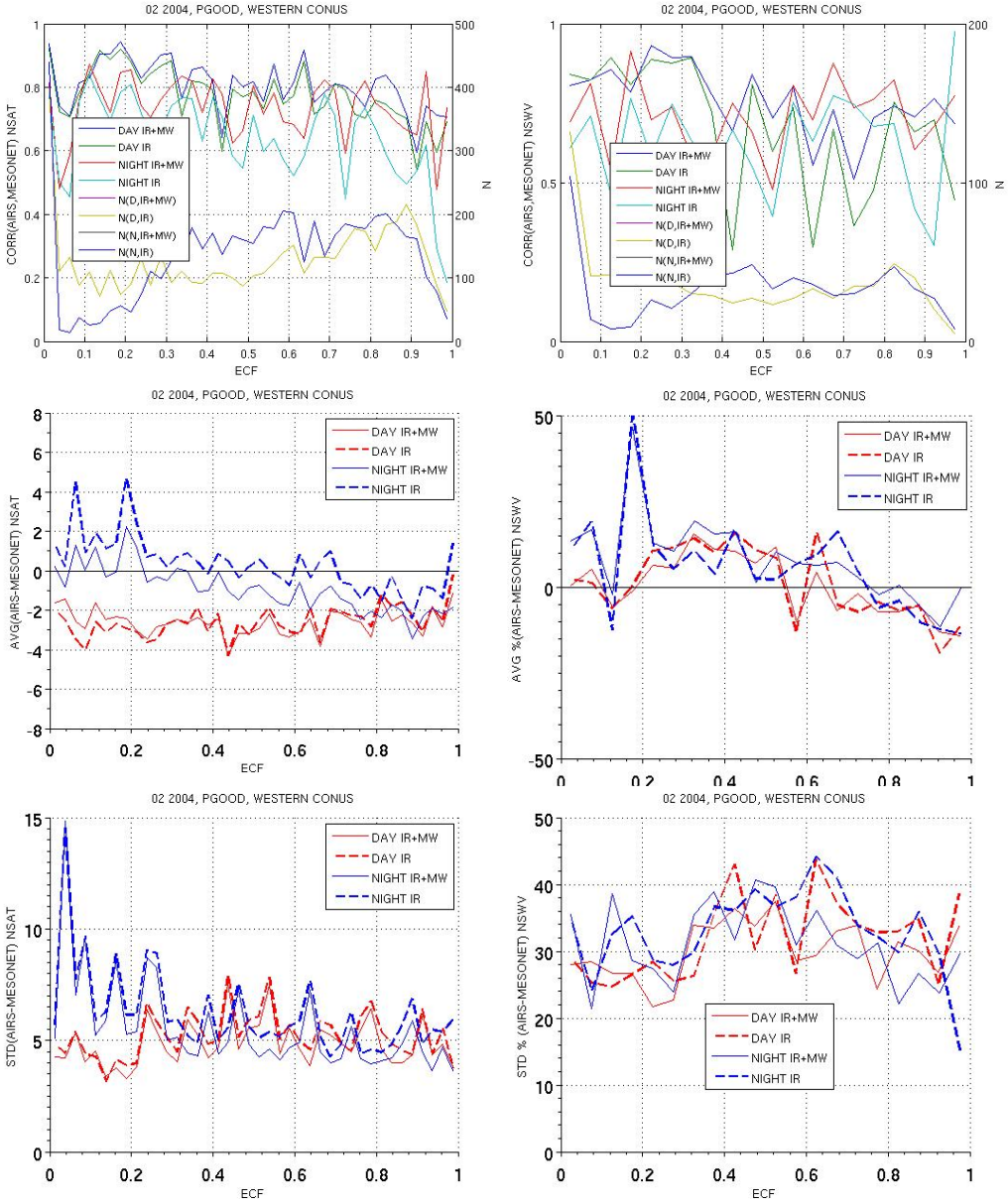

Figure 3.2.5-7. The correlation (left axis) and the count (right axis), (top row), mean bias (middle), and RMS (bottom) of the NSAT (left) and NSWV (right) of the comparison between V6 AIRS data products and collocated Mesonet observations. Both IR+MW and IR data are shown and results are separated by day and night for Western CONUS Feb 2004.

compared with IR+MW. Unlike the comparison with the buoy data, difference

between AIRS and Mesonet data do not show an increase trend with ECF. Note that the range of rms NSAT difference over land during the day is 3-5K, much wider than over the ocean, which is 1-1.5K. The large spikes of nearly 15K rms differences in NSAT are likely caused by clouds as there are disproportionately large numbers of matchups that are identified as "clear" as compared to partially cloudy FOVs.

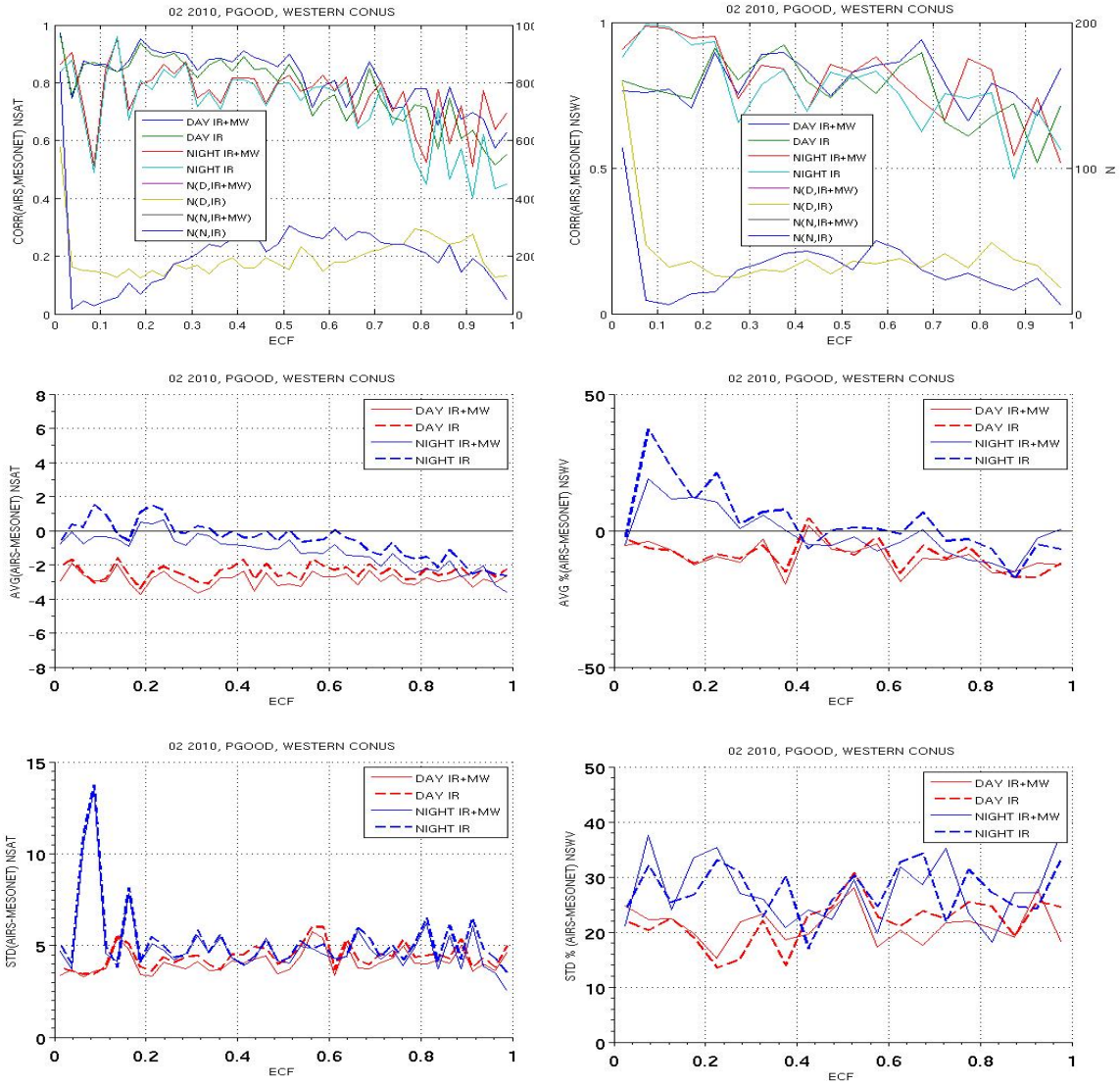

Figure 3.2.5-8. Similar to Figure 3.2.5-7, but for Feb 2010

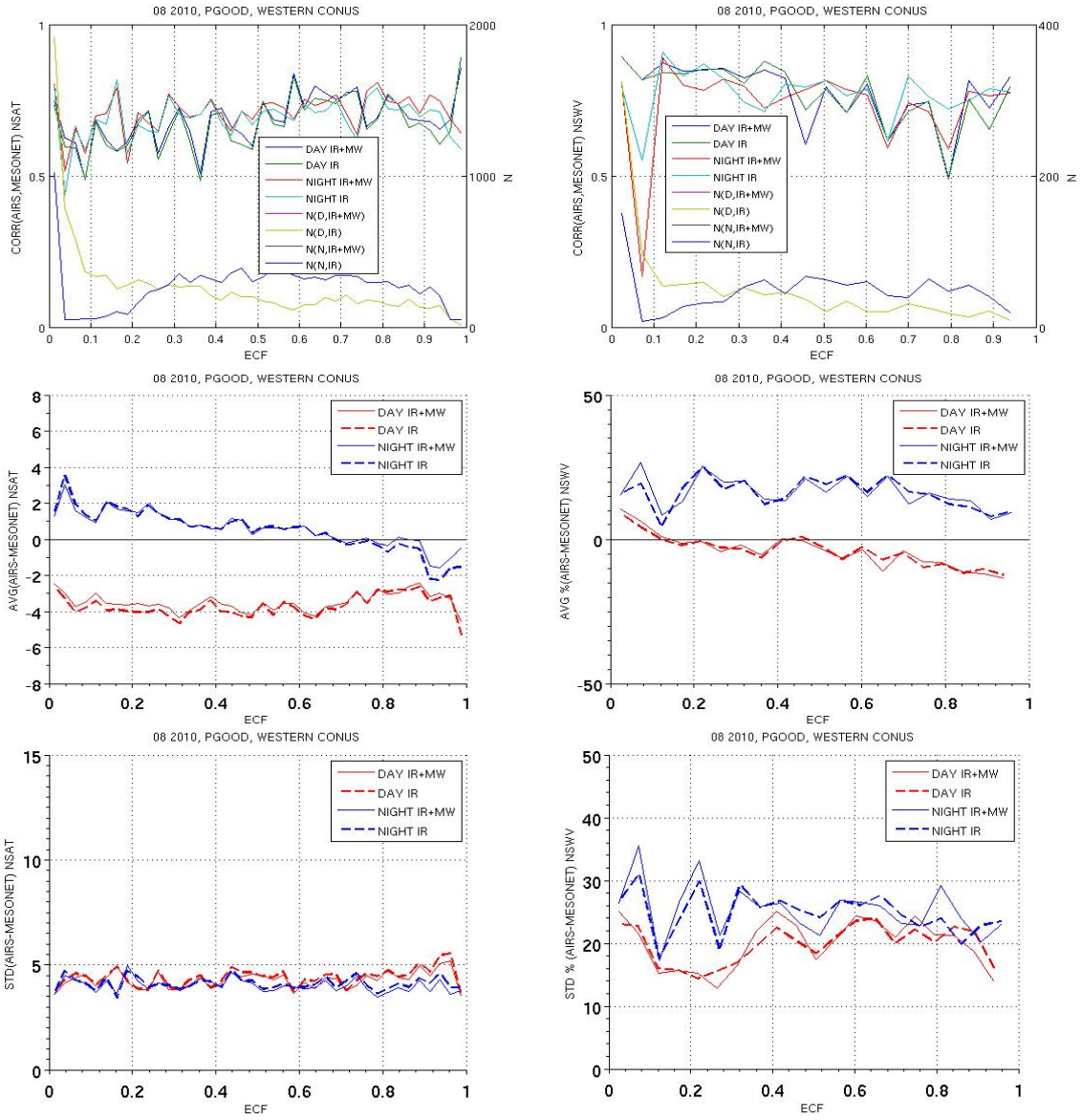

Figure 3.2.5-9. Similar to Figure 3.2.5-7, but for Aug 2010

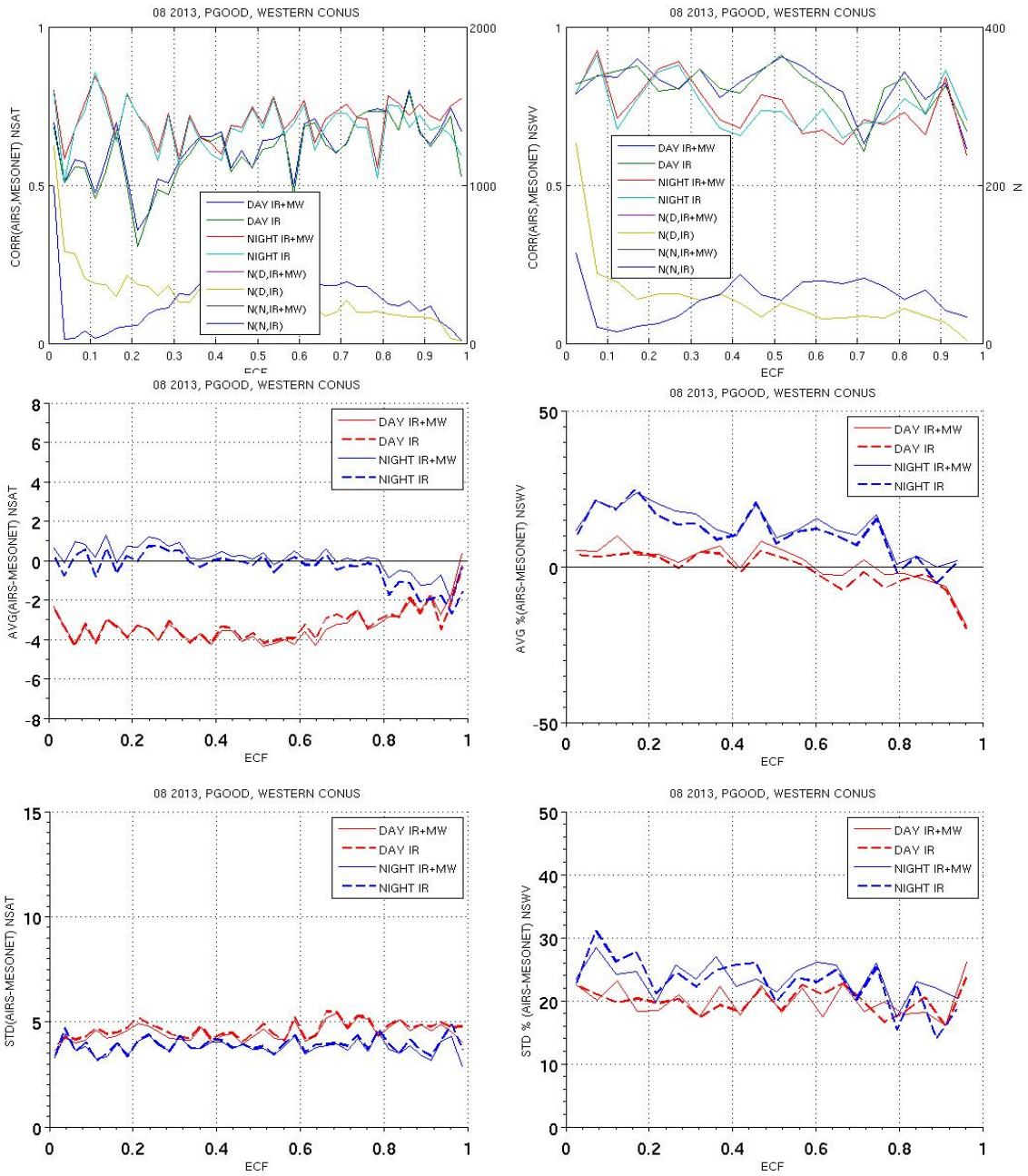

Figure 3.2.5-10. Similar to Figure 3.2.5-7, but for Aug 2013

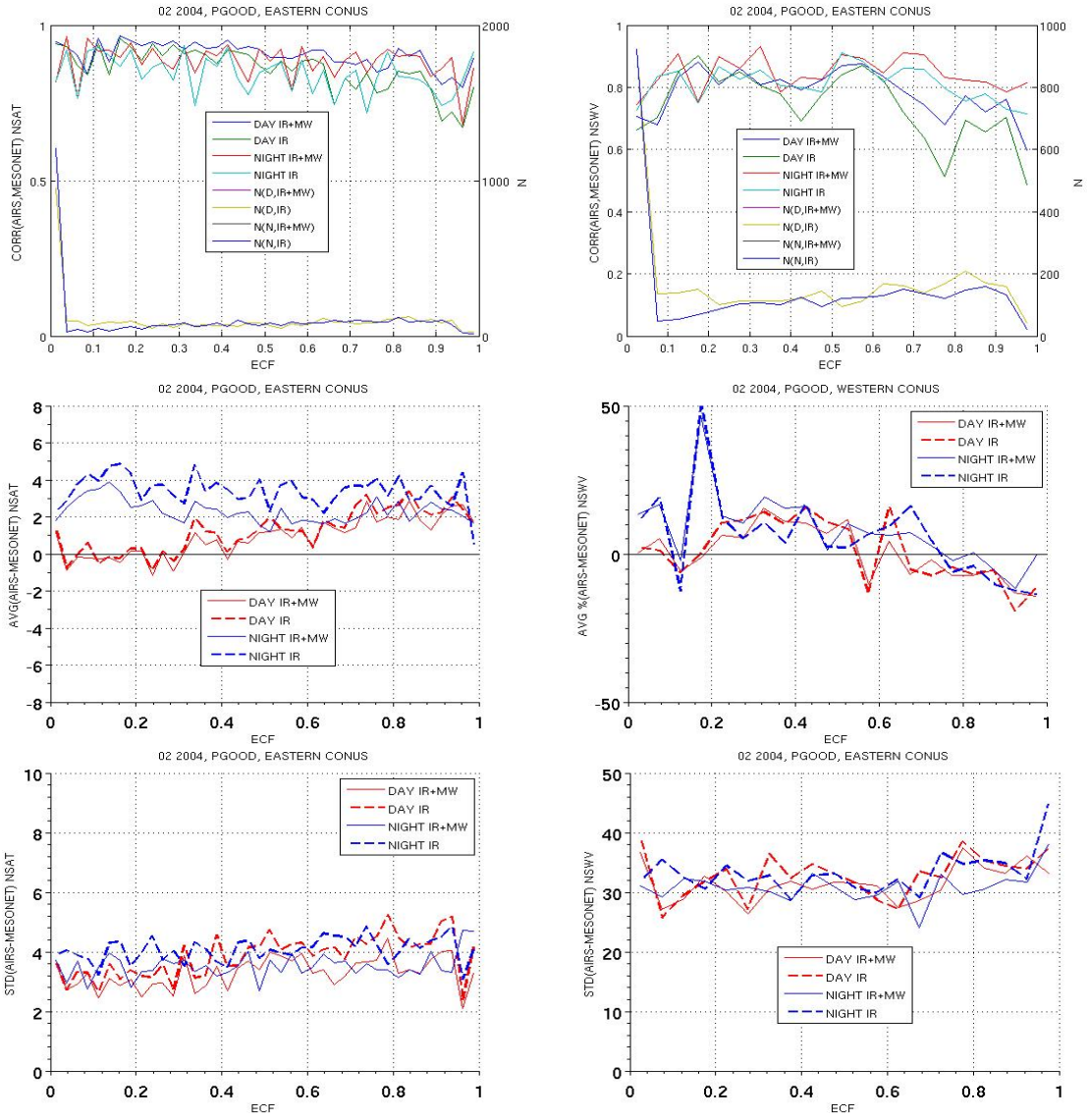

Figure 3.2.5-11. The correlation (left axis) and the count (right axis), (top row), mean bias (middle), and RMS (bottom) of the NSAT (left) and NSWV (right) of the comparison between V6 AIRS data products and collocated Mesonet observations. Both IR+MW and IR data are shown and results are separated by day and night for Eastern CONUS Feb 2004.

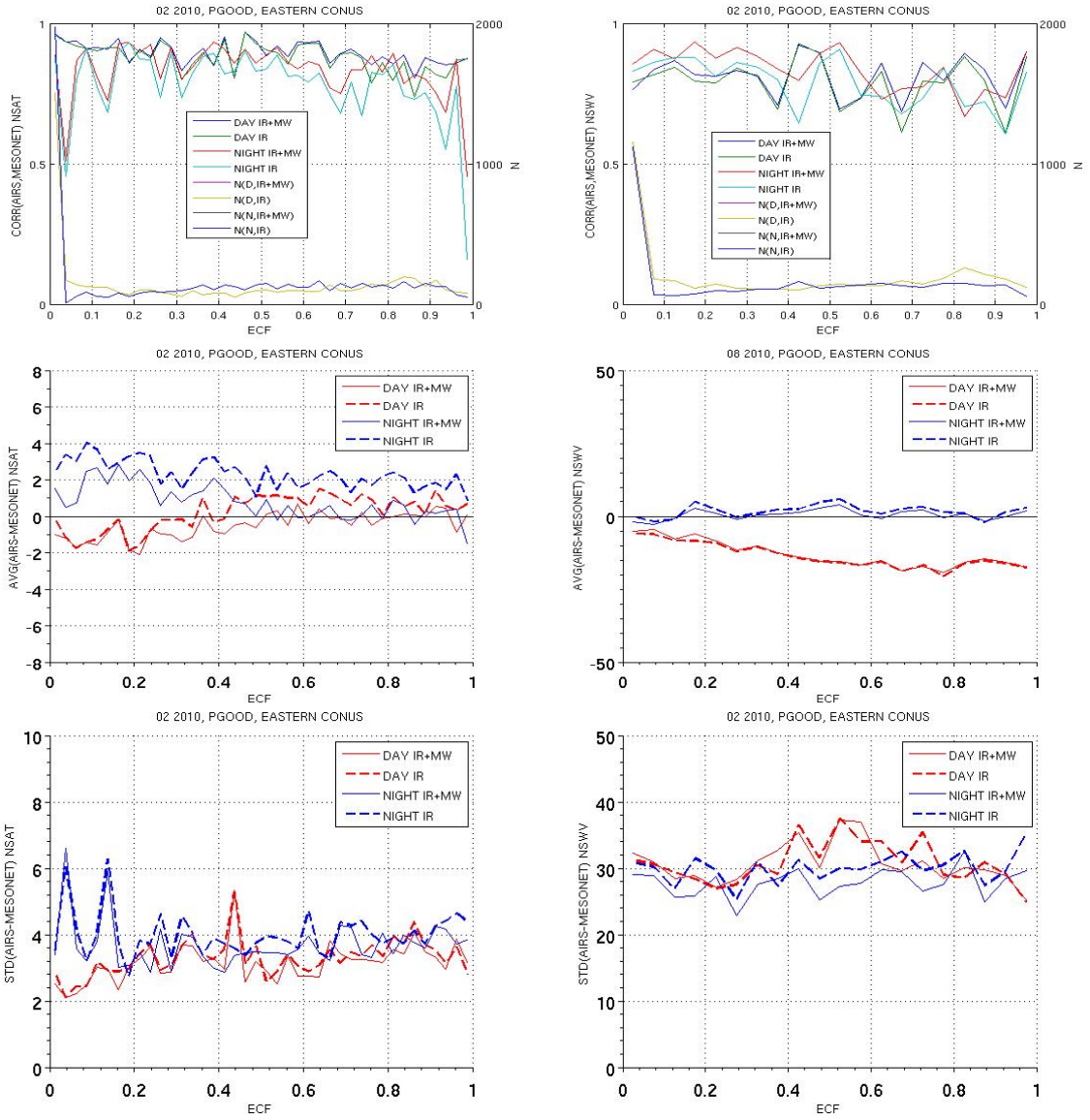

Figure 3.2.5-12. Similar to Figure 3.2.5-11, but for Feb 2010

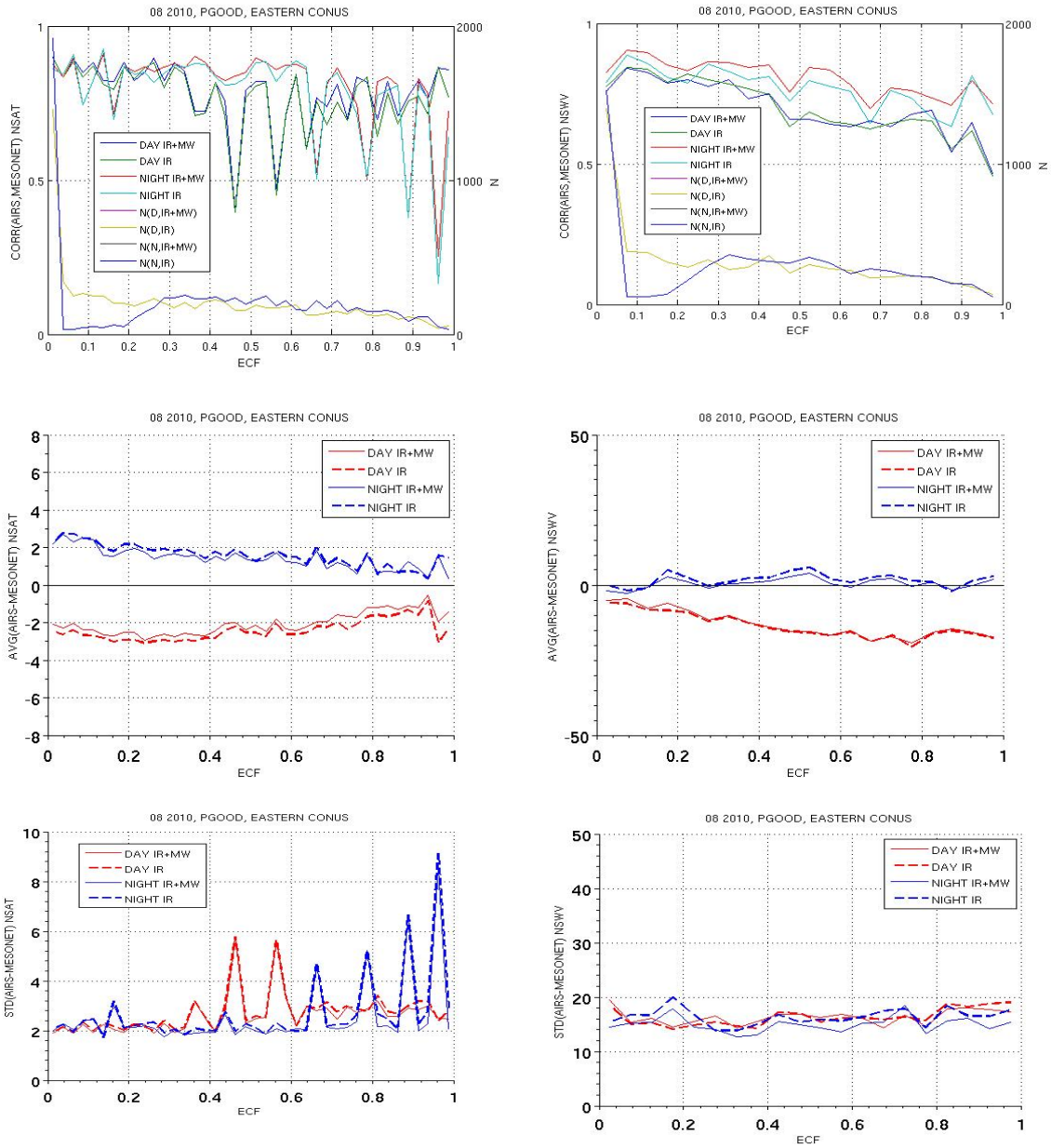

Figure 3.2.5-13. Similar to Figure 3.2.5-11, but for Aug 2010

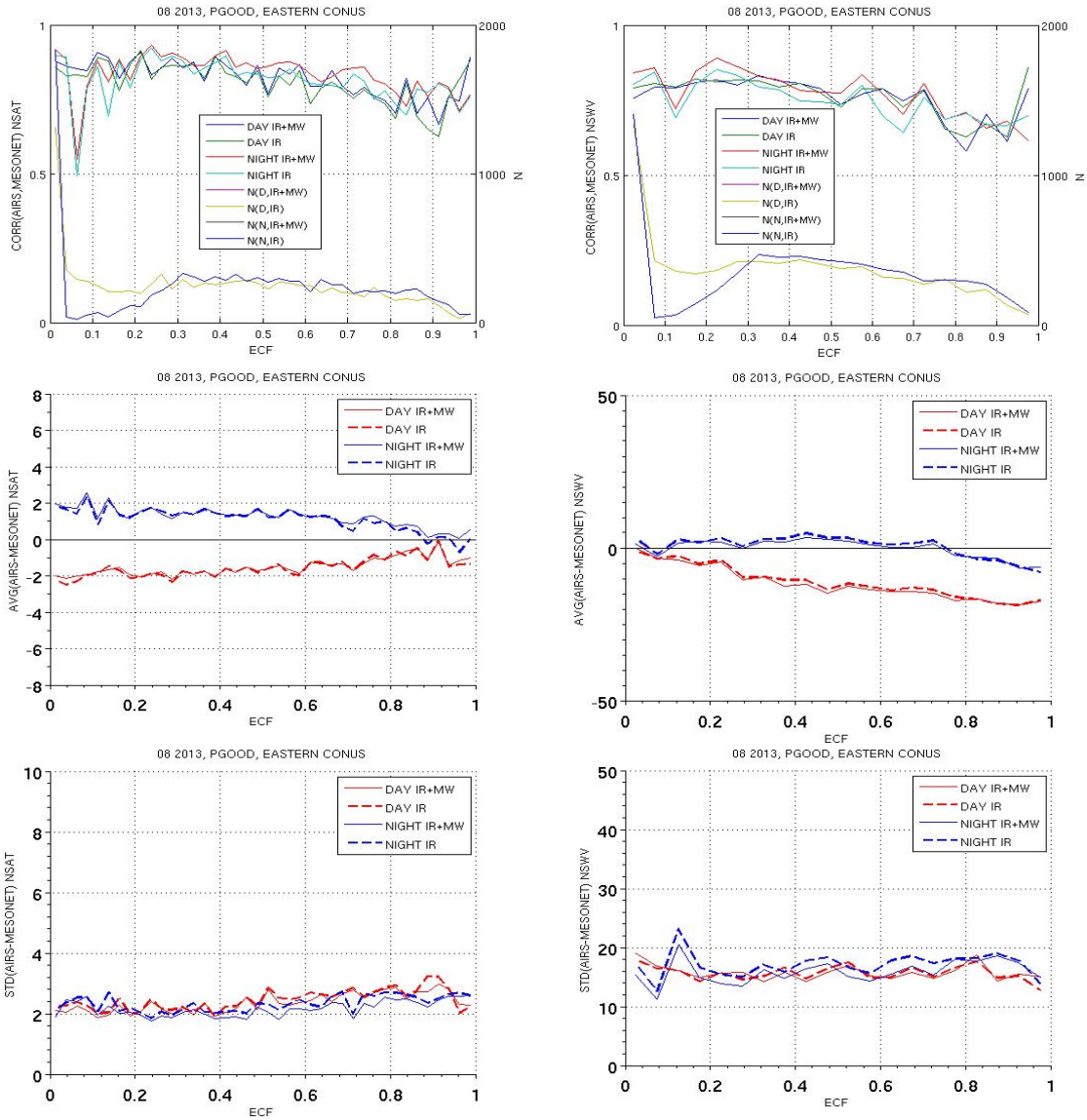

Figure 3.2.5-14. Similar to Figure 3.2.5-11, but for Aug 2013

3.2.6 AIRS mid-troposphere CO_2 compared with HIPPO air-borne measurements

Contributor: E. T. Olsen

Data

The HAIPER Pole-to-Pole transects of the mid-Pacific (Wofsy et al. 2012) provided measured CO_2 profiles useful for validating collocated Level 2 AIRS V5 IR+MW (AIRX2STC) and IR (AIRS2STC) partial column CO_2 retrievals. A subset of measured profiles from the HIPPO-2, HIPPO-3, HIPPO-4 and HIPPO-5 campaigns were selected for this purpose (see Table 3.2.6-1). The criterion for selection of these "deep profiles" was that the aircraft measurements extended above the 190 hPa pressure level to ensure good coverage of the AIRS CO_2 sensitivity profile.

Table 3.2.6-1. HIPPO campaigns used for testing and validation

Campaign	Start Date	End Date	#Deep Profiles
HIPPO-2	30 Oct 2009	22 Nov 2009	19
HIPPO-3	23 Mar 2010	16 Apr 2010	34
HIPPO-4	13 Jun 2011	30 Jun 2011	28
HIPPO-5	8 Aug 2011	10 Sep 2011	54

Methodology

The AIRS Level 2 retrievals ingested for use by the CO_2 post processing stage are filtered according to one of their internal quality factors, PGood, as well as the retrieved Tropopause pressure, PTrop. Only FOVs (at AMSU resolution) satisfying the condition

$$(PGood - PTrop) > 200\ hPa$$

are passed to the CO_2 post processing stage. This test ensures that the temperature profile is of sufficient quality from TOA to a level in the atmospheric column at least 200 hPa below the Tropopause. Tests are also applied to excise data that may be contaminated by surface emission.

The CO_2 retrieval algorithm results in an estimate for each FOV in a 2x2 array that are combined to arrive at the final product. The Level 2 CO_2 Standard Product contains retrievals meeting a spatial coherence over the 2x2 array, expressed as the standard deviation among the 4 (or 3) surviving FOVs. Retrievals for which the standard deviation is less than 2 ppm are included in the standard product.

The collocation criteria for validation against HIPPO profiles are

$$|\delta t| < 24\ hours\ \ and\ \ \Delta R < 500\ km,$$

that is, the AIRS Level 2 retrievals must take place within 24 hours of the HIPPO profile measurement mean time and within a radius of 500 km of the location of the mean location of the profile measurement.

The Level 2 CO_2 retrievals at each month are employed to display comparison of average collocated CO_2 retrievals and HIPPO profiles convolved with their averaging kernels, showing the bias of IR+MW and IR retrievals as a function of latitude for the four campaigns (see Figure 3.2.6-1).

Conclusions

The loss of MW has no direct influence upon the AIRS CO_2 post-processing algorithm because the algorithm has chosen to use channels that have minimal radiance contribution from the surface and the very lowest atmospheric layers. Thus the difference of retrieved CO_2 exhibits essentially no bias when AMSU/AIRS and AIRS (IR Only) are compared against one another or compared separately against airborne validation measurements.

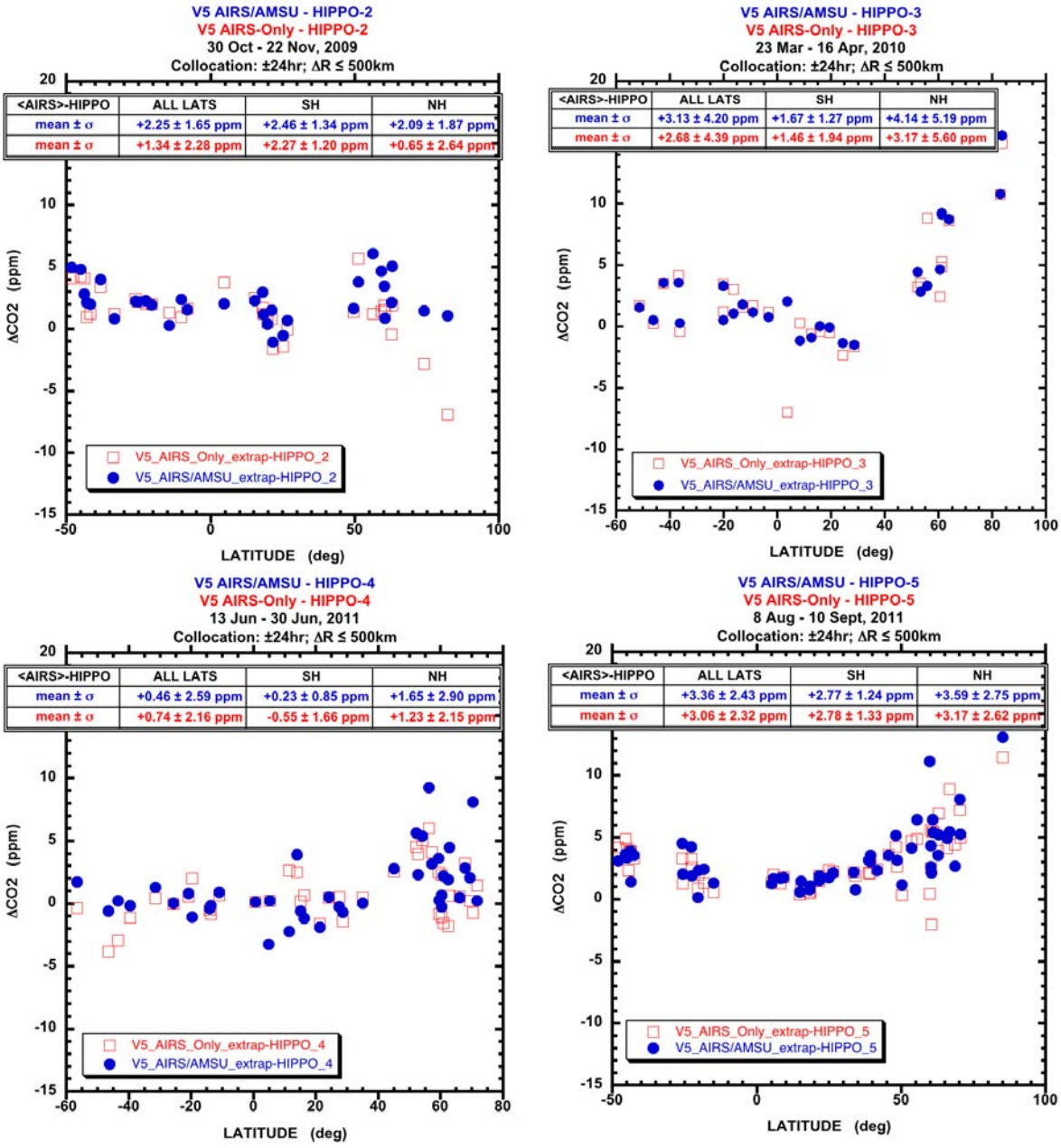

Figure 3.2.6-1. Comparison of collocated AIRS/AMSU (IR+MW) CO_2 and AIRS (IR-only) CO_2 to deep-dip HIPPO profiles convolved with their averaging kernels. Blue: <AIRS/AMSU> - HIPPO. Red: <AIRS> - HIPPO. Top left panel: Comparisons against HIPPO-2 profiles. Top right panel: Comparisons against HIPPO-3 profiles. Bottom left panel: Comparisons against HIPPO-4 profiles. Bottom right panel: Comparisons against HIPPO-5 profiles.

3.3 Test results for L3 products

For a summary of L3 test results, please see Table 1.2.

3.3.1 AIRS monthly mean surface skin temperature

Contributor: Baijun Tian

AIRS V6 L3 monthly mean surface skin temperature (SurSkinTemp) at ascending node, 1 x 1 lat-lon grids is tested by comparing the IR+MW with IR products. Global maps of SurfSkinTemp and yield by the IR retrieval and their differences with the IR+MW products are shown in Fig. 3.3.1-1. The differences between the AIRS IR-Only and IR+MW SurfSkinTemp are large (~ 3 K) over high latitude frozen land and ocean regions (e.g., Canada, Siberia, and Antarctic coast), but they are generally small over most other regions (< 1 K). The differences in yield between the AIRS IR-Only and IR+MW SurfSkinTemp are large (~ 30%) over the frozen land and ocean regions (e.g., Canada, Siberia, and Antarctic coast) and the southeastern tropical Pacific but they are generally small over most other regions (< 10%). Fore more discussion, please see Sec. 3.1.

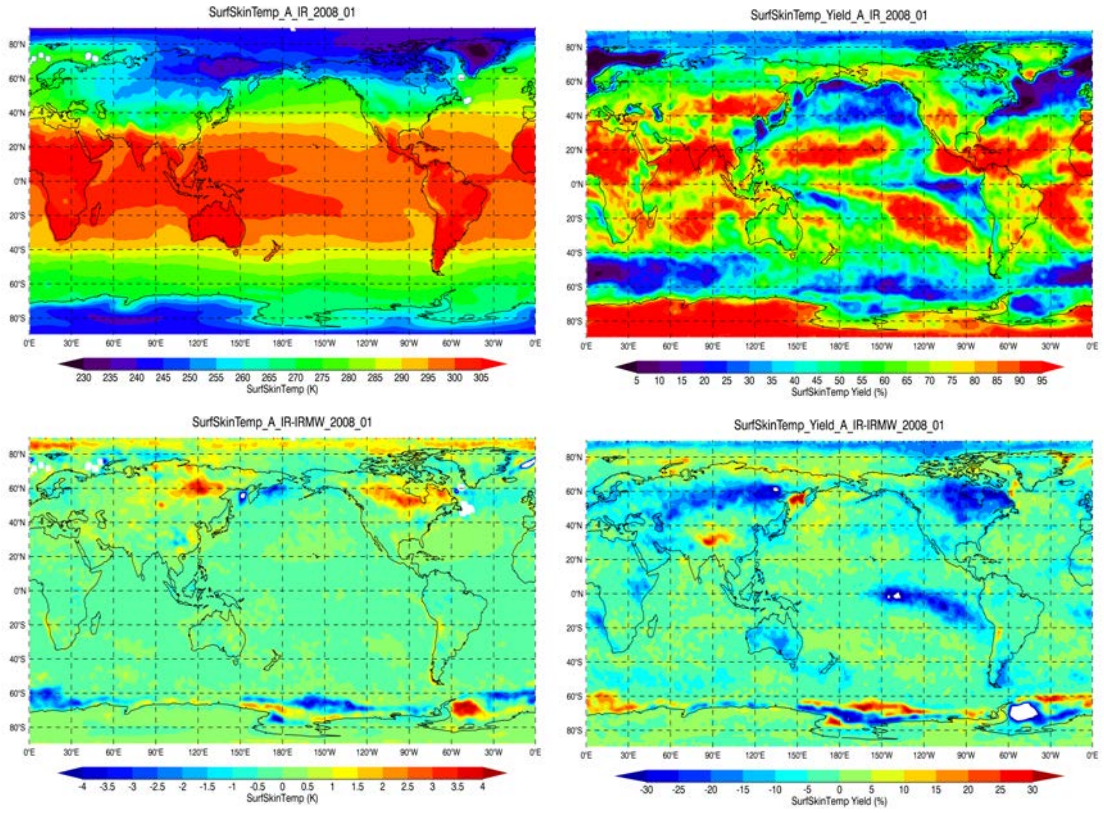

Figure 3.3.1-1. Top panels show the global map for January, 2008 SurfSkinTemp (left) and yield (right) by the IR retrieval. The bottom panels show the differences between the IR and IR+MW on the SurfskinTemp (left) and its yield (right).

3.3.2 AIRS monthly mean surface air temperature

Contributor: Baijun Tian

AIRS V6 L3 monthly mean surface air temperature (SurfAirTemp) at ascending node, 1 x 1 lat-lon grids is tested by comparing the IR+MW with IR products.

The differences between the AIRS IR-Only and IR+MW SurfAirTemp can be as large as ±3K over mid-high latitude land and ocean regions (e.g., Canada, Siberia, and Alaska coast) but they are generally small over most other regions (< 1 K). The differences in yield between the AIRS IR-Only and IRMW SurfAirTemp are large (~ 30%) over high latitude land and ocean regions (e.g., Canada and Siberia) but they are generally small over most other regions (< 10%).

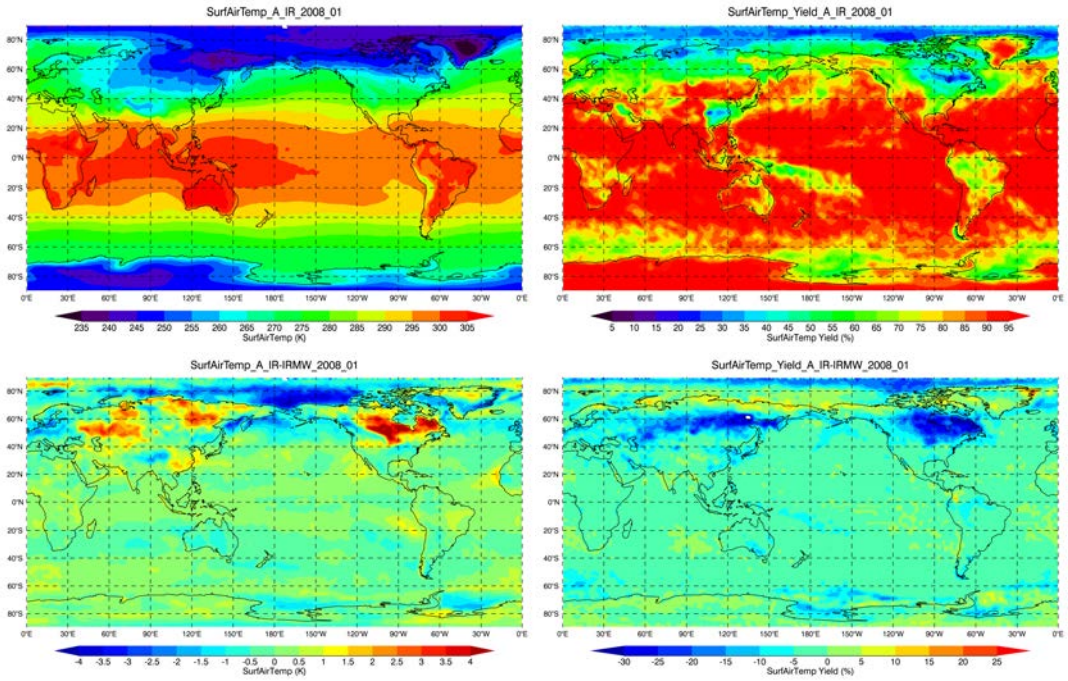

Figure 3.3.2-1. Same as Fig. 3.3.1-1 but for SurfAirTemp.

3.3.3 AIRS monthly total column water vapor comparison with AMSR-E and TMI measurements

Contributor: Baijun Tian and Eric Fetzer

AIRS V6 L3 monthly mean total column water vapor (TotH2OVap) for ascending and descending passes, 1° x 1° lat-lon grids are compared with the monthly mean column total water vapor data from AMSR-E V5 and TMI V4 products. Both the AMSRE and TMI products are at the resolution of 0.25 x 0.25 lat-lon grids. The former is available over the global ocean, and the latter is available over ocean between 40°S and 40°N, and at the resolution of 0.25° x 0.25° lat-lon grids. One month of data is used to highlight the differences between IR+MW and IR AIRS products and their differences from AMSR-E and TMI. Figure 3.3.3-1 shows the monthly mean TotH2OVap from the AMSR-E, TMI, AIRS IR ascending, and descending nodes for the month of January, 2008 as well as the AIRS retrieval yield for this month.

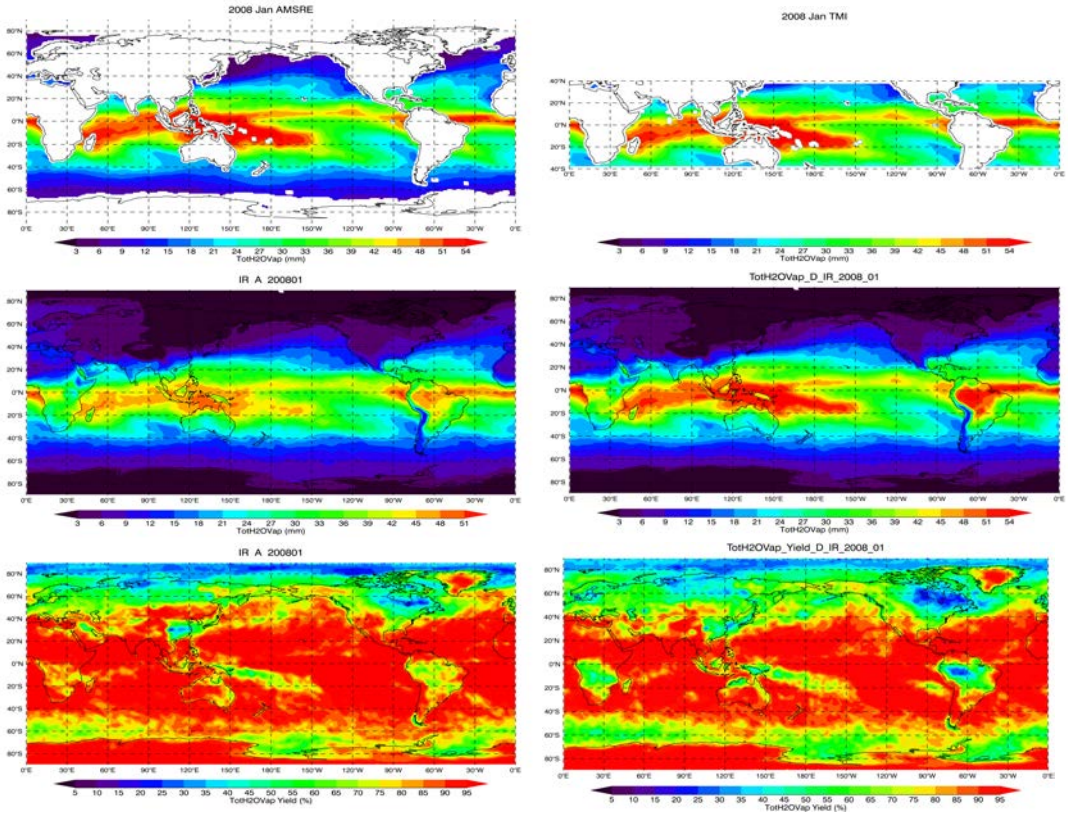

Figure 3.3.3-1. The monthly mean total column water vapor from the AMSR-E, TMI, AIRS IR ascending, and descending passes for the month of January, 2008. The yield of the AIRS IR product is also shown for ascending pass.

Figure 3.3.3-2 shows the differences between the AIRS IR+MW and IR-only retrieved totH2OVap and the AMSR-E data for ascending pass, together with the differences between the two AIRS retrievals on totH2OVap and its yield. For percentage differences relative to IR+MW monthly mean values and yield differences at a narrower

color bar range, please see Figure 3.1.4. Compared to AMSR-E and TMI, the AIRS IR-Only and IR+MW TotH2OVap products have dry biases over the tropical deep convective or high cloud regions and wet biases over the subsiding or low cloud regions and mid-latitude snow-covered land regions. The IR only retrievals have biases with the same spatial pattern but larger magnitudes than the IR+MW combined retrievals. These differences appear to be related to clouds (tropics or subtropics), surface conditions (ice or snow over the extratropical mid-latitudes) and sampling (different QCs for IR and IRMW).

The results for descending nopassesde are shown in Figure 3.3.3-3. There is a strong diurnal cycle in TotH2OVap, the biases are much bigger for the ascending passes and much smaller for the descending passes.

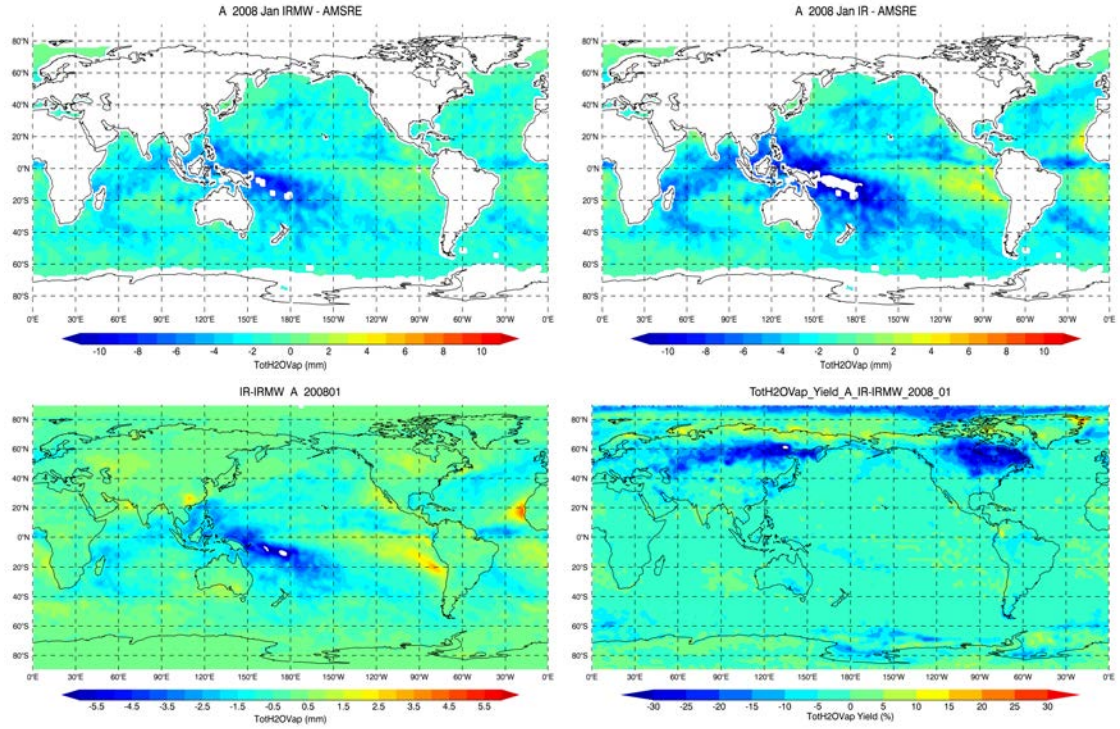

Figure 3.3.3-2. Top panels show the differences between the AIRS IR+MW (left) and IR-only (right) retrieved totH2OVap and the AMSR-E data for ascending data. The bottom panels show the differences between the two AIRS retrievals on totH2OVap (left) and its yield (right). For percent differences relative to IR+MW monthly mean values and yield differences at a narrower color bar range, please see Figure 3.1.4.

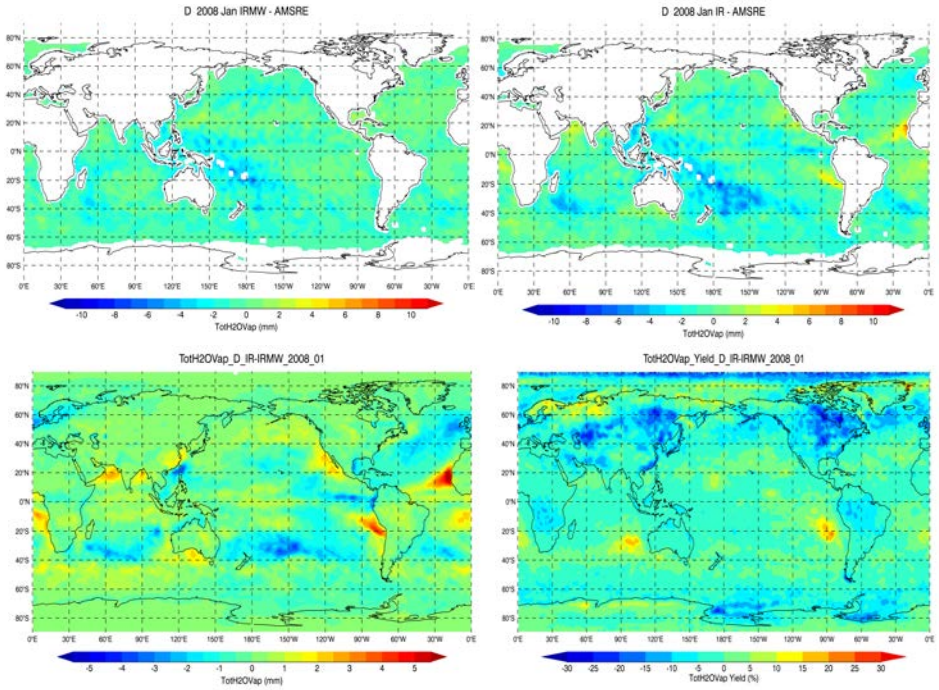

Figure 3.3.3-3. Same as Fig. 3.3.3-2, except for descending passes.

3.3.4 AIRS monthly mean tropopause parameters comparison with the GPSRO observations

Contributor: Baijun Tian

Three different tropopause parameters are tested by comparing with the GPS Radio Occultation (RO) data including tropopause height, tropopause pressure, and tropopause temperature. The AIRS L3 ascending, descending, and TqJ_Ascending data are included in the test for the month of January 2010. The daily GPSRO data is from CHAMP, GRACE, SAC-C, and COSMIC missions and at a resolution of 5° x 10° lat-lon grids (Tian et al., 2012).

From Fig. 3.3.4-1, it is clear that both the IR and IR+MW AIRS V6 L3 tropopause height have a similar spatial structure as those from GPSRO, such as high tropopause (~16.5 km) over the tropics, low tropopause (~8.5 km) over the extratropics, and a sharp drop from the tropics to the extratropics. However, there are differences, as large as ~1 km, between the AIRS and GPSRO data, especially over the transition region between the tropics and the extratropics. Similar changes are also found for tropopause pressure (Fig. 3.4.2-2) and temperature (3.4.2-3) that are consistent with those in tropopause height. The AIRS retrieved tropopause pressure/temperature can differ from GPSRO data by 50hPa/7K in the tropic-extratropic transition zone.

There are relatively larger differences between the IR-Only and IRMW AIRS tropopause parameters over the extratropics, but their differences seem to be smaller than the differences between the AIRS and GPSRO. Tropopause height difference in this region is around 300 m (20hPa and 2K for pressure and temperature, respectively), which is much smaller than the 1km difference between AIRS and GPSRO (40hPa and 7K for pressure and temperature, respectively).

The large differences in yield between the IR and IR+MW AIRS tropopause height over the snow-covered extratropical lands are probably due to the surface emissivity issue discussed in Sec. 3.1.1. The IR-Only yield seems to be smaller than the IR+MW yield.

The results shown here do not vary with whether the AIRS ascending, descending, or TQJ L3 data is used. The differences between the AIRS IR+MW and IR-only retrievals are much smaller than the differences between the AIRS and GPSRO tropopause quantities.

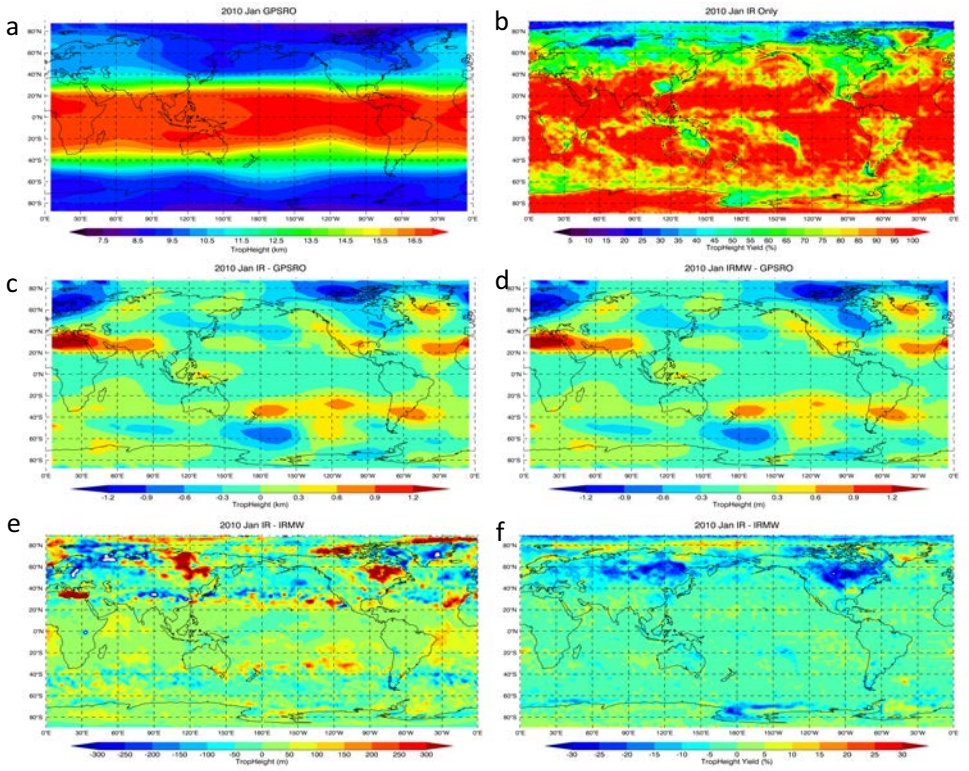

Figure 3.3.4-1. (a) The monthly mean tropopause height from GPSRO data for January 2010. (b) the AIRS IR-only retrieval yield. (c) The difference in tropopause height between AIRS IR retrieval and GPSRO. (d) The difference between AIRS IR+MW and GPSRO. (e) The difference in monthly mean tropopause height between AIRS IR and IR+MW. (f) The difference in yield for tropopause height between AIRS IR and IR+MW.

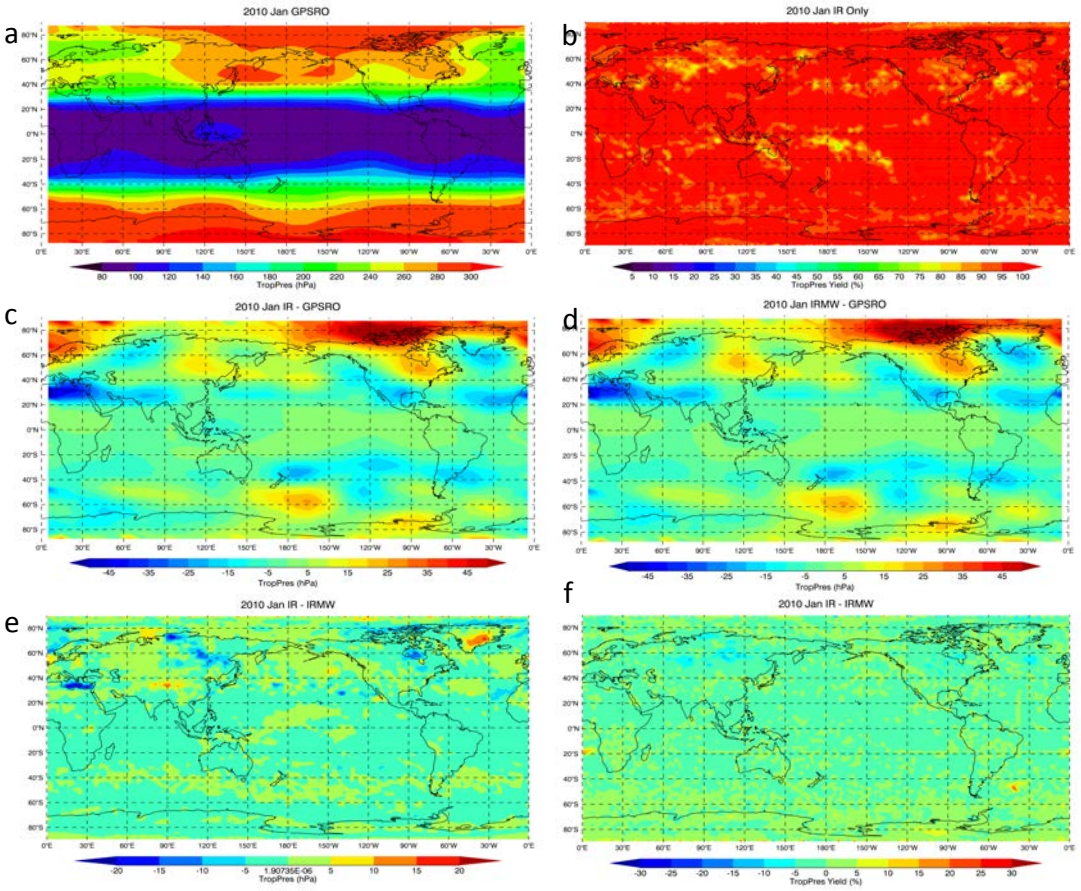

Figure 3.3.4-2. Same as Fig. 3.3.4-1 but for tropopause pressure.

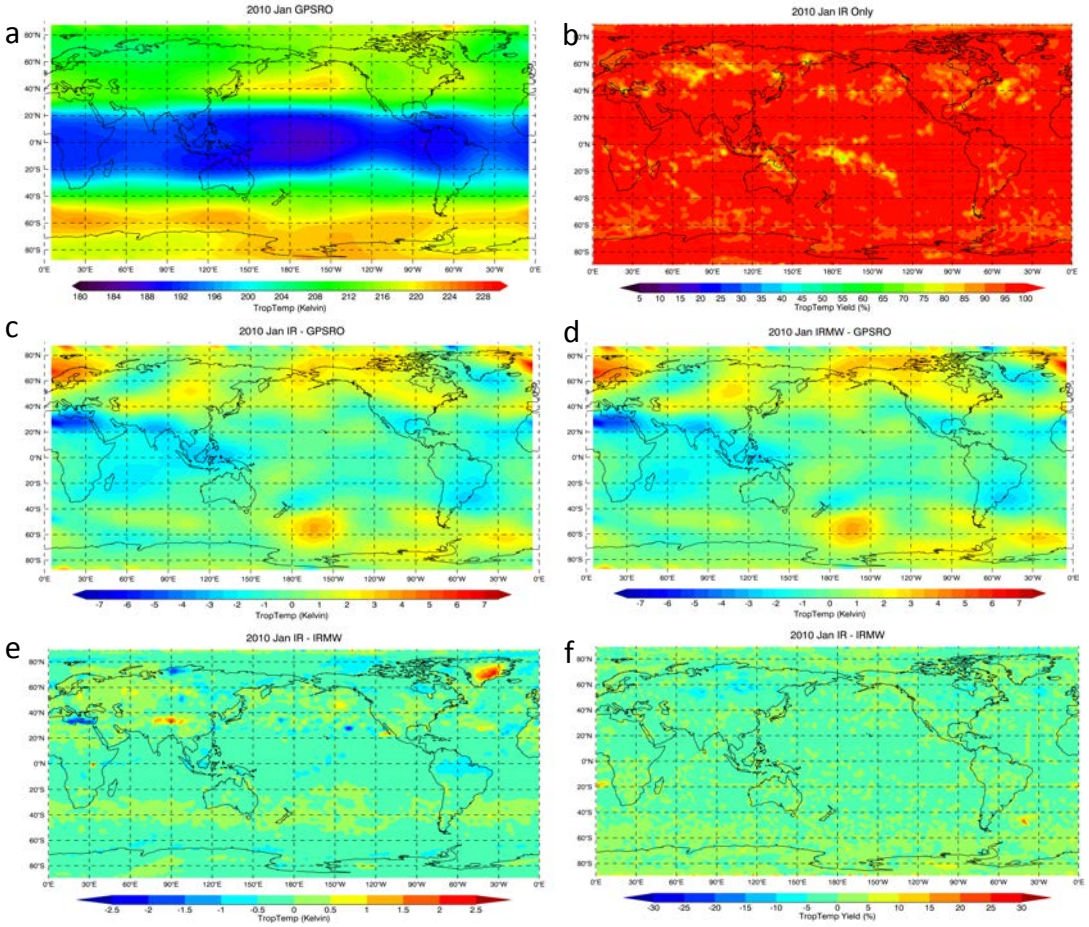

Figure 3.3.4-3. Same as Fig. 3.3.4-1 but for tropopause temperature.

3.3.5 AIRS monthly temperature and water vertical profiles

Contributor: Baijun Tian

Monthly mean temperature, water vapor mixing ratio, and relative humidity fields from IR+MW and IR retrievals are compared with each other. January 2008 ascending data is used.

3.3.5.1 Temperature profile – *Figure 3.3.5.1-1*

In the lower troposphere (850 hPa), the temperature difference between IR-Only and IR+MW can reach 3K over the mid- and high-latitude regions in the boreal winter season, but relatively small over other regions (magnitude less than ±0.6K). In the middle troposphere (500 hPa), the temperature difference between IR-Only and IRMW can reach ±1K over the high-latitude regions and the tropical deep convective regions, especially over land. In the upper troposphere (250 hPa), the IR-Only Temperature is about 1 K warmer than IR+MW over the tropical deep convective regions and about 1 K colder than IRMW over the high-latitude regions (e.g., the NH mid-latitudes). In the stratosphere (70 hPa), the temperature difference between IR-Only and IR+MW is very small.

The range of difference on yield between the IR+MW and IR increases as pressure increases. The yield for tropospheric temperature is generally lower for IR-Only than IRMW over the tropical deep convective regions due to cloud and high-latitude frozen regions due to the surface classification and emissivity issue discussed in Sec. 3.1. However, the yield difference between IR-Only and IRMW is small in the stratosphere (e.g., 70 hPa).

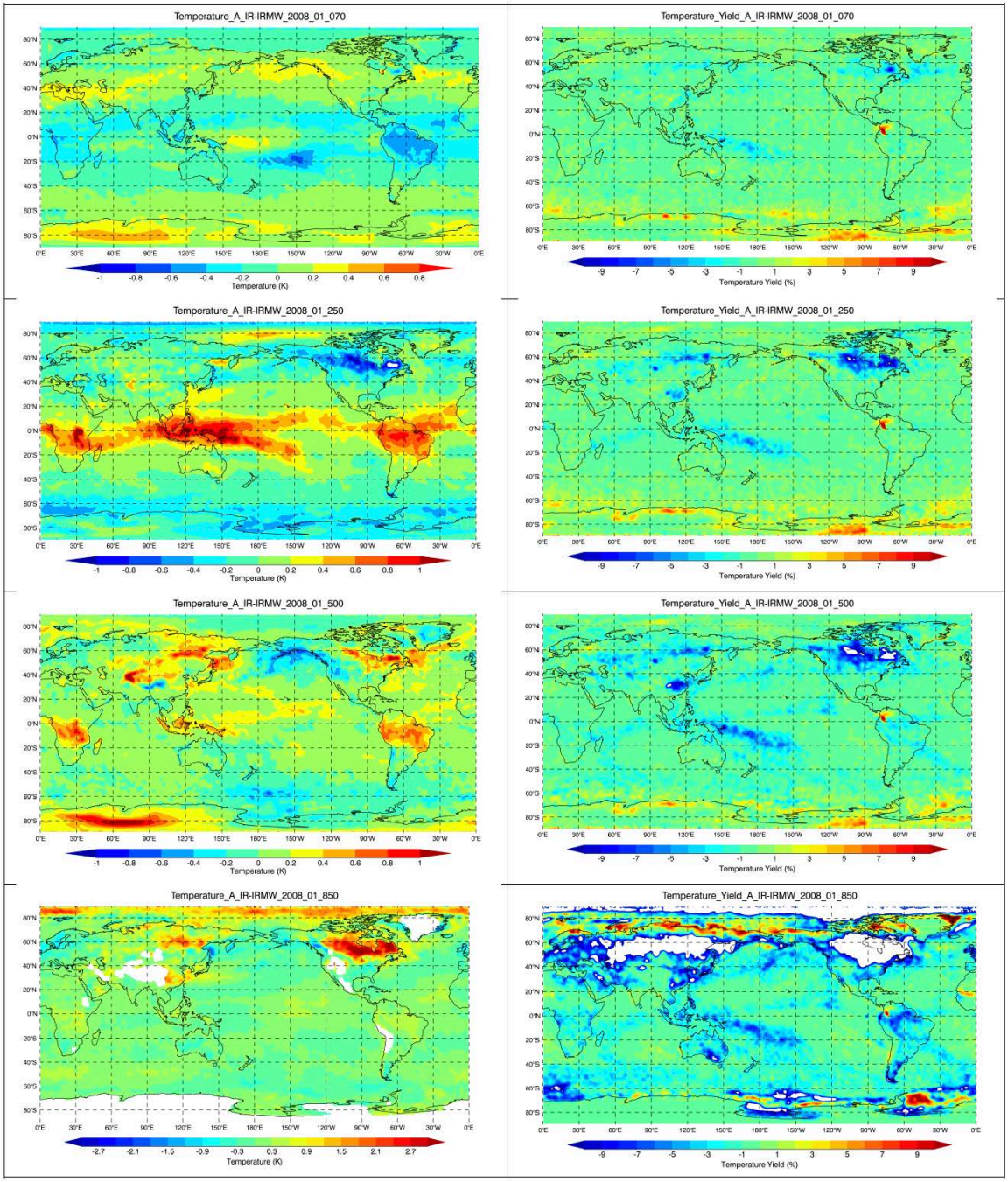

Figure 3.3.5.1-1. The differences in temperature (left) and yield (right) between AIRS V6 IR and IR+MW (IR minus IR+MW) at four levels: 70, 250,500, and 850 hPa from top to bottom. Ascending data in January 2008 is used. White color in the yield figure represents values between -10 and -35%. The narrower color range is chosen to show the finer scale of yield changes.

3.3.5.2 Water vapor mixing ratio profile (H2O_MMR) – *Figure 3.3.5.2-1*

The V6 AIRS IR-Only H2O_MMR at the lower and middle troposphere (850, 500 hPa) is lower (by about 2g/kg at 850 hPa and 0.1 g/kg at 500 hPa) than IR+MW over the tropical deep convective or high cloud regions, while it is higher than IR+MW by about 1 g/kg and 0.1g/kg than IR+MW over the subsiding or low cloud regions. This is related to the lower yield of IR-Only in these regions due to clouds (tropics or subtropics) and surface conditions (ice or snow over the NH mid-latitudes) and different QCs for IR and IRMW.

At 250 hPa, IR-Only H2O_MMR is higher than IR+MW by 0.008 g/kg over the tropical deep convective or high cloud regions. The reason for this difference is unknown although the lower yield of IR-Only in these regions may play some role.

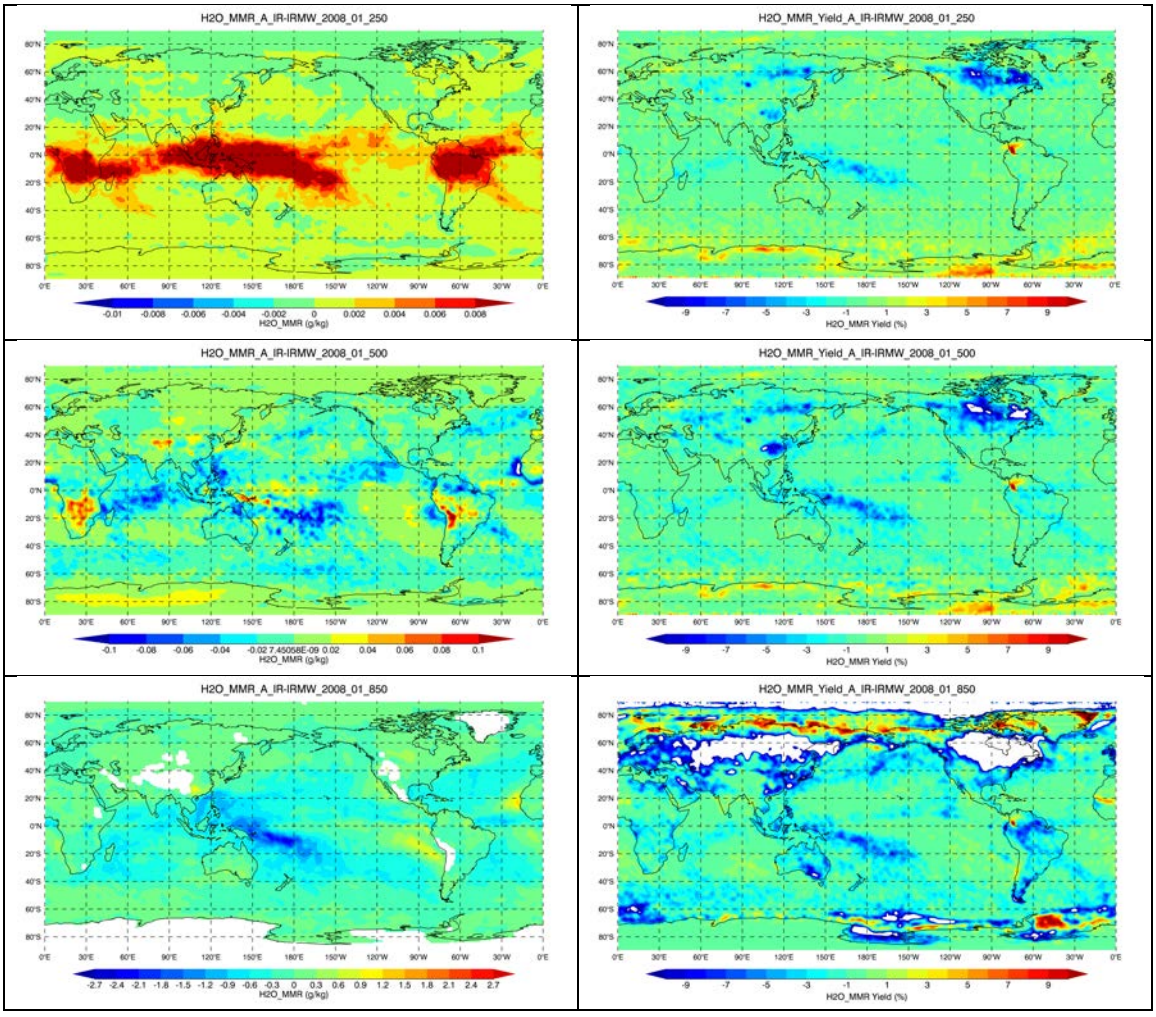

Figure 3.3.5.2-1. Same as Fig. 3.3.5.1-1, but for water vapor mixing ratio and at three levels: 250, 500, and 850 hPa from top to bottom.

3.3.5.3 Relative humidity profile (RelHum) – *Figure 3.3.5.3-1*

The differences on RelHum between the IR and IR+MW result from the combination of changes on both temperature and water vapor mixing ratio at each level. In the tropics and subtropical subsiding regions, the effect from water vapor differences plays a dominant role, thus the difference on relative humidity at these regions has the same sign with water vapor differences. The magnitude of the differences is from -15% to 8% at 850 hPa and -3% to 2% at 500hPa. In the high latitude region where temperature differences can be large, the sign of the relative humidity changes is dominated by both temperature and water vapor difference between the two retrievals.

The difference between the IR-Only and IR+MW RelHum at the upper troposphere (250 hPa) is generally small except in the Polar Regions.

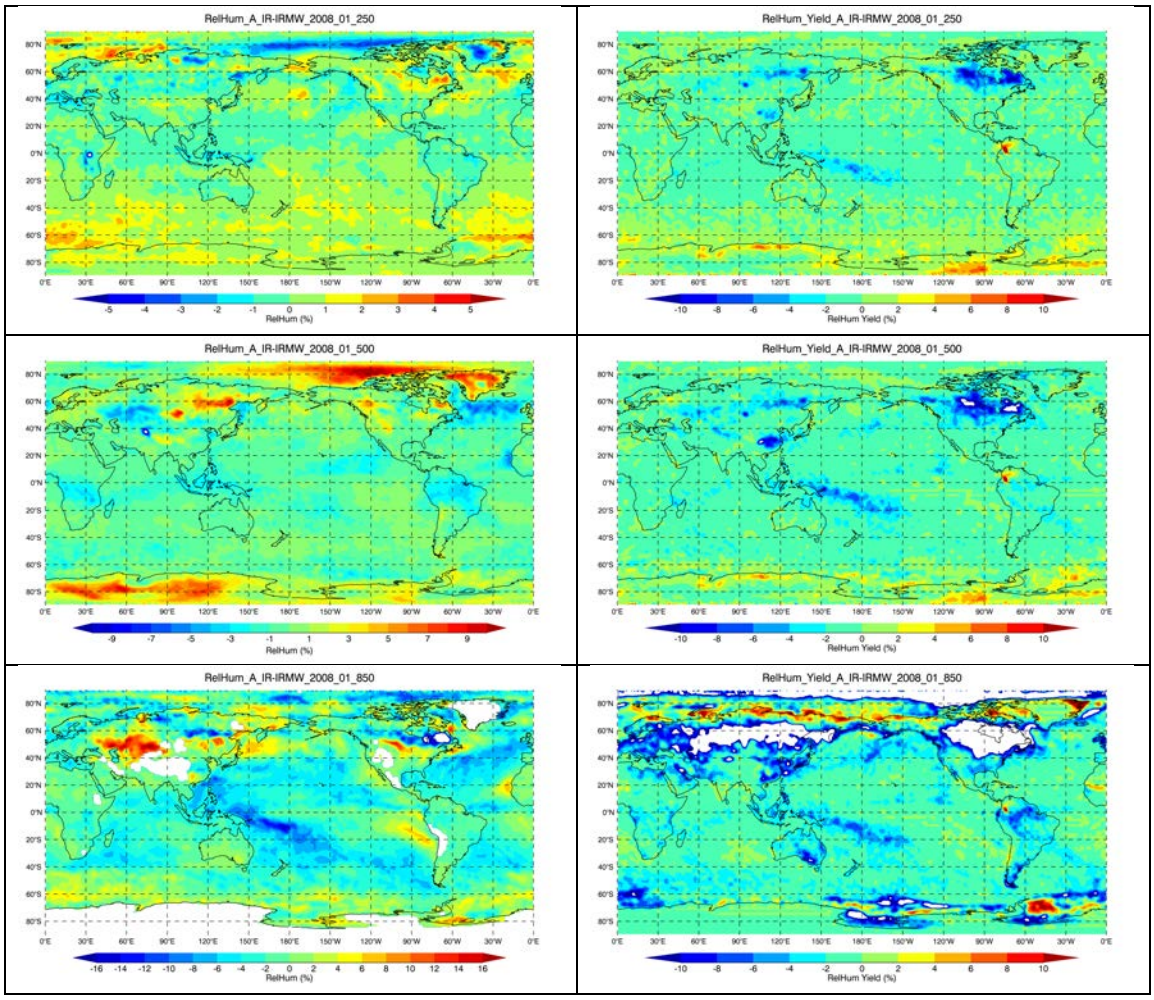

Figure 3.3.5.3-1. Same as Fig. 3.3.5.2-1, but for relative humidity.

3.3.6 AIRS monthly cloud field

Contributor: Brian Kahn

Data

The AIRS Standard Level 2 two-layer effective cloud fraction (ECF) and cloud top temperature (Tcld) and the Support Level 2 single layer ice cloud top temperature (Tcld, ice), optical thickness (tau) and effective diameter (De) is gridded to 1°×1° gridded resolution and differenced for four months in 2009 (January, April, July, and October) using the method in Kahn et al. (2014; 2015). These are not derived from the Standard and Support Level 3 files. We expect similar results if L3 data is used.

Methodology

All of the Tcld, ice, tau, and De parameters that meet the QC defined in Kahn et al. (2014) are kept in the analysis. In the case of ECF and Tcld, there is no QC applied so that we can understand some of the biggest changes in retrieval failures as well as outside of these areas. (Please refer to the granule scale comparisons in Sec. 3.2.4 for insight into this behavior.) Counts are retained for each geophysical field in each latitude/longitude bin so that these monthly maps may be averaged with other months (not shown).

Discussion, Results, and Conclusions

Figure 3.3.6-1 shows results for the upper layer TCld. (1) AIRS-IR is several Ks colder in the low latitudes than IR+MW, while the reverse is true in the high latitudes. One may ask: why is AIRS-IR colder in the tropics? One hypothesis is the possibility of increased sensitivity to more tenuous, thin-cloud tops with IR-only remote sensing, but this is not confirmed and warrants further exploration. (2) Some land/ocean contrast is noted in the difference plot but not in the TCld fields themselves, which is an indication of the role of surface changes with the loss of AMSU-A2. An additional point of reference is that ice edge effects are apparent around Antarctica. (3) The biggest differences are found in the tropical east Pacific in the 240-270K temperature range. We suspect that this is related to the type of mid-level, multi-layer, and/or convective cloud in this region. (4) There is a decrease in the TCld for AIRS-IR in subtropical Sc regions than IR+MW. The improvement in this region in v6 was notable over v5, however, the marine boundary layer cloud from the IR-only retrieval are too high and above the inversion.

Figure 3.3.6-2 shows results for the lower layer TCld. (1) AIRS-IR is several Ks warmer in most latitudes, except for a small decrease in tropical convective regions on the north side of ITCZ (the role of multilayer clouds may be at play here but that is not confirmed). (2) Some land/ocean contrast is noted in the difference plot but also in the TCld fields themselves unlike upper TCld. Ice edge effects are still apparent around Antarctica but they are more subtle than upper TCld. (3) The AIRS lower TCld is placed lower in atmosphere, possibly to compensate for higher TCld in the context of radiative consistency. This is speculative and not confirmed.

Figure 3.3.6-3 shows results for the upper layer ECF. (1) AIRS-IR ECF is reduced in low latitudes and increased in high latitudes. This appears consistent with the idea of the maintenance of radiative consistency in AIRS-MW and AIRS-IR while the individual

values of TCld and ECF can change significantly. (2) The difference plot of Upper ECF traces out convection much more closely than Upper TCld. (3) Extremely large changes are apparent around Antarctica. This appears related to the sea ice edge but also to topography on land. There may be changes in surface temperature and emissivity in the presence of large topographical features but this is speculative.

Figure 3.3.6-4 shows results for the lower layer ECF. (1) The lower layer shows a similar pattern as upper ECF but reversed in sign, with an increase most everywhere in AIRS-IR. (2) A strong resemblance of the difference pattern to convection is noted. (3) The difference plot of Lower ECF appears to have a pattern similar to lower TCld but of opposite sign. (4) It is worth noting that the differences appear larger relative to the absolute values in the case of lower ECF than in the case of upper ECF. So the lower ECF is more sensitive to AIRS-MW and AIRS-IR changes. This is not unexpected. A simplistic view is that the AIRS-IR has a harder time finding the low cloud than IR+MW.

Figure 3.3.6-5 shows the differences for ice cloud optical thickness. (1) In the thickest ITCZ and storm track ice clouds, AIRS-IR is slightly reduced over AIRS-MW. (2) In thin cirrus in the W. Pacific region, AIRS-IR is slightly increased over AIRS-MW. (3) There are significant increases of tau in high latitude regions especially over land and ice. This effect appears to mirror some of the TCld and ECF spatial pattern changes. (4) There is less change around the Antarctica ice edge that suggests these clouds are distinctly liquid phase (warm or supercooled).

Figure 3.3.6-6 shows the differences for ice cloud effective diameter. (1) The spatial pattern of differences to first order is opposite of the ice cloud optical thickness. (2) There are decreases over high latitude land and ice in AIRS-IR compared to IR+MW. (3) There are increases over low latitude and ocean for AIRS-IR, but larger changes in midlatitude storm tracks compared to tropics. (4) Very strong and notable reductions in De around and over Antarctica are noted. The same effects are seen in the Arctic in certain months (not shown). (5) We looked at ascending versus descending differences and no significant changes were seen. (6) We looked at counts between AIRS-IR and AIRS-MW. While the counts were slightly less for AIRS-IR, these appear not to explain the very large changes in high latitudes and over land.

Figure 3.3.6-7 shows the differences for ice cloud top temperature. (1) To first order, these patterns mirror the changes found in the AIRS Standard L2 Upper TCld field. The magnitude of the change is much less than the Upper TCld, however. (3) There remains a modest decrease in ice TCld,ice in the low latitudes and a modest increase in the high latitudes. It should be noted that he AIRS Upper TCld is used as a prior guess for the AIRS Ice TCld retrieval. Also recall that we assume a single layer cloud in the ice property retrieval.

Comments and Discussions

Further research is warranted to determine the cause of these differences, which could be some combination of yield, sampling in different cloud states, or changes in retrieval noise/RMSE. We have also quantified differences in the cloud thermodynamic phase algorithm in addition to these cloud properties. We decided not to show these results as they tend to be much smaller. However, there are some large changes in the “liquid” and “unknown” cloud frequencies near ice edges and over a few high latitude land surfaces that are connected to ECF changes that are in turn connected to the loss of AMSU.

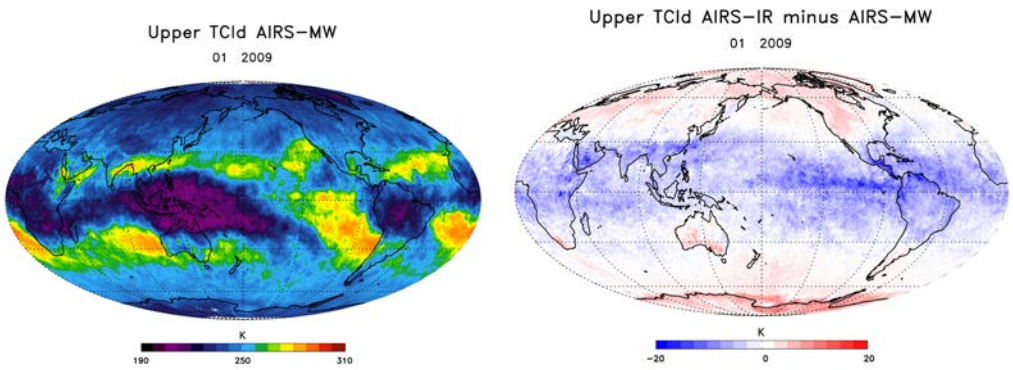

Figure 3.3.6-1. Left: AIRS-MW upper layer TCld for January 2009. Right: AIRS-IR minus AIRS-MW upper layer TCld for same time period.

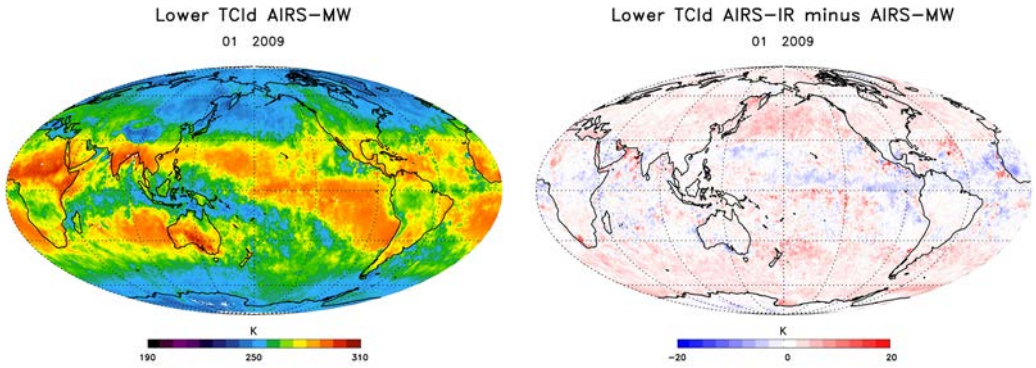

Figure 3.3.6-2. Left: AIRS-MW lower layer TCld for January 2009. Right: AIRS-IR minus AIRS-MW lower layer TCld for same time period.

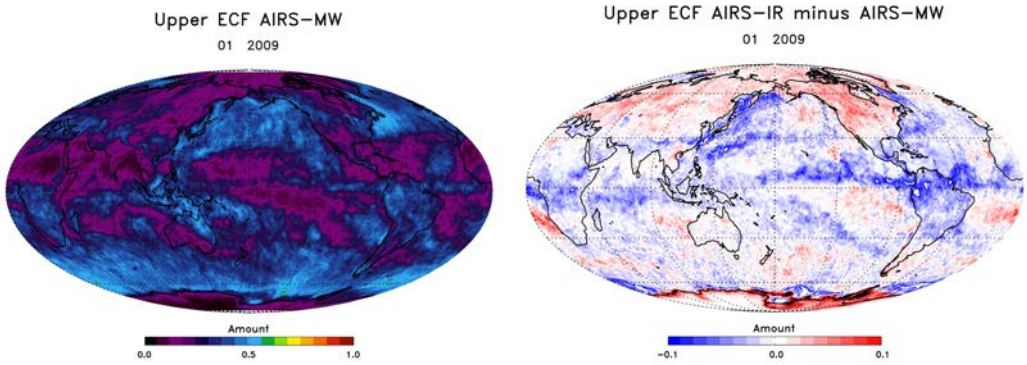

Figure 3.3.6-3. Left: AIRS-MW upper layer ECF for January 2009. Right: AIRS-IR minus AIRS-MW upper layer ECF for same time period.

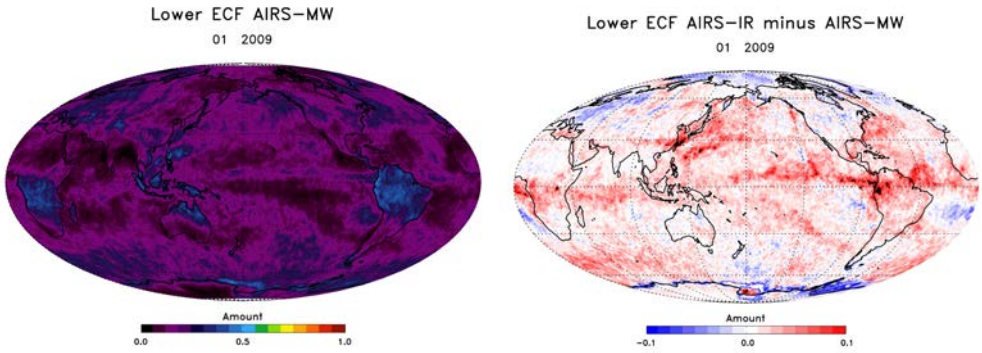

Figure 3.3.6-4. Left: AIRS-MW lower layer ECF for January 2009. Right: AIRS-IR minus AIRS-MW lower layer ECF for same time period.

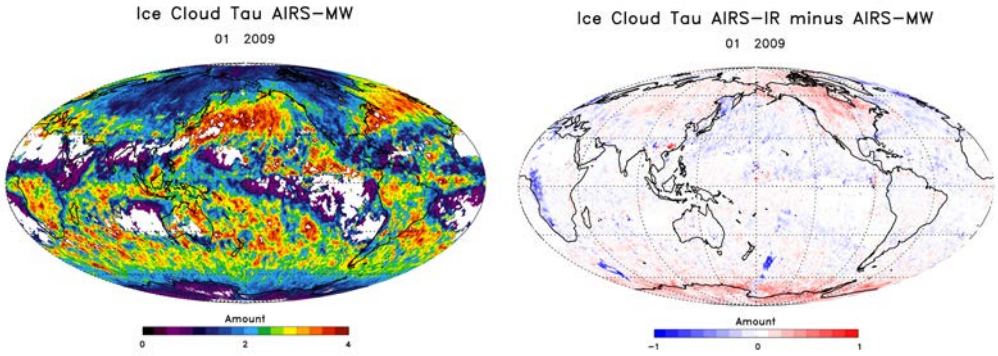

Figure 3.3.6-5. Left: AIRS-MW ice cloud optical thickness for January 2009. Right: AIRS-IR minus AIRS-MW ice cloud optical thickness for same time period.

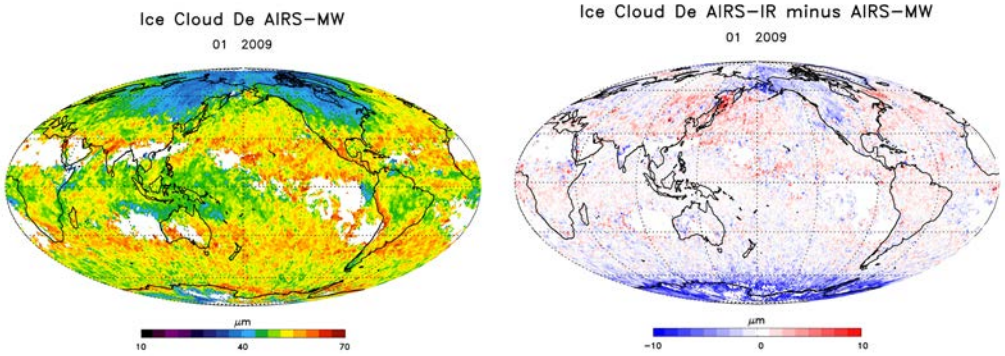

Figure 3.3.6-6. Left: AIRS-MW ice cloud effective diameter for January 2009. Right: AIRS-IR minus AIRS-MW ice cloud effective diameter for same time period.

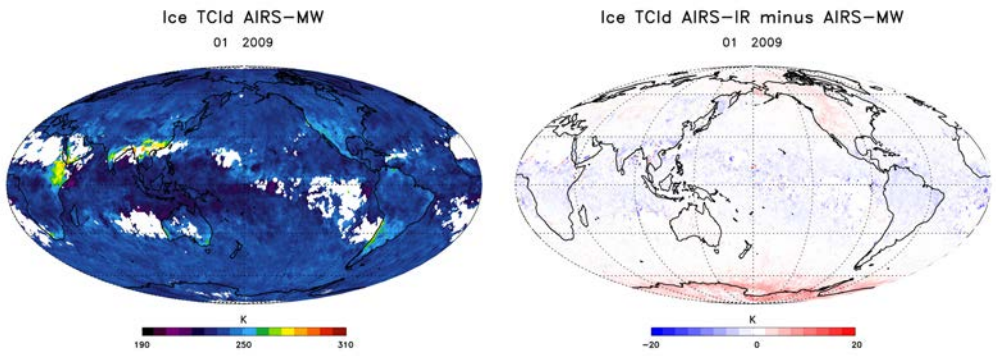

Figure 3.3.6-7. Left: AIRS-MW ice cloud top temperature for January 2009. Right: AIRS-IR minus AIRS-MW ice cloud top temperature for same time period.

3.3.7 AIRS L3 total column ozone

Contributor: Fredrick Irion

Testing of AIRS Versions 6 IR+MW and IR-only total column ozone retrievals were made by comparisons against coincident measurements by the Ozone Monitoring Instrument (OMI). This testing is meant to be a comparison of the total columns between the AIRS versions and to check for pathologies in V6 IR+MW and IR Only. This should not be viewed as a validation of any AIRS ozone product. Below in the figures, IR+MW is referred to as Version 6 and IR-only is referred to as Version 6 AIRS-only.

For total column ozone, we tested against one day of OMI data, Feb 24, 2007, using the Version 3 OMI Level 3e product, which has a 0.25°x 0.25°gridding. AIRS and OMI total ozone observations were compared if the geographical center of the AIRS observation was within the OMI grid box. Again, as we have used L3 data from OMI, this should not be taken as validation of AIRS ozone. As OMI relies on backscattered UV radiation, only sunlit measurements of AIRS could be used.

Figure 3.3.7-1 below compares the relative difference between IR+MW and IR-only and OMI total ozone (calculated as (AIRS-OMI)/OMI in percent). The general pattern is similar in both versions, with some regional biases, and that the number of observations is fewer in V6 IR-only data product. Table 3.3.7-1 compares IR+MW and IR-only against OMI, but binned by quality flag[1]. Differences are similar, although we note that in taking the differing areas of the OMI 0.25°x0.25° grid into account by using the cosine of the latitude, the V6 IR-only agreement with OMI is slightly better than IR+MW.

Table 3.3.7-1. Relative biases of V6 and V6-AIRS only total ozone compared to OMI, filtered by quality flags, for sunlit observations of Feb. 24, 2007. The upper rows are unweighted averages, while the lower rows are averages weighted by cos(latitude).

	Quality Flag Filter	V6 IR+MW avg bias vs. OMI (% ± 1s)	V6 IR+MW number of comparisons	V6 IR-only avg bias vs OMI (% ± 1σ)	V6 IR-only number of comparisons
Unweighted by cos(latitude)	all	0.77±8.11	148189	0.63±8.33	148131
	O_3 qual flag = 0	0.48±0.76	133098	0.41±6.91	127583
Weighted by cos(latitude)	All	0.71±2.42	148189	0.43±2.49	148131
	O_3 qual flag = 0	0.30±1.98	133098	0.05±1.82	127583

A comparison of the bias sensitivity to biases in the ocean skin temperature is shown

[1] The field name is 'totO3Std_QC' in Version 6. A quality flag of 0 is 'best', 1 is 'good', and 2 is 'poor.' Note that there are very few AIRS ozone observations with ozone quality flag = 1.

in Figure 3.3.7-2. Here, we compare AIRS vs OMI ozone against AIRS vs Version 7 Advanced Microwave Scanning Radiometer – EOS (AMSR-E) ocean skin temperature[2]. In both AIRS IR+MW and IR-only, the relative ozone column bias compared to OMI increases as the AIRS minus AMSR-E temperature difference decrease (more negative). (Assuming OMI and AMSR-E as 'truth,' if the AIRS ocean skin temperature is too cold, then the retrieved ozone may become too high.) Errors in the ocean skin temperature may have a significant effect on the ozone bias. Taking data with an AIRS ozone quality flag equal to zero ('best data'), a least-squares fit of the AIRS-OMI relative ozone bias vs. the AIRS-AMSR-E temperature bias (not shown) 0.30±0.01 %/K for IR+MW, and -0.34±0.01 %/K for IR-only.

Finally, we compare AIRS-OMI bias as a function of cloud top pressure and cloud fraction. The upper panel of Figure 3.3.7-3 compares the AIRS IR+MW relative ozone bias against a combined cloud-top pressure (linearly weighted by cloud fraction) as retrieved by AIRS, while the lower panel shows the number of observations in each bin. (AIRS retrieves cloud properties for up to two cloud layers.) Figure 3.3.7-4 shows the same for IR-only. Both IR+MW and IR-only ozone show similar bias against OMI as a function of cloud pressure, although in both versions, a low bias is seen for lower pressure, thicker cloud amounts. Also, with no cloud, the bias is small, but with the sign reversed. With no cloud, the relative bias for IR+MW is -(0.9 ± 8.1) % (N=17697), and for IR-only is (0.85 ± 7.62) % (N=16177).

In summary, the differences in total column ozone between IR+MW and IR-only are much smaller than the differences between AIRS and OMI.

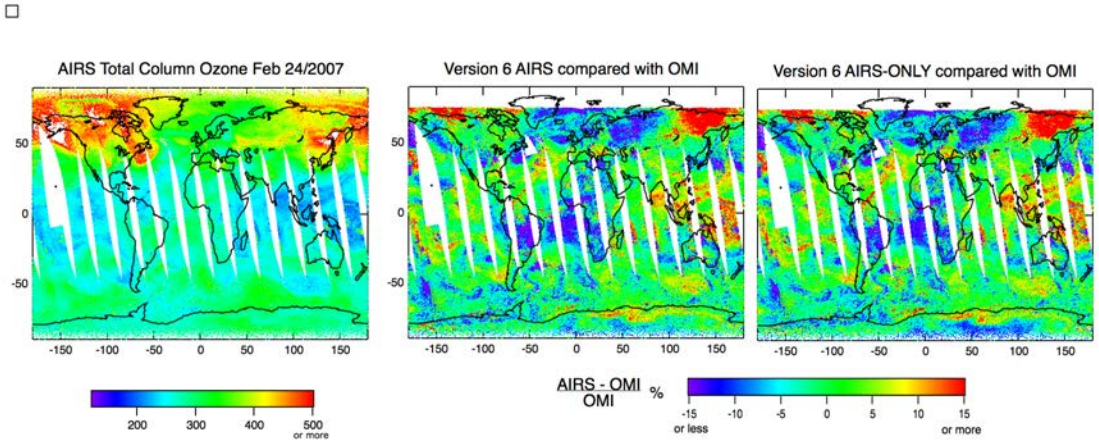

Figure 3.3.7-1: V6 IR+MW total ozone column, and relative bias of IR+MW and IR-only and Version 3 OMI total ozone for Feb. 24, 2007.

[2] AMSR-E data are produced by Remote Sensing Systems and sponsored by the NASA Earth Science MEaSUREs DISCOVER Project and the AMSR-E Science Team. Data are available at http://nsidc.org/data/amsre/.

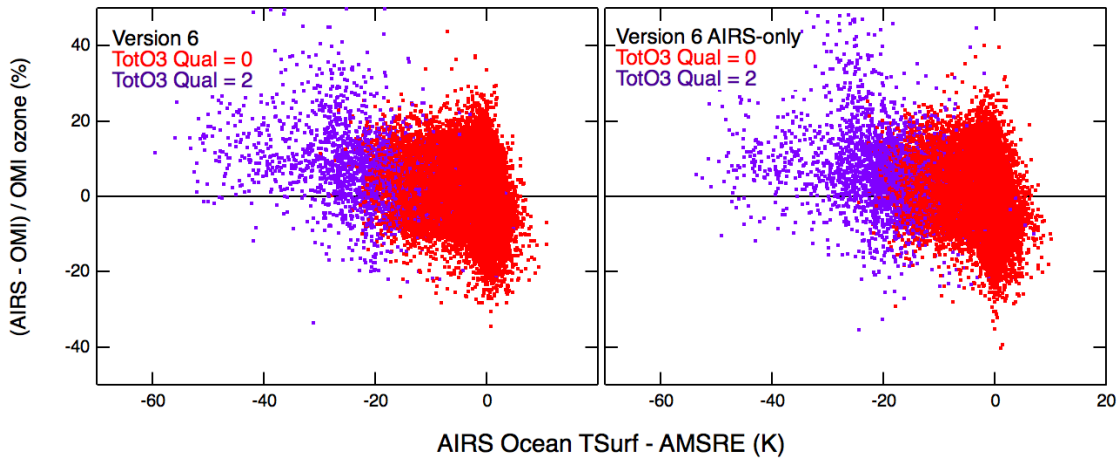

Figure 3.3.7-2. AIRS-OMI relative difference vs AIRS-AMSRe ocean surface temperature difference for Feb. 24, 2007. Left: IR+MW, right: IR-only.

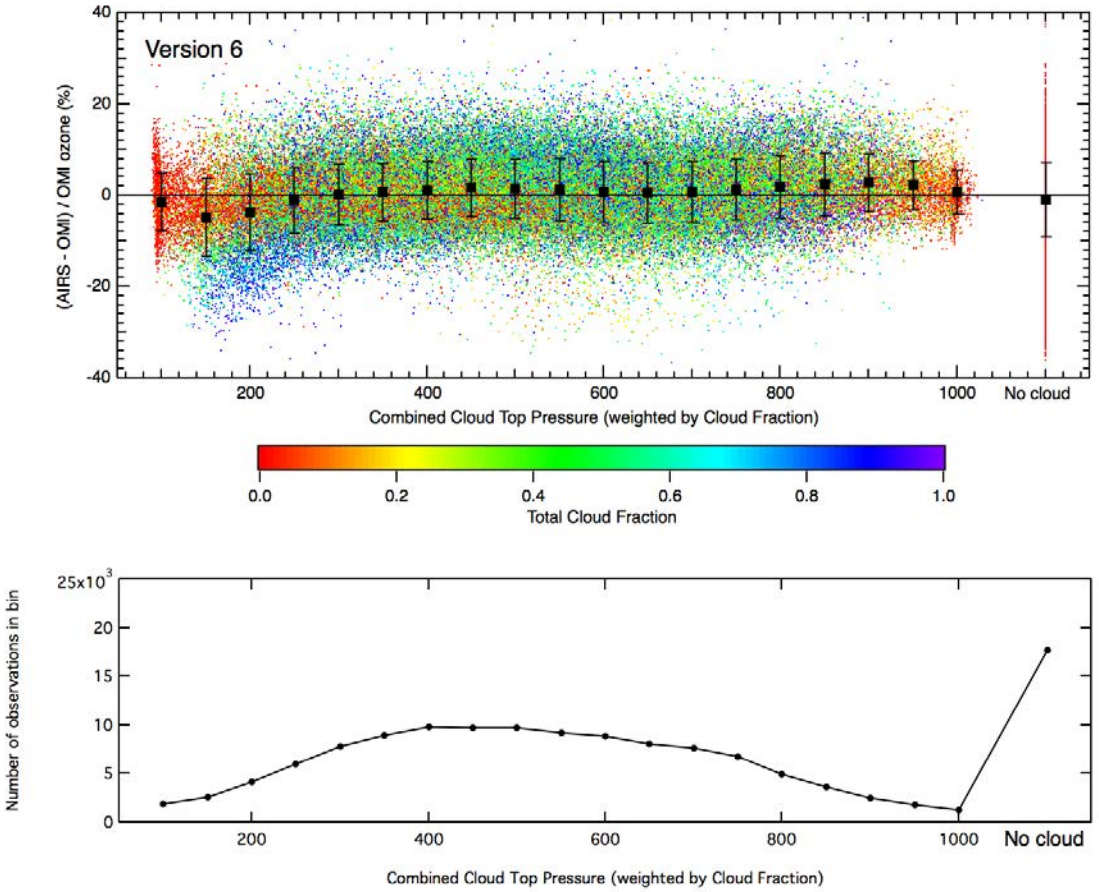

Figure 3.3.7-3: Version 6 IR+MW relative ozone bias against OMI vs combined cloud-top pressure (top panel) and number of observations in bin (bottom panel) for sunlit observations of Feb. 24, 2007. Dots are colored by the total cloud fraction. The combined cloud-top pressure is the sum of the retrieved pressures weighted by the cloud fraction in each cloud layer.

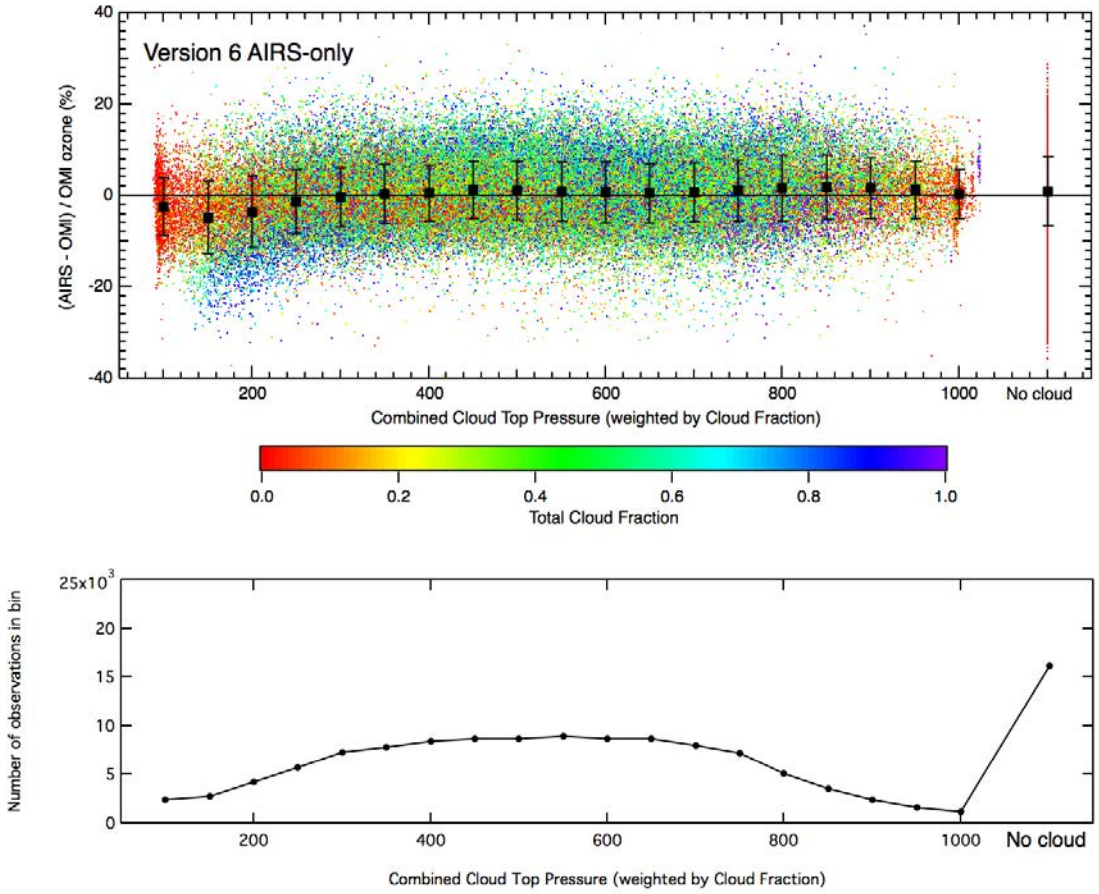

Figure 3.3.7-4: Version 6 AIRS IR-only relative ozone bias against OMI vs combined cloud-top pressure (top panel) and number of observations in bin (bottom panel) for sunlit observations of Feb. 24, 2007. Dots are colored by the total cloud fraction. The combined cloud-top pressure is the sum of the retrieved pressures weighted by the cloud fraction in each cloud layer.

3.3.8 AIRS L3 CO_2

Contributor: E. Olsen

Data

The global Level 3 AIRS/AMSU (IR+MW) and AIRS (IR Only) CO_2 products were compared over a date range spanning January 2010 to December 2011, highlighting in particular the months of January, April, July and October of 2010 to investigate the seasonal features. During 2010 AMSU Channel 5 noise level was acceptable, but during 2011 the noise level of that channel progressively degraded, more rapidly toward the end of that year. The effect upon the AIRS/AMSU CO_2 product in 2011 was to reduce the yield as the year progressed without impacting the retrieved CO_2. AMSU Channel 5 noise level was one component of the QC for the AIRS/AMSU Level 2 retrieval process, and as it increased over 2011 there were progressively fewer AIRS/AMSU Level 2 retrievals available to be ingested by the CO_2 post processing stage.

Methodology

Please refer to Sec. 3.2.6 for L2 CO_2 post processing and quality control. The monthly Level 3 comparison grids the Level 2 CO_2 retrievals within 1°x1° bins and then performs the following analyses:

(1) display the difference of average retrieved CO_2 and yield at the 1°x1° resolution for each of 12 months of 2010 (see Fig 3.3.8-1)
(2) smooth the differences by sliding a 5° diameter tophat function over the 1°x1° grids of averaged retrieved CO_2 and yield and displaying the result, carried out for Jan, Apr, Jul and Oct of 2010. (see Fig 3.3.8-2)
(3) display the area weighted global average CO_2 trend from September 2002 to June 2016, showing the transition from AIRS/AMSU to AIRS (IR-Only) with a two-year overlap from January 2010 to January 2012 (see Fig 3.3.8-3)
(4) display monthly zonal average difference of AIRS/AMSU and AIRS (IR-Only) retrieved CO_2 and yield for 2010 (See Fig 3.3.8-4)
(5) display 10° zonal trend plots (60°S to 80°N) of retrieved CO_2 and its yield for AIRS/AMSU and AIRS (IR-Only) between January 2010 and December 2012 (see Fig 3.3.8-5)

Conclusions and Comments

As shown by the L2 CO_2 comparisons with the air-borne measurements described in Sec. 3.2.6, the loss of microwave has no direct influence upon the AIRS CO_2 post-processing algorithm because the algorithm has chosen to use channels that have minimal radiance contribution from the surface and the very lowest atmospheric layers. The changes on the L3 CO_2 between IR+MW and IR are due to the changes on the yield, in particular the loss of yield in cloudy regions and over land covered by ice and snow, as

discussed in Sec. 3.1. There is an increase of yield in the subtropical low stratus cloud region.

Additional tests will be performed on the AIRS V6 CO_2 product as it becomes available in both flavors. The validation against airborne measurements will be repeated and expanded.

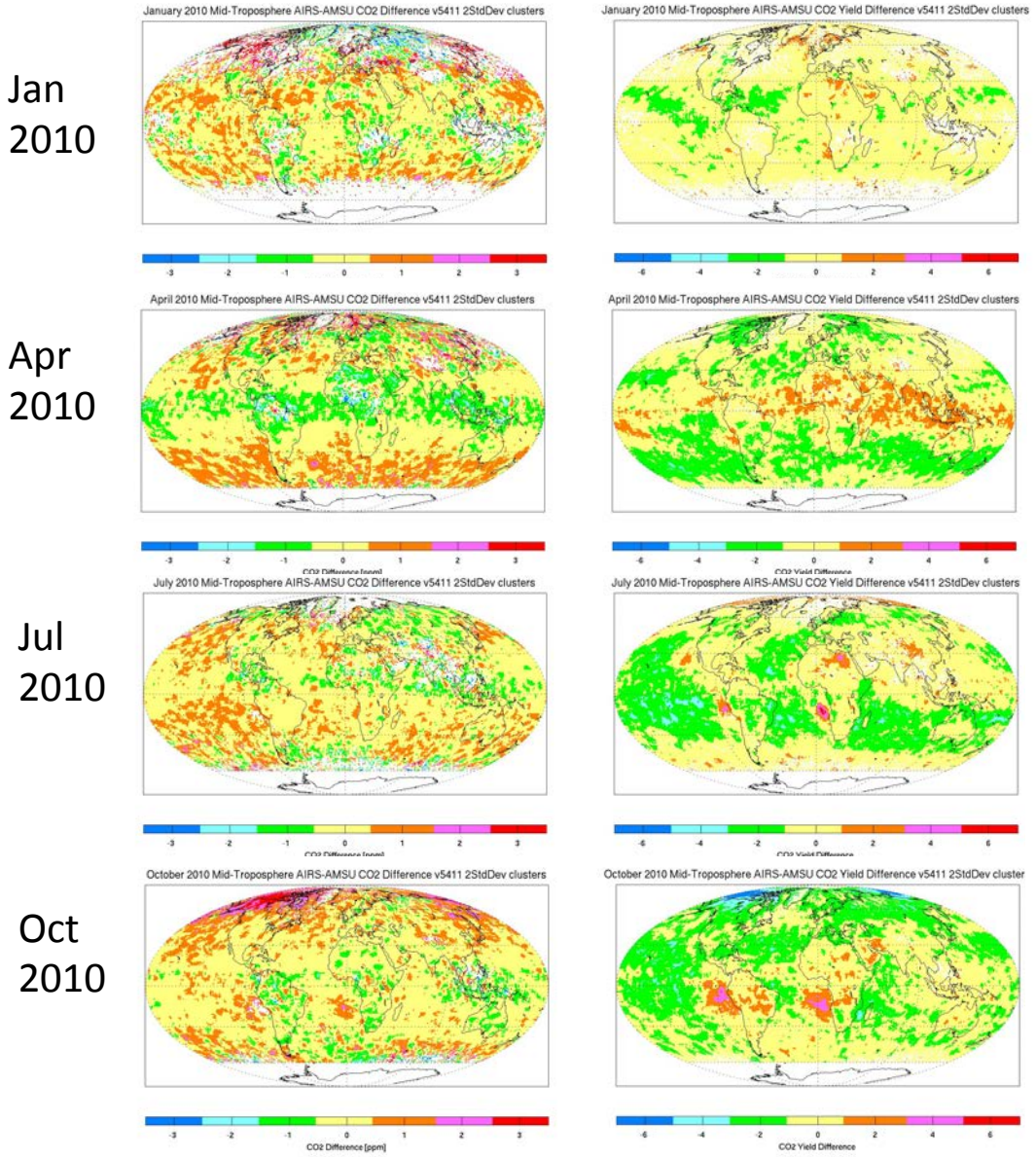

Figure 3.3.8-1. The differences of Retrieved CO_2 (left) and yield (right) between IR and IR+MW data products (IR minus IR+MW). Monthly mean data from January, April, July, and October in 2010 are plotted. Retrievals south of 60°S are not reported. January yield reduced relative to other months due to single event upset that resulted in loss of AIRS data for 15 days of that month.

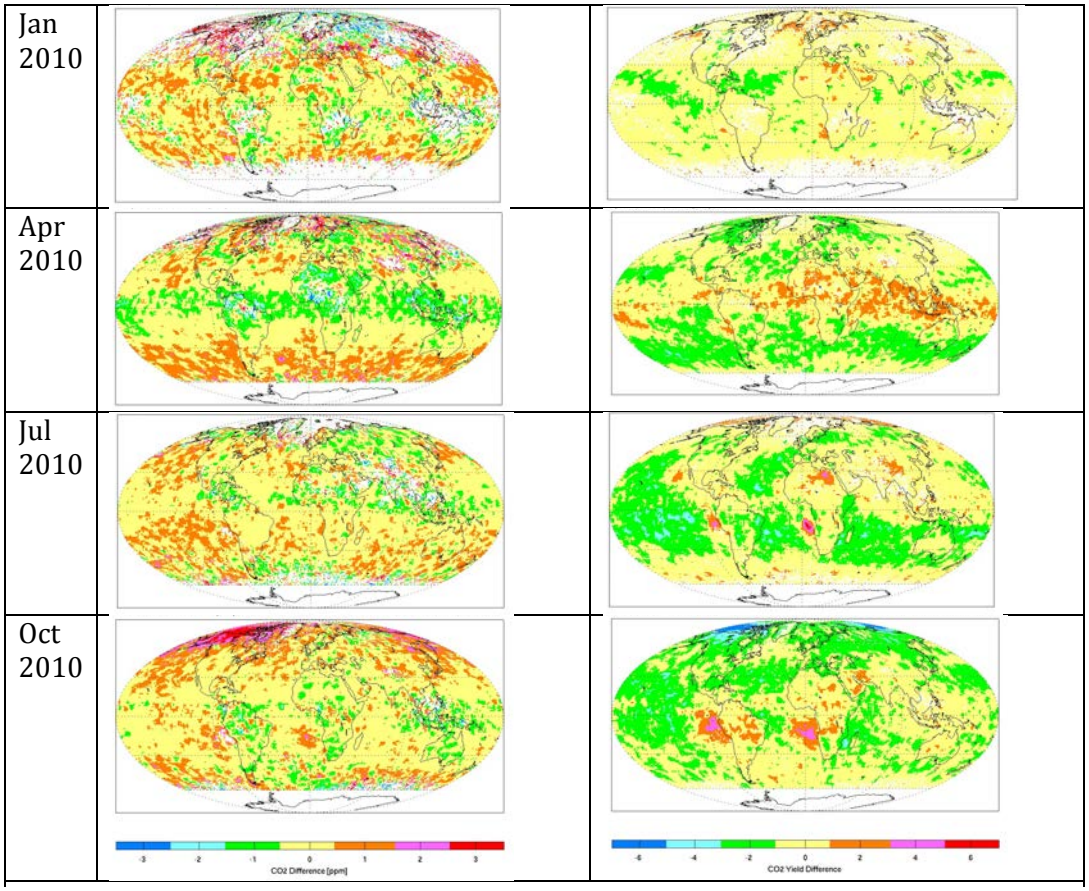

Figure 3.3.8-2. Smoothed comparison of monthly average differences of retrieved CO_2 (left) and yield (right) as a function in four different months of 2010 (IR minus IR+MW). Data at 1° grid is smoothed to 5°. Retrievals south of 60°S are not reported.

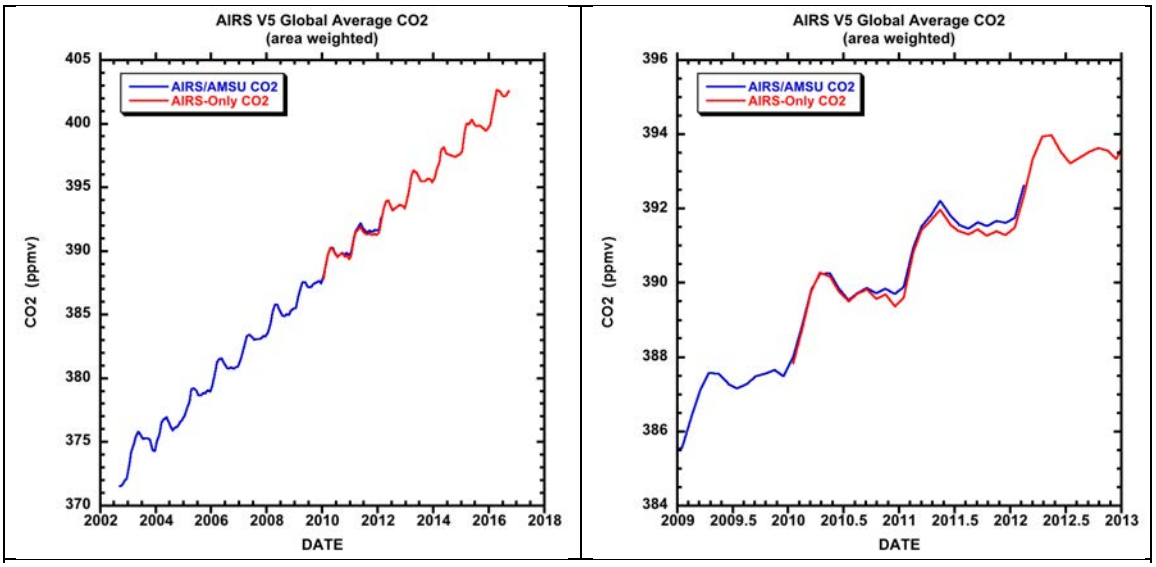

Figure 3.3.8-3. Area-weighted global average CO_2 trend calculated from monthly mean AIRS CO_2 data from September 2002 to June 2016. Left panel shows the continuity from IR+MW (blue) to IR-only (red) after 2010, and right panel shows a zoomed –view of the overlap of these two versions from January 2010 through January 2012.

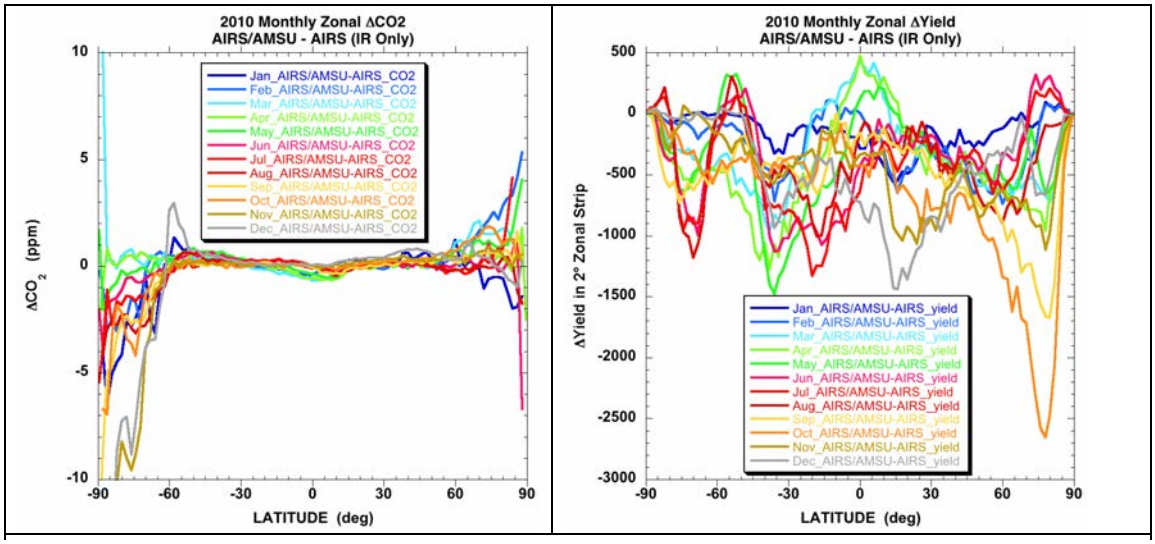

Figure 3.3.8-4. Comparisons of monthly zonal averages of retrieved CO_2 (left) and yield (right) as a function of latitude for each month of 2010 (different colors). The results of IR+MW minus IR-only are shown. Data are binned in 2° bands. Fluctuations at high latitudes (|lat| > 60°) are result of small number statistics. The zonal average difference between IR-only and IR+MW for |lat| < 60° is less than 0.5pp. Retrievals south of 60°S are not reported. Depressed IR+MW yield is due to difference in AIRS L2 QC for the two retrieval processes as well as the beginning of the progressive deterioration of AMSU channel 5.

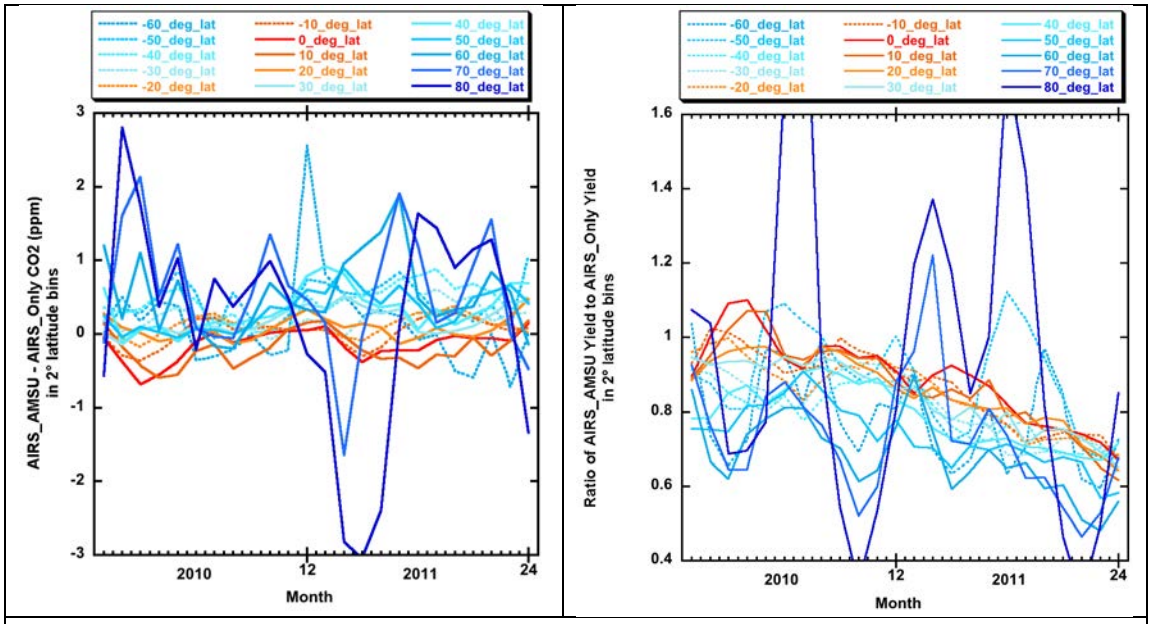

Figure 3.3.8-5. Comparison of zonal averages of retrieved CO_2 (left) and yield (right) as a function of latitude for 2010 and 2011. 10° bands are used to bin the data. Results of IR+MW minus IR are shown. Fluctuations with season in |lat| < 60° are generally small. The large fluctuations at higher latitudes are results of small samples in the statistics.

3.4 Tests of research and application using AIRS data

Since its launch in 2002, AIRS data have been widely applied in various research and application fields. It is still an ongoing effort to document the changes in these research and applications using AIRS observations from IR+MW and IR-only retrievals. Two examples are given in this section: the scaling analysis of temperature and water vapor profiles, and the drought detection using AIRS data.

3.4.1 Temperature and water vapor scaling analysis

Contributor: Brian Kahn

Data

The AIRS Standard Level 2 temperature (T) and water vapor mixing ratio (q) variance scaling is calculated and differenced for AIRS V6 IR+MW and IR-only products. The methodology follows Kahn and Teixeira (2009) and Kahn et al. (2011). Three seasons during 2009 were investigated (MAM, JJA, and SON) and zonal mean values and differences over land and ocean are shown. No 'truth' data set is used. Please refer to Kahn and Teixeira (2009) and Kahn et al. (2011) for the realism of these values and comparisons to in situ aircraft and surface observations, as well as climate model and reanalysis output.

Methodology

All T and q data are retained at vertical levels located above PGood. All T and q data at vertical levels below PGood are removed from the calculations. No filtering by cloud amount was performed as previously done in Kahn and Teixeira (2009) since power law exponents (α) do not exhibit large differences among clear and partly cloudy skies. All of the calculations of variance are performed at the daily scale, as well as for ascending and descending nodes separately, over a set of grid boxes ranging from 1.5 to 12 degrees. The scale-dependent variance is averaged from the daily snapshots and then is fit to power laws where α is derived. This is performed separately for scales less than and greater than 500 km.

Conclusions

Figure 3.4.1-1 shows the values of α for SON in 2009 over land for IR+MW. These are derived from the daily snapshots. Ascending and descending were also calculated separately but are not shown and show similar morphological patterns but are slightly higher in value.

Figure 3.4.1-2 shows the differences of α as in Figure 3.4.1-1 for IR minus IR+MW. The exponents show some significant latitude and height dependent differences between the two retrievals on the order of $\alpha=\pm0.1$. This suggests that there are important differences in the variability as a function of horizontal scale with and without the

influence of AMSU. The large-scale T reduction appears to be consistent with a reduction in variance at the largest scales due to reduced sampling in large-scale cloud structures because of the loss of AMSU. In the case of q in the low latitude boundary layer, a similar effect is seen and could be a combination of scale-dependent sampling differences or increased retrieval noise at the smallest scales. The MAM and JJA seasons show similar patterns but some latitudinal movement is noted and the magnitude of these differences can increase or decrease somewhat (not shown). Ocean exponents (not shown) in general show smaller differences between AIRS-MW and AIRS-IR than land differences.

Comments and Discussions

Further research is warranted to determine the cause of these differences, which could be some combination of yield, sampling of different cloud states, or changes in retrieval noise/RMSE. More interestingly, the differences between IR+MW and IR may yield new insights in the scale dependence of T and q variability within certain cloud states and this topic will be explored in the future.

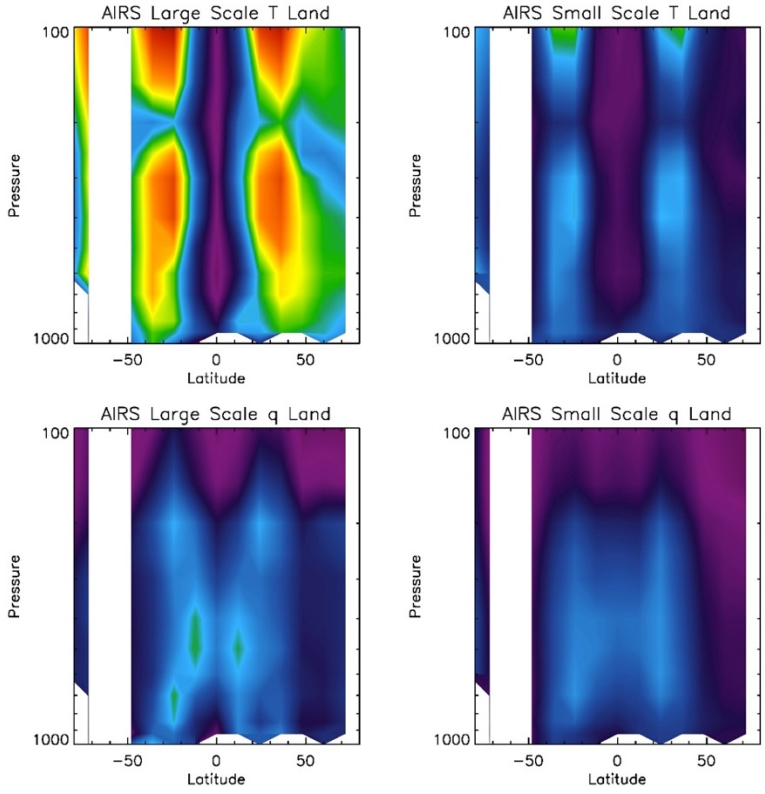

Figure 3.4.1-1. Scaling exponents for T (upper row) and q (lower row) for the large scale (left) and small scale (right) for land only. Dark purple to dark red is scaled from -0.0 to +1.0 (same color scale used in Kahn and Teixeira, 2009).

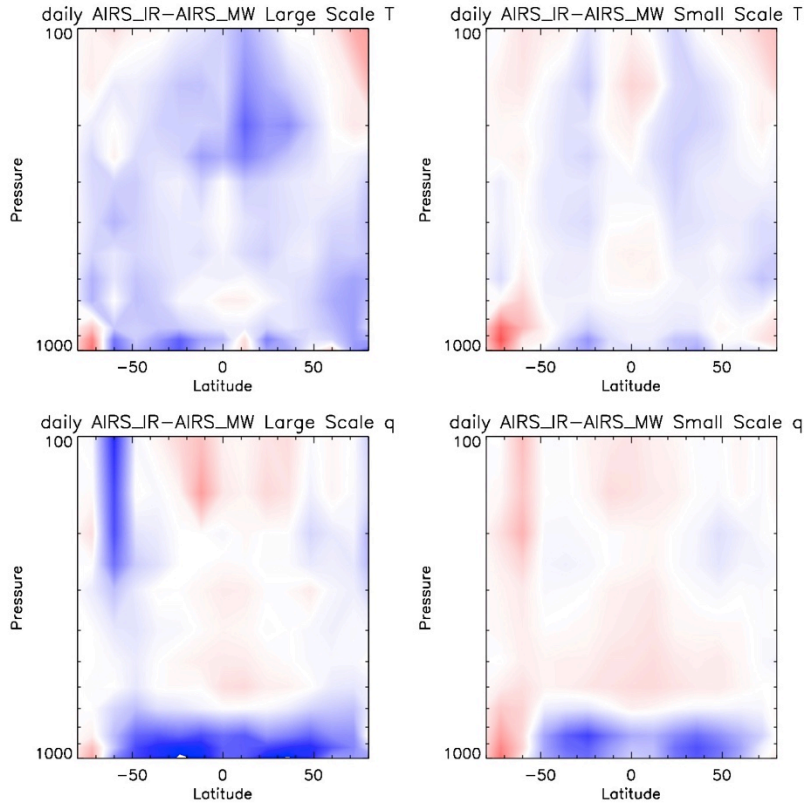

Figure 3.4.1-2. Differences between AIRS-IR and AIRS-MW for the same time period as in Figure 3.4.1-1. Dark blue to dark red is scaled from -0.1 to +0.1.

3.4.2 Drought application of AIRS data

Contributor: Ali Behrangi

Data

The AIRS Level 3 monthly near surface air temperature (Ta), and near surface RH are used to derived VPD to study two drought events.

Methodology

Monthly anomaly values of the studied variables were calculated separately for IR-only and IR+MW retrievals and compared for two case studies of recent major droughts (2011 in Texas and 2012 in Midwest). More discussion about the case studies can be found in Behrangi et al. (2015).

Conclusions

Similar results are found for the two drought events, thus only the plots for the Texas event are shown here. IR-only and IR+MW compare very well in capturing the anomaly locations and time series. No major impact on drought analysis was identified going from IR+MW to IR.

- Near surface VPD: IR-only shows slightly smaller values compared to IR+MW at very high VPDs.
- Near surface air temperature: IR-only shows slightly smaller values than IR+MW at very high temperature values.
- Near surface relative humidity: IR-only shows slightly larger values than IR+MW in very dry conditions.

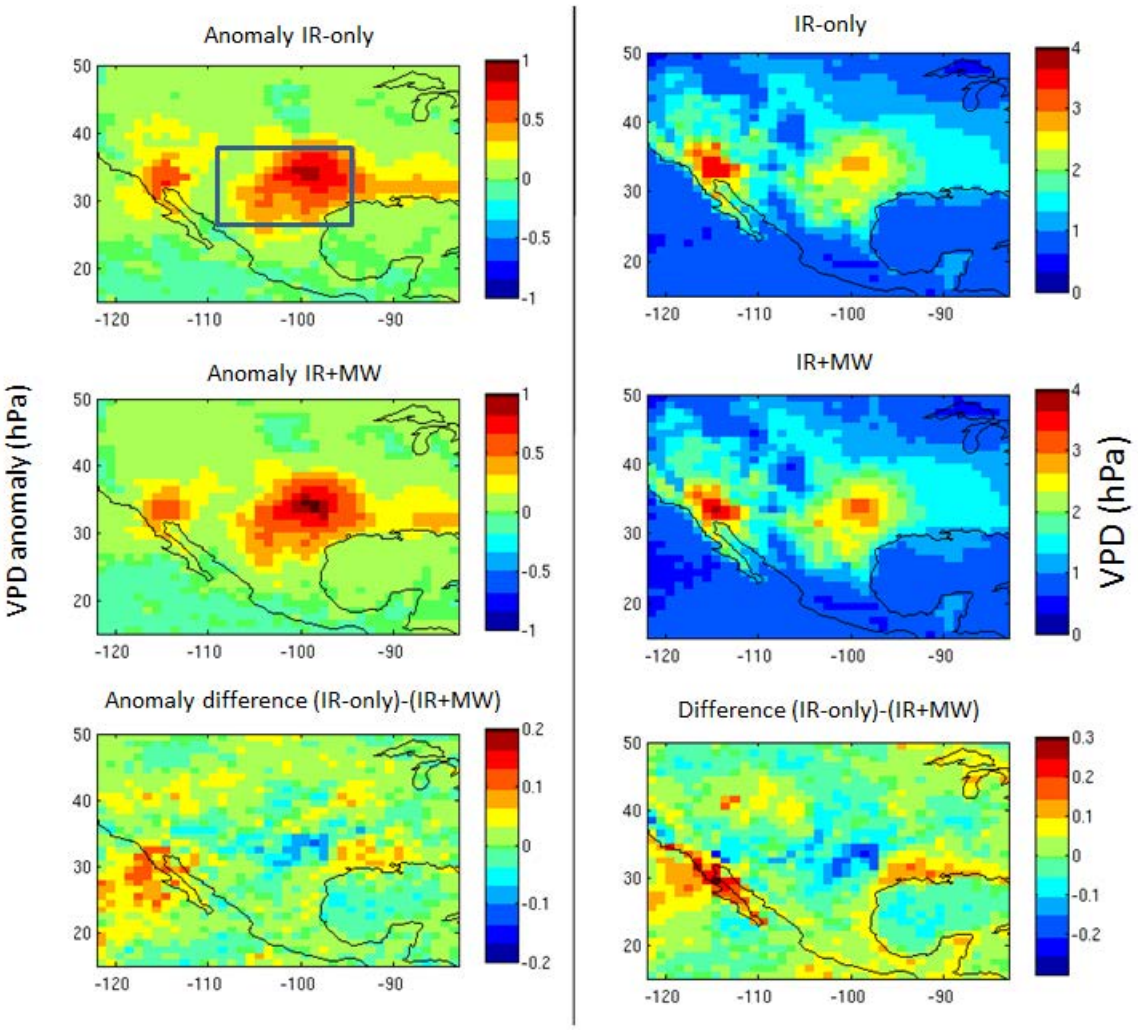

Figure 3.4.2-1. The VPD anomaly (left) and VPD (right) for Texas drought in August 2011. Top: results from IR products. Middle: results from IR+MW. Bottom: IR minus IR+MW.

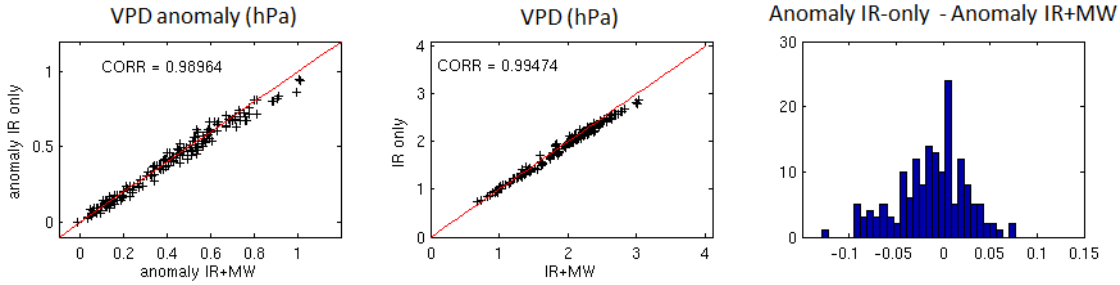

Figure 3.4.2-2. Comparisons on the daily VPD anomaly (left), VPD (middle), and the histogram of VPD anormly differences between IR and IR+MW (right) for August 2011 in Texas.

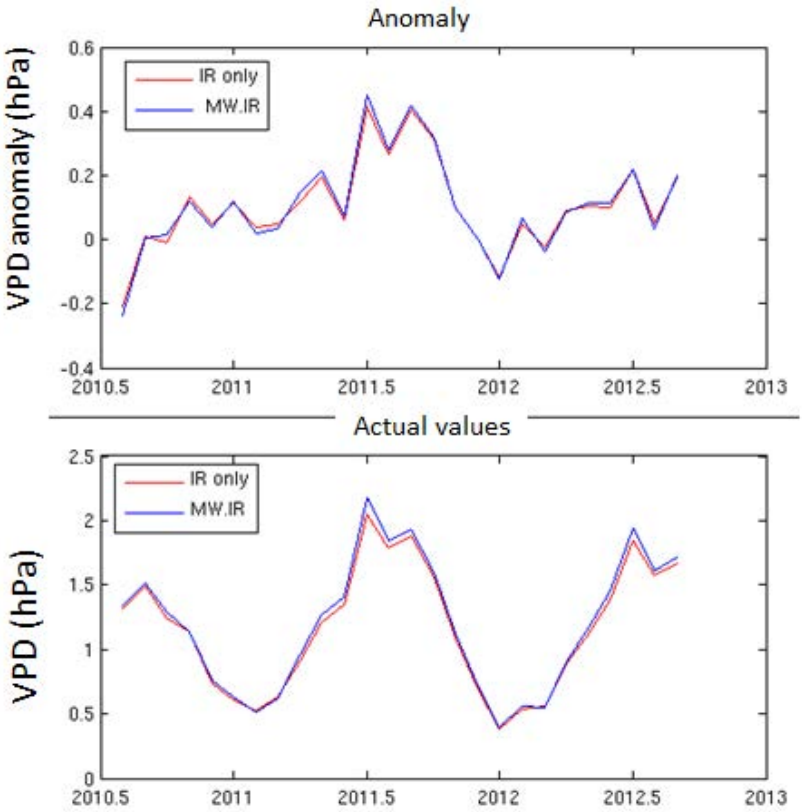

Figure 3.4.2-3. The time series of VPD anomaly and VPD during the Texas drought event in 2011. Red: IR. Blue: IR+MW.

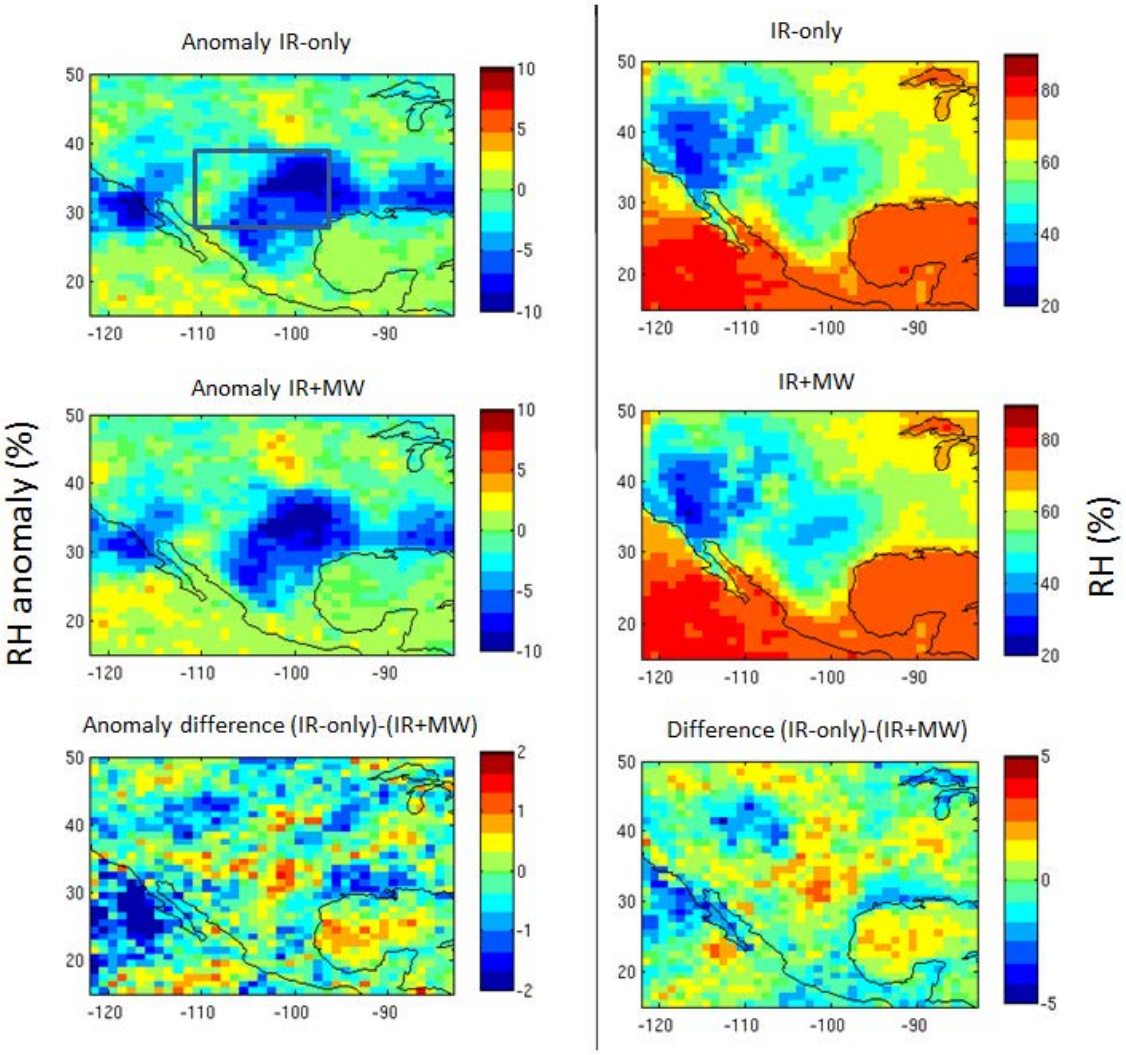

Figure 3.4.2-4. Same as Fig. 3.4.2-1 but for near surface relative humidity.

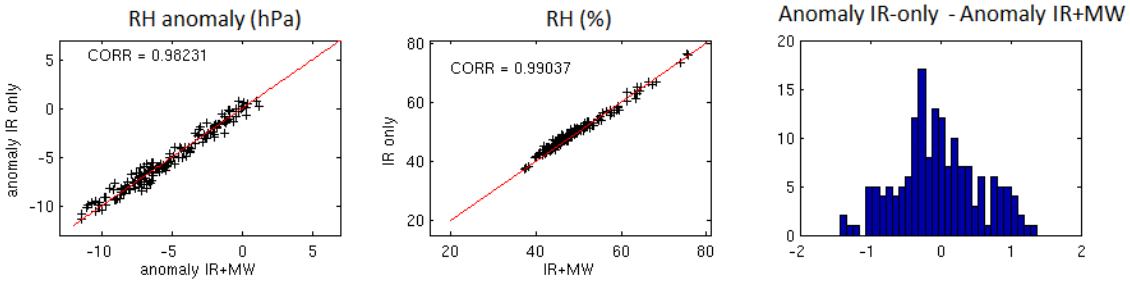

Figure 3.4.2-5. Same as Fig. 3.4.2-2 but for near surface relative humidity.

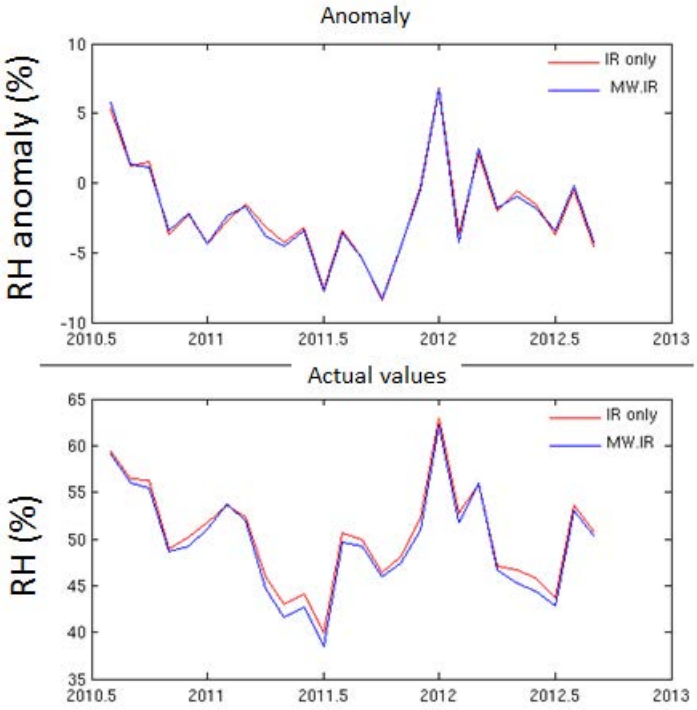

Figure 3.4.2-6. Same as Fig. 3.4.2-3 but for near surface relative humidity.

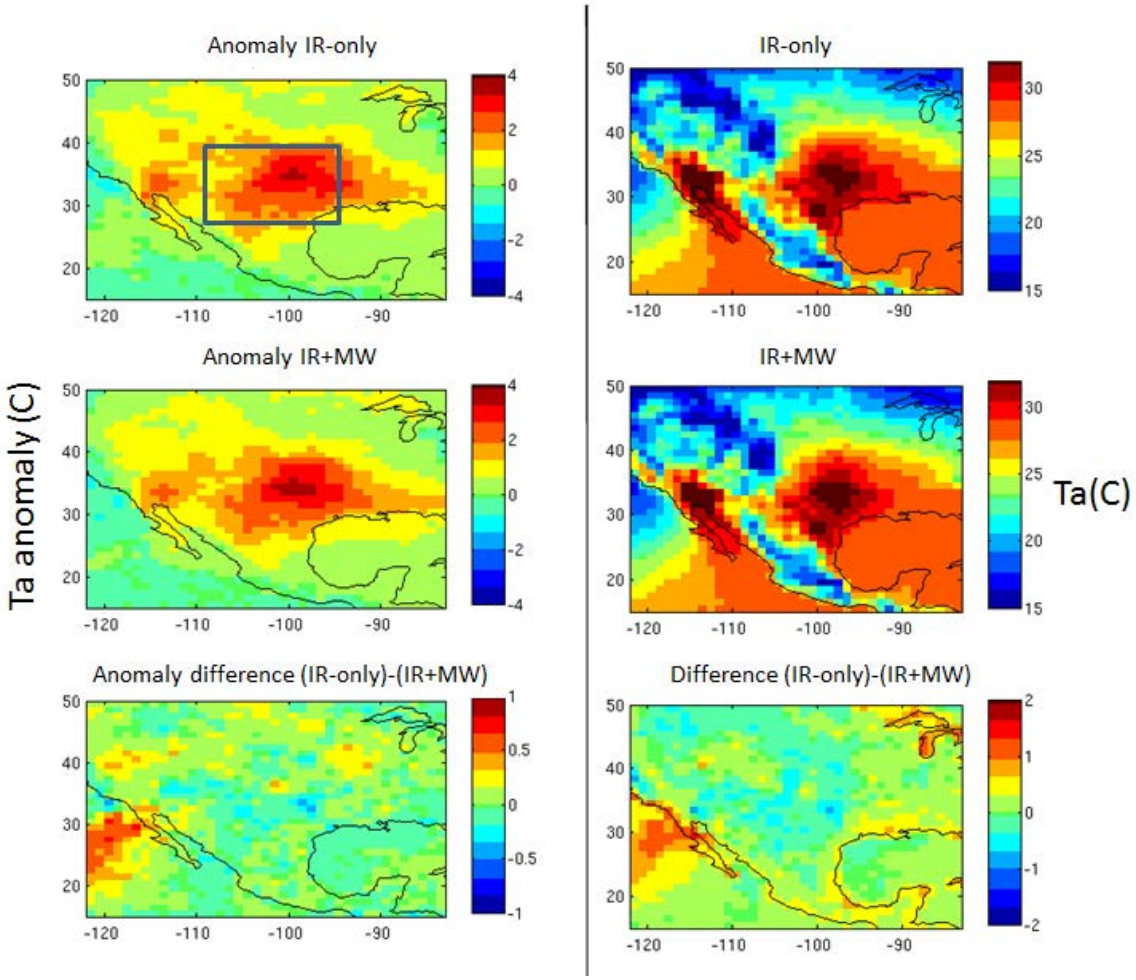

Figure 3.4.2-7. Same as Fig. 3.4.2-1 but for near surface air temperature.

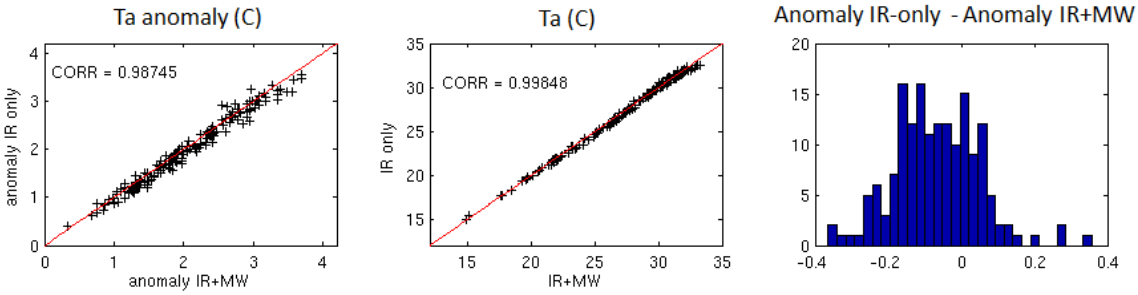

Figure 3.4.2-8. Same as Fig. 3.4.2-2 but for near surface air temperature.

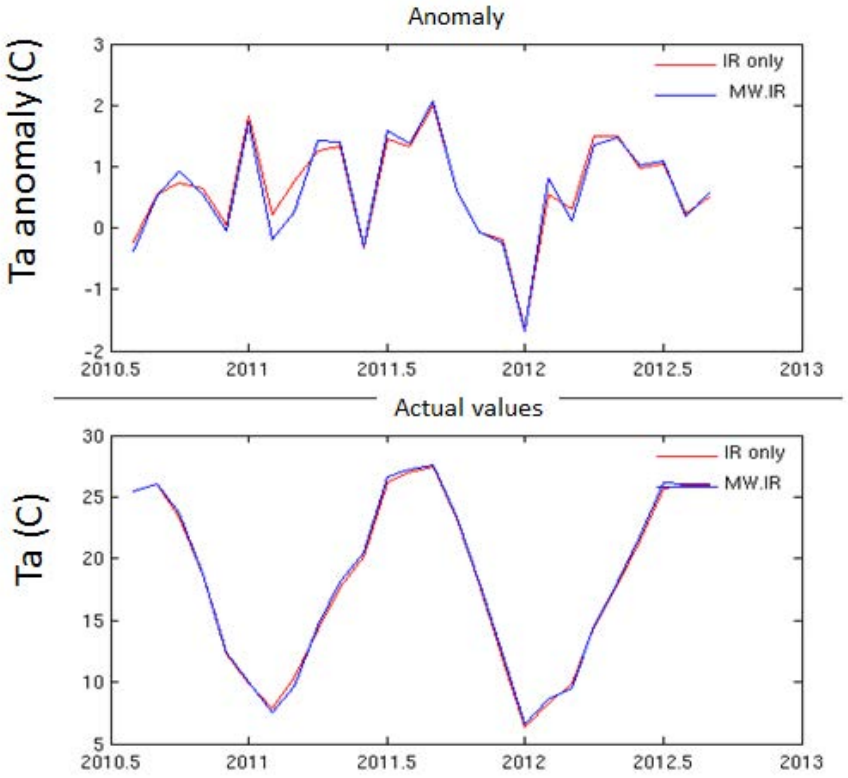

Figure 3.4.2-9. Same as Fig. 3.4.2-3 but for near surface air temperature.

4. References

Aumann, H. H., and coauthors, 2003: AIRS/AMSU/HSB on the Aqua mission: design, science objectives, data products and processing system, *IEEE Trans. Geosci. and Remote Sensing*, **41**, 253-264.

Behrangi, A., P. Loikith, E. Fetzer, H. Nguyen, and S. Granger, 2015: Utilizing Humidity and Temperature Data to Advance Monitoring and Prediction of Meteorological Drought. *Climate*, **3,** 999-1017.

Blackwell, W. J., and F. W. Chen, 2005. Neural network applications in high-resolution atmospheric remote sensing. *Lincoln Laboratory Journal*, *15*(2), p.299.

Fetzer, E., 2003: The validation of AIRS retrievals. Internaltional TOVS Study Conference-XIII. Ste. Adele, Canada.

Goldberg M. D., Y. Qu, L. McMillin, W. Wolf, L. Zhou, and M. Divakarla, 2003: AIRS near-real-time products and algorithms in support of operational numerical weather prediction. *IEEE Trans. Geosci. Remote Sens.,* **41(2),** 379–399.

Kahn, B. H., and Coauthors (2011), Temperature and water vapor variance scaling in global models: Comparisons to satellite and aircraft data, *J. Atmos. Sci.*, 68, 2156–2168, doi:10.1175/2011JAS3737.1

Kahn, B. H., and J. Teixeira (2009), A global climatology of temperature and water vapor variance scaling from the Atmospheric Infrared Sounder, *J. Climate*, 22, 5558–5576, doi: 10.1175/2009JCLI2934.1.

Kahn, B. H., F. W. Irion, V. T. Dang, E. M. Manning, S. L. Nasiri, C. M. Naud, J. Blaisdell, M. M. Schreier, Q. Yue, K. W. Bowman, E. J. Fetzer, G. C. Hulley, K. N. Liou, D. Lubin, S. C. Ou, J. Susskind, Y. Takano, B. Tian, and J. Worden (2014), The Atmospheric Infrared Sounder Version 6 cloud products, Atmos. Chem. Phys., 14, 399–426.

Kahn, B. H., M. M. Schreier, Q. Yue, E. J. Fetzer, F. W. Irion, S. Platnick, C. Wang, S. L. Nasiri, and T. S. L'Ecuyer (2015), Pixel-scale assessment and uncertainty analysis of AIRS and MODIS ice cloud optical thickness and effective radius, J. Geophys. Res., 120, doi:10.1002/2015JD023950.

Lambrigtsen, B.H., and S.-Y. Lee, 2003: Co-Alignment and Synchronization of the AIRS Instrument Suite, *IEEE Trans. Geosci. Remote Sensing*, **41**, pp. 343-351.

J. Löfgren, F. Björndahl, A. Moore, F. Webb, E. Fielding, E. Fishbein, 2010: Tropospheric correction for InSAR using interpolated ECMWF data and GPS Zenith Total Delay from the Southern California Integrated GPS Network Geoscience and Remote Sensing Symposium (IGARSS), 2010 IEEE International (2010), pp. 4503–4506. http://dx.doi.org/10.1109/IGARSS.2010.5649888.

Maddy, E. S. and C. D. Barnet, Vertical Resolution Estimates in Version 5 of AIRS Operational Retrievals, *IEEE Trans. Geosci. Remote Sens., 46(8)*, 2375-2384, 2008.

Susskind, J., C. D. Barnet, and J. M. Blaisdell (2003), Retrieval of atmospheric and surface parameters from AIRS/AMSU/HSB data in the presence of clouds, *IEEE Transactions on Geoscience and Remote Sensing*, *41*(2), 390-409.

Susskind, J., P. Piraino, L. Rokke, T. Iredell, and A. Mehta (1997), Characteristics of the TOVS Pathfinder Path A dataset, *Bulletin of the American Meteorological Society*, *78*(7), 1449-1472, doi:Doi 10.1175/1520-0477(1997)078<1449:Cottpp>2.0.Co;2.

Susskind, J., J. Rosenfield, D. Reuter, and M. T. Chahine (1984), Remote-Sensing of Weather and Climate Parameters from HIRS2 and MSU on Tiros-N, *Journal of Geophysical Research-Atmospheres*, *89*(Nd3), 4677-4697.

Tian, B., C. O. Ao, D. E. Waliser, E. J. Fetzer, A. J. Mannucci, and J. Teixeira, 2012: Intraseasonal temperature variability in the upper troposphere and lower stratosphere from the GPS radio occultation measurements. *J. Geophys. Res.*, **117**, doi:10.1029/2012jd017715.

Ware RH, Fulker DW, Stein SA, Anderson DN, al e. SuomiNet: A real-time national GPS network for atmospheric research and education. Bull Am Meteorol Soc 2000 04;81(4):677-94.

Wofsy et al, (2012), HIPPO Merged 10-second Meteorology, Atmospheric Chemistry, Aerosol Data (R_20121129), used data file "HIPPO_all_missions_merge_10s_20121129.tbl",Carbon Dioxide Information Analysis Center, OakRidge National Laboratory, Oak Ridge, Tennessee, USA, doi:10.3334/CDIAC/hippo_010.

Yue, Q., Brian H. Kahn, Eric J. Fetzer, and João Teixeira, 2011: Relationship between oceanic boundary layer clouds and lower tropospheric stability observed by AIRS, CloudSat and CALIOP, J. Geophys. Res., 116, D18212, doi:10.1029/2011JD016136.

Yue, Q., B. H. Kahn, M. Schieier, H. Xiao, E. J. Fetzer, J. Teixeira, and K. Suselj, 2013a: Transitions of cloud-topped marine boundary layers characterized by AIRS and MODIS observations, and large eddy simulations, *J. Geophys. Res.*, 118, *8598–8611* DOI: 10.1002/jgrd.50676.

Yue, Q., E. J. Fetzer, B. H. Kahn, S. Wong, G. Manipon, A. Guilaume, and B. Wilson, 2013b: Cloud-state-dependent sampling in AIRS observations based on CloudSat cloud classification, *J. of Climate*, **26**, 8357–8377, doi: http://dx.doi.org/10.1175/JCLI-D-13-00065.1.